REFERENCE MANUAL ON THE THEORY OF LIFTING SURFACE NOISE AT LOW MACH NUMBERS

M. S. Howe
Boston University, College of Engineering
110 Cummington Street, Boston MA 02215

9 January, 1998

Report AM-98-001

BOSTON UNIVERSITY
Department of Aerospace and Mechanical Engineering
110 Cummington Street
Boston, Massachusetts 02215

REFERENCE MANUAL ON
THE THEORY OF LIFTING SURFACE NOISE
AT LOW MACH NUMBERS

M. S. Howe
Boston University, College of Engineering
110 Cummington Street, Boston MA 02215
9 January, 1998

Report AM-98-001

Final Revised Report: 20 February 1998
Prepared for Dr. L. Patrick Purtell
Office of Naval Research, Code 333
Grant N00014-97-1-0963

CONTENTS

SUMMARY 1

1. INTRODUCTION 2

2. THEORY OF AERODYNAMIC SOUND 5
2.1 Lighthill's theory 5
2.2 Integral representation of aerodynamic sound 10
2.3 Theory of vortex sound 12
2.4 Compact Green's function 16
2.5 Surface force exerted by a rigid body 20
2.6 Sound generation in the presence of rigid boundaries 25
2.7 Sources adjacent to a compliant wall 30

3. SOUND GENERATED BY FLOW OVER A FLAT SURFACE 31
3.1 Wall pressure wavenumber-frequency spectrum 31
3.2 Smooth wall spectra at low Mach numbers 34
3.3 Boundary layer generated sound 36
3.4 Rough walls 37
3.5 Homogeneous elastic walls 39
3.6 Sound generated by a surface irregularity 40
3.7 Pinned elastic plate 42
3.8 Forward and backward facing steps 43
3.9 Rib-stiffened elastic wall 46
3.10 Flow excited panel radiation 49

CONTENTS continued

4. SOUND GENERATION AT THE EDGE OF A LARGE SURFACE.....51
4.1 Edge noise Green's function.....51
4.2 General representation of trailing edge noise.....55
4.3 Influence of surface geometry on edge noise.....59
4.4 Noise from flow over a right-angled wedge.....62
4.5 Influence of mean flow direction.....64

5. BLADES AND BLADE TIPS.....66
5.1 Green's functions.....66
5.2 Trailing edge self noise.....68

6. SLOTS AND FLAP SIDE-EDGES.....74
6.1 Green's function: non-compact airfoil chord.....74
6.2 Green's function: compact airfoil chord.....78
6.3 Derivation of Green's function.....78
6.4 Boundary layer generated slot noise.....80
6.5 Side-edge flap noise.....83

REFERENCES.....89

PRINCIPAL SYMBOLS.....92

SUMMARY

A summary review is made of the theory of aerodynamic sound in low Mach number flows, with particular emphasis on procedures for estimating the influence of solid boundaries on sound production. Special consideration is given to the production of sound by nominally steady flow over a lifting or control surface. Four categories of interactions are discussed involving (i) a large, nominally flat surface, (ii) a large surface with a trailing edge, (iii) a lifting surface of compact chord and finite span, and (iv) a trailing edge with a streamwise slot or part-span flap.

The relative inefficiency with which hydrodynamic energy is converted into sound means that it is not usually possible to make confident noise predictions by direct numerical simulation of a flow. However, numerical codes can accurately predict *mean* properties of complex fluid structure interactions, and the results may be incorporated into analytical models described in this report to express the sound and vibration generated by an interaction in terms of those mean properties. Mean flow numerical computations also permit 'noisy' large scale features (such as trailing vortices) to be identified, whose potential for noise generation can be investigated analytically by the methods described herein.

1. INTRODUCTION

The sound generated by unsteady flow is called *aerodynamic sound* [1, 2]. Most flows of technological interest are of high Reynolds number and turbulent, and the acoustic radiation is a very small by-product of the motion. The turbulence is usually produced by fluid motion relative to solid boundaries or by the instability of free shear layers separating a high speed flow (such as a jet) from a stationary environment. The theory of aerodynamic sound is usually concerned with the mechanism of sound *production* by a prescribed turbulent flow as opposed to the processes by which the flow is generated. In many instances, however, the backreaction of the sound on the flow can be important, and must be properly accounted for in estimating the radiation.

The aerodynamic sound problem in "free space" reduces to the study of mechanisms that convert kinetic energy of free rotational ("vortical") motions into acoustic waves involving longitudinal vibrations of fluid particles. There are two principal source types: a quadrupole, whose strength is determined by the unsteady Reynolds stress, and a dipole, which is important when mean mass density variations occur within the source region.

The quadrupole sound generated by turbulent flow near a *fixed, rigid* surface, is augmented by radiation from a distribution of surface *dipoles* whose strength is the force per unit surface area exerted on the fluid. If the surface is in accelerated motion there are additional dipoles and quadrupoles; neighboring surfaces in *relative* motion experience "potential flow" interactions that also generate sound. At the low Mach numbers M encountered in underwater applications (typically < 0.01), the *acoustic efficiency* of the surface sources exceeds the quadrupole efficiency by a large factor $\sim O(1/M^2)$. The presence of solid surfaces within low Mach number turbulence can therefore lead to substantial increases in aerodynamic sound levels.

Turbulence stresses on an elastic surface generate sound, and can also excite structural vibrations which store a substantial amount of flow energy. The vibrations are ultimately dissipated by frictional losses, but they can contribute significantly to the radiated noise, because elastic waves are "scattered" at structural discontinuities, and some of their energy is transformed into sound. Flow generated sound accordingly reaches the far field via two paths: directly from the turbulence sources and indirectly from possibly remote locations where the scattering occurs. In consequence, the effective acoustic efficiency of the flow is

often very much larger than for a geometrically similar rigid surface, even when only a small fraction of the structural energy is scattered into sound.

The first part of this report (§2) consists of a review of the theory of aerodynamic sound for low Mach number flows, including methods for estimating the contributions from solid boundaries. Subsequent sections deal with the prediction of sound generated by high Reynolds number flow over typical structural elements of a complex, underwater control surface. The flow induced sound and vibration of a submerged vehicle is attributable to the instability of boundary layers, the shedding of larger scale vortex structures from appendages, and to localized sources formed when these flow inhomogeneities interact with or impinge on geometrical and structural discontinuities, such as joints, corners, fixed and articulated lifting surfaces, shrouds, etc. With few exceptions, and because of the large number of degrees of freedom, and the relative inefficiency with which hydrodynamic energy is converted into sound, it is not possible to make confident noise predictions by direct numerical calculation of the flow.

However, because of the increasing ability of numerical codes to simulate accurately the principal *mean* properties of fluid structure interactions, the results of such calculations can be incorporated into analytical prediction schemes to estimate the sound and vibration generated by fluid-structure interactions in terms of computed mean hydrodynamic properties. For example, numerical solutions of the Reynolds-Averaged Navier-Stokes (RANS) equations, which make use of a simplified turbulence model, enable the mean flow field about geometrically complex structures to be evaluated in detail. Such solutions can be used to calculate characteristic 'wavelengths', wavenumbers and frequencies for insertion into empirical models of the unsteady surface pressure and shear stress spectra that are then used to estimate sound and vibration levels produced by boundary layer forcing of an elastic substructure. These methods also permit 'noisy' large scale features (such as trailing vortices) to be identified, whose unsteady interaction with a structural appendage or surface irregularity can be investigated by appeal to analytical models involving the perturbation of the large scale structure by a turbulence field, or from some known instability characteristic of the motion.

The purpose of this report is to review and extend where necessary the available analytical models for low Mach number flows interacting with lifting surfaces. This is done by considering four different classes of flow interactions with: (i) large, nominally flat surfaces (§3), (ii) a large surface with a trailing edge (§4), (iii) lifting surfaces of finite chord and span (§5),

and (iv) trailing edges with streamwise slots and part-span flaps (§6). Well known methods and formulae are reviewed without extensive discussion, but results not available elsewhere in the literature are treated in more detail (especially in §§4-6).

2. THEORY OF AERODYNAMIC SOUND

§2.1 Lighthill's theory

The acoustic analogy. Lighthill [1] reformulated the Navier-Stokes equation into an exact, inhomogeneous wave equation whose source terms are important only within the turbulent (vortical) region. Sound is expected to be such a very small component of the flow that, once generated, its back-reaction on the source flow is usually negligible. In a first approximation the motion in the source region may therefore be determined by neglecting the production and propagation of the sound. This would be inappropriate if the Mach number M is large enough for compressibility to be important in the source flow, when the source flow is coupled to a resonator, such as an organ pipe, or when bubbles are present in the case of liquids. However, there are many technologically important flows where M is sufficiently small that the hypothesis is obviously correct, and where the theory leads to unambiguous predictions of the sound.

Consider the sound generated by a finite region of rotational flow in an unbounded fluid at rest at infinity. Let us compare the equations for the *density* fluctuations in the real flow with those for an ideal, linear acoustic medium which coincides with the real fluid at large distances from the sources. The difference between these equations will be shown to be equivalent to a distribution of sources in the ideal acoustic medium, whose radiation field is the same as that in the real flow and may therefore be calculated by the methods of linear acoustics. To do this, body forces are neglected, and the momentum equation is written in the form

$$\partial(\rho v_i)/\partial t = -\partial \pi_{ij}/\partial x_j, \tag{2.1.1}$$

where π_{ij} is the **momentum flux** tensor

$$\pi_{ij} = \rho v_i v_j + (p - p_o)\delta_{ij} - \sigma_{ij}, \tag{2.1.2}$$

p_o is the uniform pressure at infinity, and σ_{ij} is the viscous stress tensor (other standard symbols are defined on page 92).

By integrating over a fixed region V, it can be seen that (2.1.1) equates the rate of change of momentum in V to the action of the pressure and viscous stresses on its boundary and to the convection of momentum across the boundary at a rate determined by the Reynolds stress $\rho v_i v_j$. In an ideal, linear acoustic medium, momentum transfer is produced solely

by the pressure, i.e., $\pi_{ij} \to \pi^o_{ij} = (p - p_o)\delta_{ij} \equiv c_o^2(\rho - \rho_o)\delta_{ij}$, where ρ_o and c_o are the mean density and sound speed. The equation of linear acoustics for the perturbation density $\rho - \rho_o$ is therefore

$$\left(\partial^2/c_o^2\partial t^2 - \nabla^2\right)\left[c_o^2(\rho - \rho_o)\right] = 0, \tag{2.1.3}$$

and is obtained by eliminating ρv_i between (2.1.1) (with π_{ij} replaced by π^o_{ij}) and the continuity equation

$$\partial\rho/\partial t + \mathrm{div}(\rho \mathbf{v}) = 0. \tag{2.1.4}$$

In the absence of externally applied forces or moving boundaries, equation (2.1.3) has only the trivial solution $\rho - \rho_o = 0$, since the radiation condition ensures that sound waves cannot enter from infinity.

The sound generated in the real fluid may now be seen to be exactly equivalent to that produced in an ideal, stationary acoustic medium that is forced by the stress distribution $T_{ij} = \pi_{ij} - \pi^o_{ij}$. T_{ij} is the **Lighthill stress tensor**

$$T_{ij} = \rho v_i v_j + \left((p - p_o) - c_o^2(\rho - \rho_o)\right)\delta_{ij} - \sigma_{ij}. \tag{2.1.5}$$

The Reynolds stress $\rho v_i v_j$ is nonlinear, and is significant only within the rotational source region. The second term is the *excess* of momentum transfer by the pressure over that in an ideal ("linear") fluid of density ρ_o and sound speed c_o. This is caused by wave amplitude nonlinearity, and by mean density variations in the source flow. The viscous stress tensor σ_{ij} is linear in the perturbation quantities, and properly accounts for the attenuation of the sound; in most applications the Reynolds number in the source region is sufficiently large that σ_{ij} can be neglected, and attenuation in the radiation zone is usually ignored in a first approximation.

Lighthill's **acoustic analogy** equation for the production of aerodynamic sound is obtained by first re-writing (2.1.1) as the momentum equation for an ideal, stationary fluid of density ρ_o and sound speed c_o subject to the externally applied stress T_{ij}:

$$\partial(\rho v_i)/\partial t + \partial\left(c_o^2(\rho - \rho_o)\right)/\partial x_i = -\partial T_{ij}/\partial x_j.$$

Elimination of the momentum density ρv_i between this and the continuity equation (2.1.4) yields **Lighthill's equation**, which is the exact, nonlinear counterpart of (2.1.3):

$$\left(\frac{1}{c_o^2}\frac{\partial^2}{\partial t^2} - \nabla^2\right)\left[c_o^2(\rho - \rho_o)\right] = \frac{\partial^2 T_{ij}}{\partial x_i \partial x_j}. \tag{2.1.6}$$

The fluid mechanical problem of calculating the aerodynamic sound is therefore formally equivalent to solving this equation for the radiation into a stationary, ideal fluid produced by a distribution of *quadrupole* sources whose strength per unit volume is the Lighthill stress tensor T_{ij}.

The solution with outgoing wave behavior in an unbounded fluid is given by the retarded potential integral

$$c_o^2(\rho - \rho_o) = \frac{\partial^2}{\partial x_i \partial x_j} \int \frac{T_{ij}(\mathbf{y}, t - |\mathbf{x}-\mathbf{y}|/c_o)}{4\pi|\mathbf{x}-\mathbf{y}|}\, d^3\mathbf{y}, \tag{2.1.7}$$

where $c_o^2(\rho - \rho_o) \to p - p_o$ as $|\mathbf{x}| \to \infty$ in the linearly disturbed fluid outside the source flow. This solution should strictly be regarded as an alternative, integral equation formulation of the Navier-Stokes equation, that happens to provides a useful representation of the far field sound when T_{ij} is known. T_{ij} accounts not only for the generation of sound, but also for self-modulation due to acoustic nonlinearity, convection by the flow, refraction due to sound speed variations, and attenuation due to thermal and viscous actions. Nonlinear effects on propagation and dissipation are usually sufficiently weak to be neglected within the source region, although they may affect propagation to a distant observer. Convection and refraction of sound within and near the source flow can be important, for example when the sources are contained in a turbulent shear layer, or are adjacent to a large, quiescent region of fluid whose mean thermodynamic properties differ from those in the radiation zone. Effects of this kind are accounted for by contributions to T_{ij} that are *linear* in the perturbation quantities relative to a mean background flow [2].

Thus, with the exception of flows amenable to special treatment, the practical utility of Lighthill's equation rests on the hypothesis that all of these effects, which actually depend on the *compressibility* of the source flow, can be ignored, and that adequate predictions of the aerodynamic sound are obtained by taking for T_{ij} an estimate based on the equations of motion of an incompressible fluid. This approximation is likely to be acceptable when $M^2 \ll 1$, and when the wavelength of the sound is much larger than the dimension of the source region. The remainder of this section is devoted to a consideration of such cases.

Aerodynamic sound generated by low Mach number turbulence of uniform mean density. When the mean density and sound speed are uniform, the variations in ρ produced by low Mach number, high Reynolds number velocity fluctuations are of order $\rho_o M^2$, and $\rho v_i v_j \approx \rho_o v_i v_j$ with a relative error $\sim O(M^2) \ll 1$. Similarly, $p - p_o - c_o^2(\rho - \rho_o) \approx$

$(p-p_o)(1-c_o^2/c^2) \sim O(\rho_o v^2 M^2)$. Thus, $T_{ij} \approx \rho_o v_i v_j$, when viscous stresses are neglected, and the solution (2.1.7) becomes

$$p(\mathbf{x},t) \approx \frac{\partial^2}{\partial x_i \partial x_j} \int \frac{\rho_o v_i v_j(\mathbf{y}, t-|\mathbf{x}-\mathbf{y}|/c_o)}{4\pi|\mathbf{x}-\mathbf{y}|} d^3\mathbf{y}$$

$$\approx \frac{x_i x_j}{4\pi c_o^2 |\mathbf{x}|^3} \frac{\partial^2}{\partial t^2} \int \rho_o v_i v_j(\mathbf{y}, t-|\mathbf{x}-\mathbf{y}|/c_o)\, d^3\mathbf{y}, \quad |\mathbf{x}| \to \infty, \qquad (2.1.8)$$

where $p(\mathbf{x},t) = c_o^2(\rho - \rho_o)$ is the perturbation pressure in the far field. Quantitative predictions can be made from this equation provided the behavior of the Reynolds stress is known.

The order of magnitude of p can be estimated in terms of the characteristic velocity v and length scale ℓ (of the energy containing eddies) in the source region. ℓ is determined by the scale of the mechanism responsible for turbulence production, such as the width of a jet mixing layer. Fluctuations in $v_i v_j$ occurring in different regions of the turbulent flow separated by distances $> O(\ell)$ will tend to be statistically independent, and the sound may therefore be considered to be generated by a collection of V_o/ℓ^3 independent eddies, where V_o is the volume occupied by the turbulence. The dominant frequency of the motion $\sim v/\ell$, so that the wavelength of the radiated sound $\sim \ell/M \gg \ell$ ($M \sim v/c_o$), and each eddy is therefore acoustically *compact*. Hence, the acoustic pressure generated by a single eddy is of order $p \sim (\ell/|\mathbf{x}|)\rho_o v^2 M^2$, and the acoustic power it radiates $\sim 4\pi|\mathbf{x}|^2 p^2/\rho_o c_o \approx \ell^2 \rho_o v^8/c_o^5 = \ell^2 \rho_o v^3 M^5$. This is Lighthill's "eighth power" law. The total acoustic power is $\Pi_a \approx (\mathrm{V}_o/\ell^3)(\ell^2 \rho_o v^3 M^5) = \rho_o v^3 M^5 \mathrm{V}_o/\ell$. Dimensional arguments and experiment [3, 4] indicate that the rate of decay of the turbulence kinetic energy $\sim O(\mathrm{V}_o \rho_o v^3/\ell)$. In a statistically steady state this must equal the rate Π_o, say, at which energy is supplied to the flow by the action of external forces. The *efficiency* Π_a/Π_o with which this energy is converted into sound is therefore proportional to M^5, confirming Lighthill's hypothesis that the flow generated sound is an infinitesimal by-product of the motion.

Aerodynamic sound generated by low Mach number turbulence of variable mean density. When the mean density in the source region is not constant, the Reynolds stress quadrupoles are augmented by a distribution of *dipoles*, the dipole strength being proportional to the hydrodynamic force experienced by a fluid particle of density ρ relative to the force the same particle would experience had its density been equal to ρ_o. This dipole is "hidden" within the Lighthill quadrupole T_{ij}, and is estimated by first writing

the solution (2.1.7) in the form

$$p(\mathbf{x},t) \approx \frac{1}{4\pi c_o^2}\frac{\partial^2}{\partial t^2}\int \left[\rho v_i v_j\right]\frac{(x_i-y_i)(x_j-y_j)d^3\mathbf{y}}{|\mathbf{x}-\mathbf{y}|^3} + \frac{1}{4\pi}\int \frac{\partial^2}{\partial t^2}\left[\frac{p-p_o}{c_o^2}-(\rho-\rho_o)\right]\frac{d^3\mathbf{y}}{|\mathbf{x}-\mathbf{y}|}, \quad |\mathbf{x}-\mathbf{y}|\to\infty \tag{2.1.9}$$

where the square brackets [ ] indicate evaluation at the retarded time $t-|\mathbf{x}-\mathbf{y}|/c_o$.

The density of a fluid particle changes by $(p-p_o)/c^2$ when isentropically compressed by departures of p from the ambient pressure p_o, where c is the local speed of sound. Let us assume that the motion of each fluid particle is isentropic, but that the mean density, which will be denoted by $\bar{\rho}(\mathbf{x},t)$, varies from point to point in the source region, where $(\bar{\rho}-\rho_o)/\rho_o$ need not necessarily be small. This means that $(p-p_o)/c^2 = \rho-\bar{\rho}$ and $D\bar{\rho}/Dt = 0$. The Reynolds stress on the right (2.1.9) must be replaced by $\bar{\rho}v_iv_j$, and the integrand of the second term in (2.1.9) becomes

$$\frac{\partial^2}{\partial t^2}\left\{\frac{p-p_o}{c_o^2}-(\rho-\rho_o)\right\} = \frac{\partial^2}{\partial t^2}\left\{(p-p_o)\left(\frac{1}{c_o^2}-\frac{1}{c^2}\right)\right\} - \frac{\partial^2}{\partial t^2}(\bar{\rho}-\rho_o).$$

The first term on the right is already in a form suitable for estimating the acoustic radiation. However, the second term would yield zero when retarded time variations are neglected over a coherent source region of constant mass. To deal with this the relation $D(\bar{\rho}-\rho_o)/Dt = 0$ is used to show that

$$\frac{\partial^2}{\partial t^2}(\bar{\rho}-\rho_o) = -\frac{\partial}{\partial x_j}\left((\bar{\rho}-\rho_o)\frac{Dv_j}{Dt}\right) + \frac{\partial^2}{\partial x_i\partial x_j}((\bar{\rho}-\rho_o)v_iv_j) + \frac{\partial}{\partial t}((\bar{\rho}-\rho_o)\mathrm{div}\,\mathbf{v}) - \frac{\partial}{\partial x_j}(v_j(\bar{\rho}-\rho_o)\mathrm{div}\,\mathbf{v}). \tag{2.1.10}$$

This is further simplified by substitution from the momentum equation $Dv_j/Dt = (-1/\rho)\partial p/\partial x_j$, and from the continuity equation $\mathrm{div}\,\mathbf{v} = (-1/\rho c^2)Dp/Dt \approx -D[(p-p_o)/\rho c^2]/Dt$. The amplitude of sound produced by the final term on the right of (2.1.10) is $O(M)$ relative to the preceding one and is neglected.

Inserting these results into (2.1.9), and discarding the overbar on $\bar{\rho}$, we obtain

$$\begin{aligned} p(\mathbf{x},t) \approx\ & \frac{x_ix_j}{4\pi c_o^2|\mathbf{x}|^3}\frac{\partial^2}{\partial t^2}\int\left[\rho_o v_iv_j\right]d^3\mathbf{y} + \frac{\rho_o x_j}{4\pi c_o|\mathbf{x}|^2}\frac{\partial}{\partial t}\int\left[\left(\frac{1}{\rho_o}-\frac{1}{\rho}\right)\frac{\partial p}{\partial y_j}\right]d^3\mathbf{y} \\ & + \frac{\rho_o}{4\pi|\mathbf{x}|}\frac{\partial^2}{\partial t^2}\int\left[\left(\frac{1}{\rho_o c_o^2}-\frac{1}{\rho c^2}\right)(p-p_o)\right]d^3\mathbf{y}, \quad |\mathbf{x}|\to\infty, \end{aligned} \tag{2.1.11}$$

where quantities in square braces are evaluated at time $t-|\mathbf{x}-\mathbf{y}|/c_o$. The new terms in this formula, in addition to the Reynolds stress radiation of (2.1.8), are respectively non-zero when the mean density in the source region $\rho \neq \rho_o$, and when $\rho_o c_o^2 \neq \rho c^2$, and are the sound fields of dipole and monopole sources.

All of these source types occur in the turbulent mixing region of a hot gas jet exhausting into cold air: "hot spots" or "entropy inhomogeneities" behave as scattering centers at which dynamic pressure fluctuations are converted directly into sound. The dipole source strength is proportional to $(1/\rho - 1/\rho_o)\nabla p$, i.e., to the difference between the acceleration of fluid of density ρ in the jet and that which fluid of ambient mean density ρ_o would experience in the same pressure gradient. For an ideal gas with $p-p_o \sim O(\rho_o v^2)$ in the jet, the order of magnitude of the dipole sound from an eddy of scale ℓ is

$$p \sim (\ell/|\mathbf{x}|)(1-\rho_o/\rho)\rho_o v^2 M \approx (\ell/|\mathbf{x}|)(\Delta T/T)\rho_o v^2 M,$$

where $\Delta T/T \approx (\rho-\rho_o)/\rho$ is the fractional temperature difference between the hot spot and its environment, which can be large. The sound power $\sim \ell^2(\Delta T/T)^2\rho_o v^3 M^3$ exceeds that from a Reynolds stress quadrupole

by a factor of order $(\Delta T/T)^2/M^2$. Thus, "entropy noise" may be an important component of the noise of a hot gas jet at very low Mach numbers [5].

The final term on the right of (2.1.11) is a monopole whose strength is determined by the difference between the adiabatic compressibilities ($K_s = 1/\rho c^2$) in the source region and in the ambient medium. In an ideal gas $K_s = 1/\gamma p$, so that this source is generally small, although it may be significant during the turbulent mixing of gases with different values of the specific heat ratios γ. It can be very important in multiphase flows where, for example, the presence of small air bubbles in water often leads to an immense increase in the turbulence generated noise [6].

§2.2. Integral representation of aerodynamic sound

Most practical problems of sound generation by flow involve moving boundaries, moving sources interacting with boundaries, or turbulence in shear layers separating a quiescent medium from a high speed flow. To apply Lighthill's equation in these circumstances **control surfaces** S are introduced. These may coincide with the surface of a moving solid, or mark a convenient interface between fluid regions of widely differing mean properties. A solution is then sought by imposing boundary conditions on S, either by first performing subsidiary calculations to determine the pressure or velocity on S or, when S coincides with the surface of a solid, by application of suitable impedance conditions.

Let $f(\mathbf{x},t)$ be an indicator function that vanishes on S and satisfies $f(\mathbf{x},t) > 0$ in the fluid where Lighthill's equation is to be solved, and $f(\mathbf{x},t) < 0$ elsewhere, and set

$$p'_{ij} = (p - p_o)\delta_{ij} - \sigma_{ij}. \tag{2.2.1}$$

Multiply the momentum equation (2.1.1) by the Heaviside step function $\mathrm{H}(f)$ and rearrange into the form

$$\frac{\partial}{\partial t}\left(\rho v_i \mathrm{H}(f)\right) + \frac{\partial}{\partial x_i}\left(\rho v_i \mathrm{H}(f) c_o^2(\rho - \rho_o)\right) = -\frac{\partial}{\partial x_j}\left(\mathrm{H}(f) T_{ij}\right) + \left(\rho v_i(v_j - \bar{v}_j) + p'_{ij}\right)\frac{\partial \mathrm{H}}{\partial x_j}(f)\ ,$$

where $\bar{\mathbf{v}}$ is the velocity of S (so that $\partial \mathrm{H}(f)/\partial t = -\bar{v}_j \partial \mathrm{H}(f)/\partial x_j$), and ρ_o, c_o are the mean density and sound speed in $f > 0$. To simplify the notation we shall henceforth write H instead of $\mathrm{H}(f)$ when there is no danger of confusion. The same procedure applied to the equation of continuity, supplies

$$\frac{\partial}{\partial t}\left(\mathrm{H}(\rho - \rho_o)\right) + \frac{\partial}{\partial x_i}\left(\mathrm{H}\rho v_i\right) = \left(\rho(v_i - \bar{v}_i) + \rho_o \bar{v}_i\right)\frac{\partial \mathrm{H}}{\partial x_i}.$$

The elimination of $\mathrm{H}\rho v_i$ between these two equations yields the differential *Ffowcs Williams - Hawkings equation*

$$\left(\frac{1}{c_o^2}\frac{\partial^2}{\partial t^2} - \nabla^2\right)[\mathrm{H}c_o^2(\rho-\rho_o)] = \frac{\partial^2(\mathrm{H}T_{ij})}{\partial x_i \partial x_j} - \frac{\partial}{\partial x_i}\left([\rho v_i(v_j-\bar{v}_j)+p'_{ij}]\frac{\partial \mathrm{H}}{\partial x_j}\right) + \frac{\partial}{\partial t}\left([\rho(v_j-\bar{v}_j)+\rho_o\bar{v}_j]\frac{\partial \mathrm{H}}{\partial x_j}\right). \quad (2.2.2)$$

This equation is valid throughout the whole of space. By using the free space Green's function

$$G(\mathbf{x},\mathbf{y},t-\tau) = \frac{1}{4\pi|\mathbf{x}-\mathbf{y}|}\delta(t-\tau-|\mathbf{x}-\mathbf{y}|/c_o) \quad (2.2.3)$$

to write down the formal, outgoing wave solution, it is transformed into an integral equation known as the

Ffowcs Williams - Hawkings equation [7]

$$\mathrm{H}c_o^2(\rho-\rho_o) = \frac{\partial^2}{\partial x_i \partial x_j}\int_{\mathrm{V}(\tau)}\left[T_{ij}\right]\frac{d^3\mathbf{y}}{4\pi|\mathbf{x}-\mathbf{y}|} - \frac{\partial}{\partial x_i}\oint_{\mathrm{S}(\tau)}\left[\rho v_i(v_j-\bar{v}_j)+p'_{ij}\right]\frac{d\mathrm{S}_j(\mathbf{y})}{4\pi|\mathbf{x}-\mathbf{y}|} + \frac{\partial}{\partial t}\oint_{\mathrm{S}(\tau)}\left[\rho(v_j-\bar{v}_j)+\rho_o\bar{v}_j\right]\frac{d\mathrm{S}_j(\mathbf{y})}{4\pi|\mathbf{x}-\mathbf{y}|}, \quad (2.2.4)$$

where quantities in the square braces [ ] are evaluated at the retarded time $\tau = t-|\mathbf{x}-\mathbf{y}|/c_o$, the surface integrals are over the retarded surface $\mathrm{S}(\tau)$ defined by $f(\mathbf{y},\tau)=0$, with the surface element $d\mathbf{S}$ directed into the region $\mathrm{V}(\tau)$ where $f>0$.

If the control surface is stationary ($\bar{\mathbf{v}}=0$), S is defined by $f(\mathbf{y},t)\equiv f(\mathbf{y})=0$, and (2.2.4) reduces to

Curle's equation [8]

$$\mathrm{H}c_o^2(\rho-\rho_o) = \frac{\partial^2}{\partial x_i \partial x_j}\int_{\mathrm{V}}\left[T_{ij}\right]\frac{d^3\mathbf{y}}{4\pi|\mathbf{x}-\mathbf{y}|} - \frac{\partial}{\partial x_i}\oint_{\mathrm{S}}\left[\rho v_i v_j + p'_{ij}\right]\frac{d\mathrm{S}_j(\mathbf{y})}{4\pi|\mathbf{x}-\mathbf{y}|} + \frac{\partial}{\partial t}\oint_{\mathrm{S}}\left[\rho v_j\right]\frac{d\mathrm{S}_j(\mathbf{y})}{4\pi|\mathbf{x}-\mathbf{y}|}, \quad (2.2.5)$$

which is a generalization of Kirchhoff's formula of linear acoustics. When S is stationary and *rigid*, this simplifies to

$$\mathrm{H}c_o^2(\rho-\rho_o) = \frac{\partial^2}{\partial x_i \partial x_j}\int_{\mathrm{V}}\left[T_{ij}\right]\frac{d^3\mathbf{y}}{4\pi|\mathbf{x}-\mathbf{y}|} - \frac{\partial}{\partial x_i}\oint_{\mathrm{S}}\left[p'_{ij}\right]\frac{d\mathrm{S}_j(\mathbf{y})}{4\pi|\mathbf{x}-\mathbf{y}|}. \quad (2.2.6)$$

The surface integrals in these formulae may be interpreted as distributions of monopole or dipole sources. They are associated with mass and momentum transfer across S, but their

values cannot normally be specified independently. Indeed, because the acoustic power is usually a mere fraction of the total power, small errors made in prescribing the surface terms can seriously impair the accuracy of predictions of the flow-generated sound.

§2.3. Theory of vortex sound

The rôle of vorticity in Lighthill's theory. At low Mach numbers the velocity defining the Reynolds stress quadrupole in Lighthill's equation can be determined by regarding the source flow as incompressible, and using the Biot-Savart law [9] to express $\mathbf{v}$ in terms of the vorticity. This suggests the existence of a fundamental relation between the sound waves, which diverge from the source region and transport energy to the whole of space, and the vorticity, which is confined by Kelvin's theorem [9] to a finite domain where most of its kinetic energy is ultimately dissipated by the action of viscosity.

Consider an acoustically compact, homentropic vorticity distribution $\boldsymbol{\omega}$ of scale ℓ centered on the coordinate origin in a medium of density ρ_o and sound speed c_o. The velocity $\mathbf{v} = \mathbf{u} + \nabla\varphi$, where $\mathbf{u}$ is defined in terms of the vorticity $\boldsymbol{\omega}$ by the Biot-Savart formula

$$\mathbf{u}(\mathbf{x},t) = \operatorname{curl} \int \frac{\boldsymbol{\omega}(\mathbf{y},t)d^3\mathbf{y}}{4\pi|\mathbf{x}-\mathbf{y}|}, \tag{2.3.1}$$

which is a purely kinematic relation between $\boldsymbol{\omega}$ and a velocity $\mathbf{u}$ that vanishes at infinity. Since $\int \boldsymbol{\omega}(\mathbf{x},t)\, d^3\mathbf{x} \equiv \mathbf{0}$, it follows that $u \sim O(1/|\mathbf{x}|^3)$ as $|\mathbf{x}| \to \infty$. Also div $\mathbf{u} = 0$, so that the value of φ is determined by the compressibility of the fluid. In the source region $p - p_o \sim \rho_o u^2$, and the characteristic time of the source flow $\sim \ell/u$. Thus, $Dp/Dt \sim \rho_o u^3/\ell$, and the continuity equation $\nabla^2\varphi + D\rho/\rho Dt \approx \nabla^2\varphi + (1/\rho_o c_o^2)Dp/Dt = 0$ implies that

$$\nabla\varphi = O(uM^2), \quad M = u/c_o \text{ for } |\mathbf{x}| \sim \ell. \tag{2.3.2}$$

We can use the identity

$$\partial^2(u_iu_j)/\partial x_i\partial x_j = \operatorname{div}(\boldsymbol{\omega}\wedge\mathbf{u}) + \nabla^2\left(u^2/2\right) \tag{2.3.3}$$

to express the solution (2.1.8) of Lighthill's equation in the form

$$p(\mathbf{x},t) = p_1(\mathbf{x},t) + p_2(\mathbf{x},t),$$

$$p_1(\mathbf{x},t) = \frac{-\rho_o x_i}{4\pi c_o|\mathbf{x}|^2}\frac{\partial}{\partial t}\int\left[(\boldsymbol{\omega}\wedge\mathbf{u})_i\right]d^3\mathbf{y}, \quad p_2(\mathbf{x},t) = \frac{\rho_o}{4\pi c_o|\mathbf{x}|}\frac{\partial^2}{\partial t^2}\int\left[\frac{1}{2}u^2\right]d^3\mathbf{y}, \quad |\mathbf{x}| \to \infty, \tag{2.3.4}$$

where [ ] denotes evaluation at time $t - |\mathbf{x}-\mathbf{y}|/c_o \approx t - |\mathbf{x}|/c_o + \mathbf{x}.\mathbf{y}/c_o|\mathbf{x}|$. When retarded time variations across the source region are neglected the identity (2.3.3) and the divergence theorem imply that $\int[\boldsymbol{\omega}\wedge\mathbf{u}]d^3\mathbf{y} \equiv \mathbf{0}$, since $u \sim O(1/|\mathbf{y}|^3)$ as $|\mathbf{y}| \to \infty$. To estimate the value of the first integral in (2.3.4) it is therefore necessary to expand $(\boldsymbol{\omega}\wedge\mathbf{u})(t-|\mathbf{x}-\mathbf{y}|/c_o)$ in powers of the retarded time element $\mathbf{x}.\mathbf{y}/c_o|\mathbf{x}|$. The first term in the expansion yields,

$$p_1(\mathbf{x},t) \approx \frac{-\rho_o x_i x_j}{4\pi c_o^2|\mathbf{x}|^3}\frac{\partial^2}{\partial t^2}\int y_i(\boldsymbol{\omega}\wedge\mathbf{u})_j(t-|\mathbf{x}|/c_o)\,d^3\mathbf{y} \;\sim\; O(\ell/|\mathbf{x}|)\rho_o u^2 M^2 \tag{2.3.5}$$

where $\partial/\partial t \sim u/\ell$.

The order of magnitude of $p_2(\mathbf{x},t)$ is estimated by first writing the momentum equation in the form,

$$\partial\mathbf{u}/\partial t + \nabla\left(\int dp/\rho + v^2/2 + \partial\varphi/\partial t\right) = -\boldsymbol{\omega}\wedge\mathbf{u} - \boldsymbol{\omega}\wedge\nabla\varphi.$$

Take the scalar product with $\mathbf{u}$

$$\partial(\tfrac{1}{2}u^2)/\partial t + \operatorname{div}\left(\mathbf{u}(\textstyle\int dp/\rho + \frac{1}{2}v^2 + \partial\varphi/\partial t)\right) = -\mathbf{u}.\boldsymbol{\omega}\wedge\nabla\varphi,$$

and integrate over the whole of space. The contribution from the divergence vanishes because $\mathbf{u}(\int dp/\rho + \frac{1}{2}v^2 + \partial\varphi/\partial t)$ tends to zero at least as fast as $1/|\mathbf{y}|^3$ as $|\mathbf{y}| \to \infty$. Hence, using (2.3.2)

$$\frac{\partial}{\partial t}\int \frac{1}{2}u^2(\mathbf{y},t)d^3\mathbf{y} = -\int(\mathbf{u}.\boldsymbol{\omega}\wedge\nabla\varphi)(\mathbf{y},t)d^3\mathbf{y} \sim \ell^2u^3M^2, \tag{2.3.6}$$

where the final estimate is really a crude upper bound, that takes no account of the details of the interactions between the vorticity and irrotational velocity.

Thus,

$$p_2(\mathbf{x},t) \sim O\left((\ell/|\mathbf{x}|)\rho_o u^2 M^4\right),$$

and by comparison with (2.3.5) we see that $p_2 \sim O(M^2)p_1 \ll p_1$ when $M \ll 1$. The component $\operatorname{div}(\rho_o\boldsymbol{\omega}\wedge\mathbf{v})$ of $\partial^2(\rho_o v_i v_j)/\partial x_i\partial x_j$ is therefore the principal source of sound at low Mach numbers [10, 11]. This is consistent with Lighthill's hypothesis that the back-reaction of the sound on the flow is negligible, because (2.3.6) states that the rate of change of the kinetic energy of the source flow due to compressible effects is at most of order $\rho_o u^3M^2/\ell$ per unit volume, which is much smaller than the power $\rho_o u^3/\ell$ needed to maintain the flow.

Acoustic analogy in terms of the total enthalpy. This analysis and the discussion at the end of §2.1 show that the dominant aeroacoustic sources at low Mach numbers are vorticity and entropy fluctuations. In order to cast Lighthill's equation in a form that emphasizes vorticity and entropy as the sound sources, it is necessary to select the *total enthalpy* $B =$

$w+\frac{1}{2}v^2$ an the independent acoustic variable (w being the specific enthalpy). This reduces to -$\partial\varphi/\partial t$ in irrotational regions, where φ is the velocity potential of the unsteady motion. B is therefore constant in steady irrotational flow, and far from the acoustic sources perturbations in $B = -\partial\varphi/\partial t$ represent acoustic waves.

To reformulate Lighthill's equation in terms of B for a *homogeneous* fluid, whose chemical composition is the same everywhere, we start from Crocco's form of the momentum equation [9]

$$\partial \mathbf{v}/\partial t + \nabla B = -\boldsymbol{\omega} \wedge \mathbf{v} + T\nabla s + \boldsymbol{\sigma} \tag{2.3.7}$$

$$\sigma_i = (1/\rho)\partial\sigma_{ij}/\partial x_j, \tag{2.3.8}$$

and re-arrange the continuity equation (2.1.4) to read

$$\frac{1}{\rho c^2}\frac{Dp}{Dt} + \operatorname{div}\mathbf{v} = \frac{\hat{\beta}T}{c_p}\frac{Ds}{Dt}, \tag{2.3.9}$$

where $D\rho/Dt$ has been eliminated by means of the thermodynamic relations

$$d\rho = \frac{dp}{c^2} + \left(\frac{\partial\rho}{\partial s}\right)_p ds \quad \text{and} \quad \left(\frac{\partial\rho}{\partial s}\right)_p = \left(\frac{\partial\rho}{\partial T}\right)_p \left(\frac{\partial T}{\partial s}\right)_p \equiv \frac{-\hat{\beta}\rho T}{c_p},$$

$\hat{\beta}$ and c_p being respectively the coefficient of expansion and the specific heat at constant pressure. For an ideal gas $\hat{\beta} = 1/T$.

Subtract the divergence of (2.3.7) from the time derivative of (2.3.9):

$$\frac{\partial}{\partial t}\left(\frac{1}{\rho c^2}\frac{Dp}{Dt}\right) - \nabla^2 B = \operatorname{div}(\boldsymbol{\omega} \wedge \mathbf{v} - T\nabla s - \boldsymbol{\sigma}) + \frac{\partial}{\partial t}\left(\frac{\hat{\beta}T}{c_p}\frac{Ds}{Dt}\right). \tag{2.3.10}$$

This equation is already in a form that strongly suggests that the terms on the right hand side constitute the most important sources of flow generated sound, because they are unchanged when the compressibility $\mathrm{K}_s = 1/\rho c^2 \to 0$, and accordingly dominate the hydrodynamic far field of B which must ultimately match the outgoing sound waves.

The first term on the left of (2.3.10) is expanded as follows:

$$\frac{\partial}{\partial t}\left(\frac{1}{\rho c^2}\frac{Dp}{Dt}\right) = \frac{D}{Dt}\left(\frac{1}{\rho c^2}\frac{\partial p}{\partial t}\right) + \frac{1}{\rho c^2}\frac{\partial v_j}{\partial t}\frac{\partial p}{\partial x_j} + v_j\left\{\frac{\partial}{\partial t}\left(\frac{1}{\rho c^2}\right)\frac{\partial p}{\partial x_j} - \frac{\partial}{\partial x_j}\left(\frac{1}{\rho c^2}\right)\frac{\partial p}{\partial t}\right\}. \tag{2.3.11}$$

The last term on the right will be discarded. It vanishes when the adiabatic compressibility $\mathrm{K}_s = 1/\rho c^2$ is a function of the pressure alone, i.e., when the motion is homentropic, or in

the particular case of an ideal gas where $K_s = 1/\gamma p$ and $\gamma = c_p/c_v$ = constant. Variations of γ in a real gas are significant only in the presence of large temperature gradients; problems of this kind are best treated separately. In liquids the compressibility may be regarded as constant; acoustic sources involving variations of K_s are important only when gas bubbles are present. The other terms on the right of (2.3.11) are transformed as follows. First:

$$\frac{1}{\rho}\frac{\partial p}{\partial t} = \frac{1}{\rho}\frac{Dp}{Dt} - \frac{1}{\rho}\mathbf{v}.\nabla p = \frac{DB}{Dt} - T\frac{Ds}{Dt} - \mathbf{v}.\boldsymbol{\sigma}, \tag{2.3.12}$$

where the thermodynamic identity $dw = Tds + dp/\rho$ and the momentum equation have been used, and second, from (2.3.7),

$$\frac{\partial v_j}{\partial t}\frac{\partial p}{\partial x_j} = -\nabla p.\left(\nabla B + \boldsymbol{\omega}\wedge\mathbf{v} - T\nabla s - \boldsymbol{\sigma}\right). \tag{2.3.13}$$

Thus, substituting from (2.3.11) into (2.3.10), we arrive at the acoustic analogy equation for the total enthalpy

$$\left(\frac{D}{Dt}\left(\frac{1}{c^2}\frac{D}{Dt}\right) - \frac{\nabla p.\nabla}{\rho c^2} - \nabla^2\right)B = \left(\frac{\partial}{\partial \mathbf{x}} + \frac{\nabla p}{\rho c^2}\right).(\boldsymbol{\omega}\wedge\mathbf{v} - T\nabla s - \boldsymbol{\sigma}) + \frac{\partial}{\partial t}\left(\frac{\hat{\beta}T}{c_p}\frac{Ds}{Dt}\right)$$
$$+\frac{D}{Dt}\left\{\frac{1}{c^2}\left(T\frac{Ds}{Dt} + \mathbf{v}.\boldsymbol{\sigma}\right)\right\}. \tag{2.3.14}$$

Vorticity and entropy sources. The operator on the left of this equation is nonlinear. All terms on the right hand side vanish in irrotational regions, and in the absence of such terms and of boundary motions, B = constant. The radiation condition ensures that the terms on the right may be identified as acoustic sources. They are confined to the region in which $\boldsymbol{\omega} \neq \mathbf{0}$ and where $\nabla s \neq \mathbf{0}$. The wave operator describes propagation of the sound through the non-uniform flow although, as for Lighthill's equation, it will not usually be permissible to neglect the interaction of the aerodynamically generated sound with the vorticity and entropy gradients when the source flow is very extensive. The following special cases should be noted:

High Reynolds number, homentropic flow: When dissipation is neglected and s = constant (2.3.14) becomes

$$\left(\frac{D}{Dt}\left(\frac{1}{c^2}\frac{D}{Dt}\right) - \frac{1}{\rho}\nabla.(\rho\nabla)\right)B = \frac{1}{\rho}\mathrm{div}(\rho\boldsymbol{\omega}\wedge\mathbf{v}). \tag{2.3.15}$$

At the low Mach numbers relevant in underwater applications, when the flow may be assumed to be at rest at infinity (where $\rho = \rho_o$ and $c = c_o$) further simplification is possible by (a)

neglecting nonlinear effects of propagation and the scattering of sound by the vorticity, and (b) taking $c = c_o$, and $\rho = \rho_o$. Then

$$\left(\frac{1}{c_o^2}\frac{\partial^2}{\partial t^2} - \nabla^2\right) B = \text{div}(\boldsymbol{\omega} \wedge \mathbf{v}), \tag{2.3.16}$$

and in the far field the acoustic pressure is given by the linearized approximation

$$p(\mathbf{x}, t) \approx \rho_o B(\mathbf{x}, t). \tag{2.3.17}$$

Non-homentropic source flow: When the source region is not homentropic, it is important to distinguish between terms on both sides of (2.3.14) that account principally for *scattering* of the sound, and those (on the right) that can unequivocally be recognized as sources. For compact sources we can argue that the correct source terms are those remaining when the fluid is temporarily taken to be *incompressible*. These are the sources on the right of (2.3.10). When dissipation is ignored, (2.3.14) then reduces to

$$\left\{\left(\frac{\partial}{\partial t} + \mathbf{U}.\nabla\right)\left[\frac{1}{c^2}\left(\frac{\partial}{\partial t} + \mathbf{U}.\nabla\right)\right] - \frac{1}{\rho}\nabla.(\rho\nabla)\right\} B = \text{div}(\boldsymbol{\omega} \wedge \mathbf{v} - T\nabla s) + \frac{\partial}{\partial t}\left(\frac{\hat{\beta}T}{c_p}\frac{Ds}{Dt}\right). \tag{2.3.18}$$

This approximation is useful when the background mean flow may be regarded as irrotational (steady flow past a streamlined body, for example) at mean velocity $\mathbf{U}(\mathbf{x})$ and density and sound speed $\rho(\mathbf{x})$ and $c(\mathbf{x})$. At very small Mach numbers it simplifies further to

$$\left(\frac{1}{c_o^2}\frac{\partial^2}{\partial t^2} - \nabla^2\right) B = \text{div}(\boldsymbol{\omega} \wedge \mathbf{v} - T\nabla s) + \frac{\partial}{\partial t}\left(\frac{\hat{\beta}T}{c_p}\frac{Ds}{Dt}\right). \tag{2.3.19}$$

The final entropy source on the right of (2.3.18) and (2.3.19) represents the production of sound by unsteady *heating* of the fluid. According to the equation of continuity (2.3.9) this source is equivalent to a volume monopole of strength,

$$q(\mathbf{x}, t) = \frac{\hat{\beta}T}{c_p}\frac{Ds}{Dt}. \tag{2.3.20}$$

§2.4. Compact Green's Function

The compact Green's function provides a formal and intuitive procedure for calculating the leading order monopole and dipole terms in the multipole expansion of the sound produced by sources near a solid body.

Green's function is the *causal* solution of the wave equation

$$\left(\frac{1}{c_o^2}\frac{\partial^2}{\partial t^2} - \nabla^2\right) G(\mathbf{x}, \mathbf{y}, t - \tau) = \delta(\mathbf{x} - \mathbf{y})\delta(t - \tau), \quad G(\mathbf{x}, \mathbf{y}, t - \tau) = 0 \text{ for } t < \tau; \tag{2.4.1}$$

the time-harmonic (*frequency domain*) Green's function satisfies

$$\left(\nabla^2 + \kappa_o^2\right) G(\mathbf{x}, \mathbf{y}; \omega) = \delta(\mathbf{x} - \mathbf{y}), \quad \kappa_o = \omega/c_o. \tag{2.4.2}$$

For the time harmonic case all quantities vary in proportion to $e^{-i\omega t}$, and $G(\mathbf{x},\mathbf{y};\omega)$ has *outgoing* wave behavior. The frequency and time domain Green's functions are related by

$$G(\mathbf{x},\mathbf{y},t-\tau) = \frac{-1}{2\pi}\int_{-\infty}^{\infty} G(\mathbf{x},\mathbf{y};\omega)e^{-i\omega(t-\tau)}\,d\omega, \tag{2.4.3}$$

where the path of integration in the ω-plane runs *above* all singularities of $G(\mathbf{x},\mathbf{y};\omega)$.

The time-harmonic Green's function satisfies the reciprocal property [12]

$$G(\mathbf{x},\mathbf{y};\omega) = G(\mathbf{y},\mathbf{x};\omega). \tag{2.4.4}$$

Time-harmonic problems. Consider the Green's function $G(\mathbf{x},\mathbf{y};\omega)$ in the presence of an acoustically compact body of diameter ℓ in the particular case in which the source point $\mathbf{y}$ is close to S and the observer at $\mathbf{x}$ is in the *acoustic far field.* Let G have *vanishing normal derivative* on S. The compactness condition implies that $\kappa_o\ell \ll 1$.

Formula (2.4.4) enables the problem of determining $G(\mathbf{x},\mathbf{y};\omega)$ to be posed as a *reciprocal* scattering problem in which the spherical wave

$$G_o(\mathbf{y},\mathbf{x};\omega) = \frac{-e^{i\kappa_o|\mathbf{x}-\mathbf{y}|}}{4\pi|\mathbf{x}-\mathbf{y}|} \tag{2.4.5}$$

generated by a point source $\delta(\mathbf{x}-\mathbf{y})$ at the far field point $\mathbf{x}$ is incident on S, and $G(\mathbf{x},\mathbf{y};\omega)$ is calculated by taking the independent variable in (2.4.2) to be $\mathbf{y}$ rather than $\mathbf{x}$. Then, if the coordinate origin is within S and $\mathbf{y}$ is close to S, the condition $\kappa_o\ell \ll 1$ permits $G(\mathbf{x},\mathbf{y};\omega)$ to be expanded in the form [13 - 15]

$$G(\mathbf{x},\mathbf{y};\omega) = \frac{-e^{i\kappa_o|\mathbf{x}|}}{4\pi|\mathbf{x}|}\left(1 - \frac{i\kappa_o x_i}{|\mathbf{x}|}\big(y_i - \varphi_i^*(\mathbf{y})\big) + \sum_{n\geq 2}(\kappa_o\ell)^n\Phi_n\left(\frac{\mathbf{x}}{|\mathbf{x}|},\mathbf{y}\right)\right),$$

$$\mathbf{y}\sim O(\ell),\ |\mathbf{x}|\to\infty. \tag{2.4.6}$$

The first term in the large braces represents the incident wave (2.4.5) evaluated at $\mathbf{y}=\mathbf{0}$. The next term is $O(\kappa_o\ell)$ and includes a component $-i\kappa_o x_i y_i/|\mathbf{x}|$ from the incident wave plus a correction $-i\kappa_o x_i\varphi_i^*(\mathbf{y})/|\mathbf{x}|$ due to S. To this order of approximation $Y_i(\mathbf{y}) \equiv y_i - \varphi_i^*(\mathbf{y})$ is a solution of Laplace's equation satisfying $\partial Y_i/\partial y_n = 0$ on S. Since $\varphi_i^*(\mathbf{y})$ must decay with distance from S, this implies that φ_i^* is simply the velocity potential of the incompressible motion that would be produced by translational motion of S as a *rigid body* at unit speed in the i-direction. The remaining terms in (2.4.6) are of order $(\kappa_o\ell)^2$ or smaller. When they

are neglected the resulting approximation for G can be used to determine the monopole and dipole terms in the multipole expansion of the solution of a fluid-structure interaction problem.

The potentials φ_i^* are uniquely defined by the shape of the body and satisfy

$$\frac{\partial \varphi_i^*}{\partial y_n}(\mathbf{y}) = n_i \quad \text{on S}, \tag{2.4.7}$$

where $\mathbf{n}$ is the unit normal on S directed into the fluid. When the body is rigid they also determine the *added mass* tensor M_{ij} [9], which is symmetric and given by

$$\mathrm{M}_{ij} = -\rho_o \oint_{\mathrm{S}} \varphi_i^*(\mathbf{y}) n_j d\mathrm{S}(\mathbf{y}) = -\rho_o \oint_{\mathrm{S}} \varphi_i^* \partial \varphi_j^* / \partial y_n d\mathrm{S}(\mathbf{y}) \equiv -\rho_o \oint_{\mathrm{S}} \varphi_j^* \partial \varphi_i^* / \partial y_n d\mathrm{S}(\mathbf{y}) \tag{2.4.8}$$

A body in translational accelerated motion at velocity $\mathbf{U}(t)$ in an ideal, incompressible fluid experiences a reaction force from the fluid equal to $-\partial(\mathrm{M}_{ij}U_j)/\partial t$ in the i-direction [9]. An external force F_i acting through the center of mass of a body of mass m therefore produces accelerated motion determined by $\partial(mU_i + \mathrm{M}_{\mathrm{ij}}U_j)/\partial t = F_i$.

Time-domain problems. The general solution of the inhomogeneous wave equation

$$\left(\frac{1}{c_o^2}\frac{\partial^2}{\partial t^2} - \nabla^2\right) p(\mathbf{x}, t) = \mathcal{F}(\mathbf{x}, t), \tag{2.4.9}$$

in the region *outside* a stationary surface S can be written

$$\begin{aligned} p(\mathbf{x}, t) \;=\; & \oint_{\mathrm{S}} \left\{ p(\mathbf{y}, \tau) \frac{\partial G}{\partial y_j}(\mathbf{x}, \mathbf{y}, t-\tau) + \rho_o \frac{\partial v_j}{\partial \tau}(\mathbf{y}, \tau) G(\mathbf{x}, \mathbf{y}, t-\tau) \right\} n_j d\mathrm{S}(\mathbf{y}) d\tau \\ & + \int G(\mathbf{x}, \mathbf{y}, t-\tau) \mathcal{F}(\mathbf{y}, \tau) d^3\mathbf{y} d\tau, \end{aligned} \tag{2.4.10}$$

When S is *rigid* we choose Green's function to have vanishing normal derivative on S. Then, using the expansion (2.4.5) to calculate $G(\mathbf{x}, \mathbf{y}, t-\tau)$ from (2.4.3), we find

$$\begin{aligned} p(\mathbf{x}, t) \;\approx\; & \frac{1}{4\pi|\mathbf{x}|}\Big(\int \mathcal{F}(\mathbf{y}, t - |\mathbf{x}|/c_o) d^3\mathbf{y} + \frac{x_i}{c_o|\mathbf{x}|}\frac{\partial}{\partial t} \int Y_i(\mathbf{y}) \mathcal{F}(\mathbf{y}, t - |\mathbf{x}|/c_o) d^3\mathbf{y} \\ & + \sum_{n \geq 2} \frac{(i\ell)^n}{c_o^n} \frac{\partial^n}{\partial t^n} \int \Phi_n(\mathbf{x}/|\mathbf{x}|, \mathbf{y}) \mathcal{F}(\mathbf{y}, t - |\mathbf{x}|/c_o) d^3\mathbf{y} \Big), \quad |\mathbf{x}| \to \infty. \end{aligned} \tag{2.4.11}$$

The term of order n in the series $\sim \mathrm{O}((\omega\ell/c_o)^n)$. When the body is compact, so that $\omega\ell/c_o \ll 1$, it is usually sufficient to retain only the first two terms in the large brackets, the

monopole and dipole. This is equivalent to approximating Green's function by

$$\begin{aligned} G(\mathbf{x},\mathbf{y},t-\tau) &\approx \frac{1}{4\pi|\mathbf{x}|}\left(\delta(t-\tau-|\mathbf{x}|/c_o)+\frac{\mathbf{x}.\mathbf{Y}}{c_o|\mathbf{x}|}\delta'(t-\tau-|\mathbf{x}|/c_o)\right) \\ &\approx \frac{1}{4\pi|\mathbf{x}|}\delta\big(t-\tau-(|\mathbf{x}|-\mathbf{x}.\mathbf{Y}/|\mathbf{x}|)/c_o\big) \\ &\approx \frac{1}{4\pi\,|\mathbf{x}-\mathbf{Y}|}\delta\big(t-\tau-|\mathbf{x}-\mathbf{Y}|/c_o\big), \quad |\mathbf{x}|\to\infty. \end{aligned} \tag{2.4.12}$$

This result can be made symmetric, in accordance with reciprocity, by replacing $\mathbf{x}$ by $\mathbf{X}\equiv\mathbf{x}-\boldsymbol{\varphi}^*(\mathbf{x})$, after which we define the

Compact Green's function for a body bounded by a surface S:

$$G(\mathbf{x},\mathbf{y},t-\tau)=\frac{1}{4\pi\,|\mathbf{X}-\mathbf{Y}|}\delta\big(t-\tau-|\mathbf{X}-\mathbf{Y}|/c_o\big), \tag{2.4.13}$$

where $X_i=x_i-\varphi_i^*(\mathbf{x})$, $Y_i=y_i-\varphi_i^*(\mathbf{y})$, and φ_i^* is the velocity potential of the incompressible flow that would be produced by rigid body motion of S at unit speed in the i-direction, so that $\partial G(\mathbf{x},\mathbf{y},t-\tau)/\partial x_n=\partial G(\mathbf{x},\mathbf{y},t-\tau)/\partial y_n=0$ on S.

In the frequency domain the corresponding approximation is

$$G(\mathbf{x},\mathbf{y};\omega)=\frac{-e^{i\kappa_o|\mathbf{X}-\mathbf{Y}|}}{4\pi|\mathbf{X}-\mathbf{Y}|}. \tag{2.4.14}$$

Note that, because of the symmetrical manner in which $\mathbf{x}$ and $\mathbf{y}$ occur in (2.4.13) and (2.4.14), the location of the coordinate origin is now arbitrary. However, it is still necessary that *either* $\mathbf{x}$ or $\mathbf{y}$ should lie in the far field of the body. When *both* $\mathbf{x}$ and $\mathbf{y}$ are in the far field predictions made with the compact Green's function will be the same as when the body is *absent*. This is because, for distant sources the amplitude of the sound scattered by a compact rigid object is $O((\kappa_o\ell)^2)$ smaller than the incident sound, i.e., is of *quadrupole* intensity [12].

§2.5. Surface force exerted by a rigid body

Force exerted on an incompressible fluid. At low Mach numbers the sound generated by turbulent flow interacting with a compact body depends on the surface forces calculated as if the fluid is incompressible (see §2.6). The force $\mathbf{F}(t)$ exerted on the fluid by a solid in rigid body motion at velocity

$$\mathbf{U} = \mathbf{U}_o + \boldsymbol{\Omega} \wedge (\mathbf{x} - \mathbf{x}_o(t)),$$

where $\mathbf{U}_o = d\mathbf{x}_o/dt$ is the velocity of its center of volume $\mathbf{x}_o(t)$, and $\boldsymbol{\Omega}(t)$ is its angular velocity (Figure 2.1), is given by the following general formula in terms of $\mathbf{U}_o$ and $\boldsymbol{\omega}$ [16]

$$\mathbf{F}(t) = \frac{1}{2}\frac{d}{dt}\int_{\mathrm{V}} \rho_o \mathbf{x} \wedge \boldsymbol{\omega} d^3\mathbf{x} - m_o \frac{d\mathbf{U}_o}{dt}, \tag{2.5.1}$$

where m_o is the mass of the fluid displaced by the body. This equation is applicable for three dimensional bodies. In two dimensions m_o is the mass displaced per unit span and the factor of $\frac{1}{2}$ is omitted.

The integral in (2.5.1) defines the *impulse* of the coupled system [9], which is an invariant of the motion when the body is absent. To evaluate the integral the vorticity must be defined *everywhere* including the region occupied by the body, i.e., vortex lines must be continued into the interior of S to form re-entrant filaments. For a non-rotating body, vortex lines meeting the surface form re-entrant loops by continuation on the surface. The impulse then becomes a function of time because the motion of these vortex lines within and on S is no longer governed by the Navier-Stokes equations. For *irrotational* flow $\boldsymbol{\omega} = \mathbf{0}$ in the fluid, but not on S, where it must be taken as the singular distribution of *bound vorticity* $\boldsymbol{\omega}_o \equiv \mathbf{n} \wedge (\nabla\varphi - \mathbf{U})\delta(f)$, where $f(\mathbf{x}, t) = 0$ defines the surface S moving at velocity $\mathbf{U}$, and φ is the velocity potential of the irrotational flow; inside S we must take $\boldsymbol{\omega} = 2\boldsymbol{\Omega}$.

At high Reynolds numbers, involving the interaction of turbulent flows with S, the surface boundary layers are often very thin, and the exterior fluid motion can frequently be approximated by irrotational flow with a superposed distribution of vorticity. In these circumstances it would be convenient to have an expression for $\mathbf{F}$ that minimizes the contribution from the bound vorticity. Such a formula can be derived for a body in *translational* motion [17 - 19].

To do this, suppose the fluid is at rest at infinity, and write the force in the form

$$F_i = \frac{d}{dt}\int_{\mathrm{V}} \rho_o v_i d^3\mathbf{x} + \oint_{\Sigma} p n_i d\mathrm{S}, \tag{2.5.2}$$

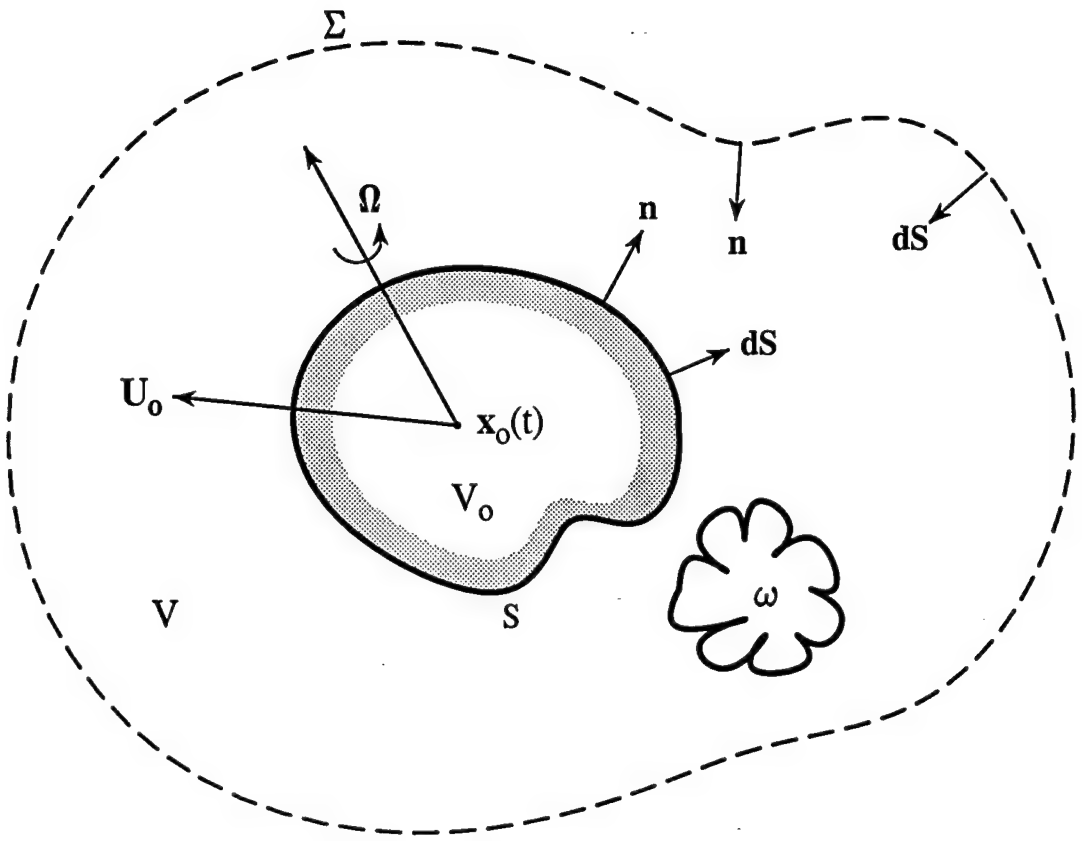

Figure 2.1. Motion of a rigid body in fluid at rest at infinity.

where V here denotes the fluid between S and a large fixed control surface Σ (Figure 2.1) whose normal $\mathbf{n}$ is directed into V. To express the right hand side of this formula in terms of the vorticity and the translational velocity of the body, we first cast the momentum equation for incompressible flow in the form

$$\frac{\partial(\rho_o \mathbf{v})}{\partial t} + \nabla\left(p + \frac{1}{2}\rho_o v^2\right) = -\rho_o \boldsymbol{\omega} \wedge \mathbf{v} - \eta \operatorname{curl} \boldsymbol{\omega}. \tag{2.5.3}$$

The scalar product of this equation with $\nabla X_i(\mathbf{x},t) = \nabla\left(x_i - \varphi_i^*(\mathbf{x},t)\right)$ is then integrated over V. X_i is the function used in §2.4 to define the compact Green's function; it is here dependent on time because of the translation of S. By applying the divergence theorem, the integrated equation can be manipulated to yield an alternative representation of the right hand side of (2.5.1). Using the definition (2.4.8) of the added mass tensor, the following formula is then obtained for the

Force exerted on an incompressible fluid by a body in translational motion

$$F_i = \mathrm{M}_{ij}\frac{dU_j}{dt} - \rho_o \int_{\mathrm{V}} \nabla X_i . \boldsymbol{\omega} \wedge \mathbf{v}_{rel} d^3\mathbf{x} + \eta \oint_{\mathrm{S}} \boldsymbol{\omega} \wedge \nabla X_i . d\mathbf{S}, \tag{2.5.4}$$

where $\mathbf{v}_{rel} = \mathbf{v} - \mathbf{U}$ is the fluid velocity relative to S. Bound vorticity makes no contribution to the volume integral because (i) $\mathbf{v}_{rel} = \mathbf{0}$ on S for viscous flow, or (ii) $\nabla X_i . \boldsymbol{\omega} \wedge \mathbf{v}_{rel} \equiv 0$ on S for an ideal fluid, since ∇X_i, $\boldsymbol{\omega}$ and $\mathbf{v}_{rel}$ are then all locally parallel to the surface.

This formula expresses the force as a sum of three essentially distinct components: (i) the inertia due to the added mass of the body, (ii) the vector sum of the normal stresses induced on S by the vorticity, (iii) the viscous skin friction.

Force exerted by a semi-infinite surface. The unsteady normal force F_2 produced by turbulence near an infinitely long, stationary, rigid strip (Figure 2.2a) of chord $2a$ is given by (2.5.4) by taking

$$X_2 = \mathrm{Re}\left(-i\sqrt{z^2 - a^2}\right), \qquad z = x_1 + ix_2, \tag{2.5.5}$$

where the strip occupies $|x_1| < a$, $x_2 = 0$, $-\infty < x_3 < \infty$.

Consider vorticity confined to the neighborhood of the edge $x_1 = +a$ of the strip within a distance $\sim \ell$ from the edge. When $\ell \ll 2a$, X_2 can be approximated within the vortical region by

$$X_2 \approx \sqrt{2a}\,\varphi^*(\mathbf{x}), \tag{2.5.6}$$

where (Figure 2.2b)

$$\varphi^*(\mathbf{x}) \equiv \sqrt{r}\sin\left(\frac{\theta}{2}\right), \quad x_1 - a = r\cos\theta, \quad x_2 = r\sin\theta. \tag{2.5.7}$$

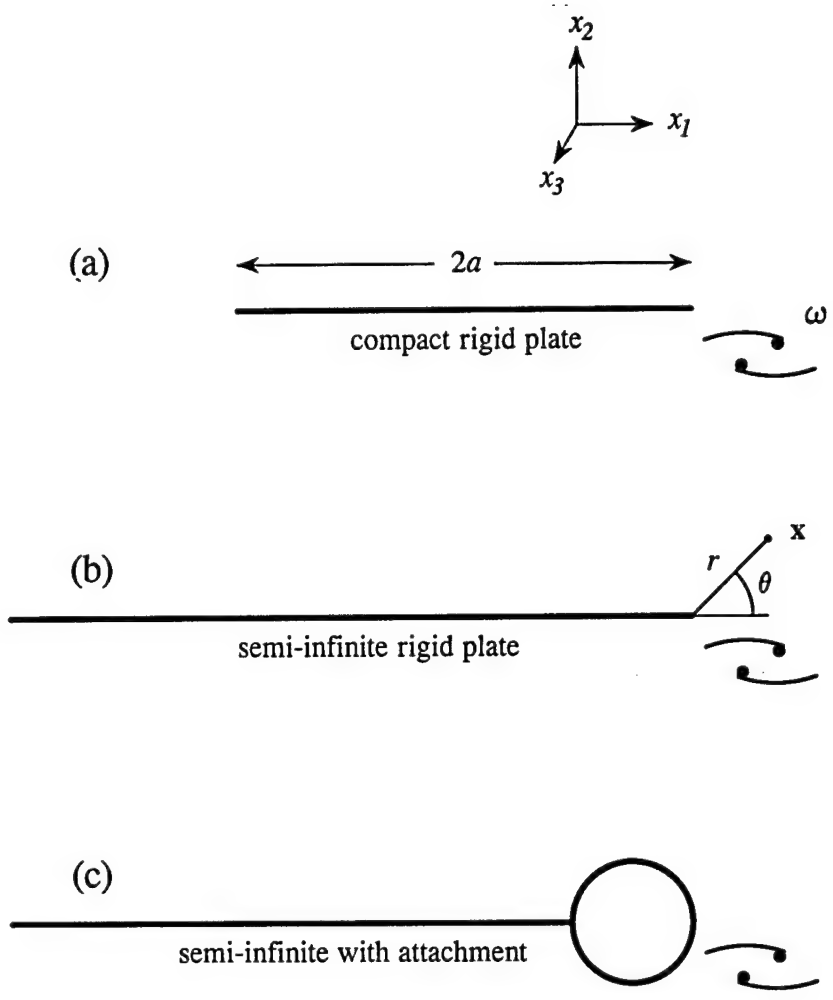

Figure 2.2. Force generated by vortex-edge interaction.

$\varphi^*(\mathbf{x})$ is just the velocity potential of an incompressible flow around the edge ($x_1 = +a$) of a *semi-infinite* rigid half plane extending to $x_1 = -\infty$. The order of magnitude of the surface force is then

$$F_2 = -\sqrt{2a}\int \rho_o(\boldsymbol{\omega}\wedge\mathbf{v})(\mathbf{x},t).\nabla\varphi^*(\mathbf{x})d^3\mathbf{x} \;\sim\; \rho_o v^2\ell^2\sqrt{\frac{a}{\ell}},$$

which is unbounded as $a/\ell \to \infty$.

But in this limit the airfoil chord ultimately becomes non-compact, and it is necessary to take account of compressibility in calculating the surface force, in which case it might be anticipated that the role of the chord length $2a$ in determining the surface force is then played by the characteristic acoustic wavelength of the aerodynamically generated sound. If the edge region occupied by the vorticity is acoustically compact, the force can be calculated by making use of the approximation given below in equation (4.1.4) to Green's function for a rigid halfplane, which yields the:

Frequency domain force

$$F_2(\omega) \approx \frac{2e^{\frac{i\pi}{4}}}{\sqrt{\pi\kappa_o}}\int \rho_o(\boldsymbol{\omega}\wedge\mathbf{v})(\mathbf{x},\omega).\nabla\varphi^*(\mathbf{x})d^3\mathbf{x} \;=\; \frac{\sqrt{2\lambda}e^{\frac{i\pi}{4}}}{\pi}\int \rho_o(\boldsymbol{\omega}\wedge\mathbf{v})(\mathbf{x},\omega).\nabla\varphi^*(\mathbf{x})d^3\mathbf{x}, \tag{2.5.8}$$

where $\lambda = 2\pi/\kappa_o$ is the acoustic wavelength;

Time domain force

$$F_2(t) \approx \frac{2\sqrt{c_o}}{\pi}\int_{-\infty}^{t} d\tau \int \frac{(\boldsymbol{\omega}\wedge\mathbf{v})(\mathbf{x},\tau).\nabla\varphi^*(\mathbf{x})}{\sqrt{t-\tau}}\, d^3\mathbf{x}. \tag{2.5.9}$$

These formulae remain valid when the edge of the half plane supports a rigid, "attachment" (Figure 2.2c) along its span whose cross-section is acoustically compact and whose length scale of variation in the spanwise (x_3) direction is compact. In this case the potential function $\varphi^*(\mathbf{x}) \equiv \varphi^*(x_1,x_2)$ must be replaced by $\Phi^*(\mathbf{x}) \equiv \Phi^*(x_1,x_2,x_3)$ which describes potential flow around the irregular edge, and satisfies

$$\Phi^*(x_1,x_2,x_3) \to \varphi^*(x_1,x_2) \equiv \sqrt{r}\sin\left(\frac{\theta}{2}\right), \quad \text{as } r = \sqrt{(x_1-a)^2+x_2^2} \to \infty.$$

§2.6 Sound generation in the presence of rigid boundaries

The Ffowcs Williams - Hawkings equation (2.2.4) enables the aerodynamic sound to be expressed as the sum of the sound generated by quadrupole sources together with contributions from monopole and dipole sources distributed on boundaries. For turbulent flow near a fixed rigid surface, the direct sound from the quadrupoles T_{ij} is augmented by radiation from surface dipoles whose strength is the force per unit surface area exerted on the fluid. If the surface is in accelerated motion there are additional dipoles and quadrupoles, and neighboring surfaces in relative motion produce "potential flow" interactions that generate sound. At low Mach numbers the acoustic efficiency of the surface dipoles exceeds the efficiency of the volume quadrupoles by a large factor $\sim O(1/M^2)$. Thus, the presence of solid surfaces within low Mach number turbulence can lead to substantial increases in aerodynamic sound levels.

Acoustically compact bodies. Consider the production of sound by turbulence near a compact, stationary rigid body. Let the fluid have uniform mean density ρ_o and sound speed c_o, and assume the Mach number is sufficiently small that convection of the sound by the flow may be neglected. The acoustic pressure in the far field is given by Curle's equation (2.2.5) in the form

$$p(\mathbf{x},t) \approx \frac{x_i x_j}{4\pi c_o^2 |\mathbf{x}|^3} \frac{\partial^2}{\partial t^2} \int \left[\rho_o v_i v_j\right] d^3\mathbf{y} + \frac{x_i}{4\pi c_o |\mathbf{x}|} \frac{\partial}{\partial t} \oint_S \left[n_j p'_{ij}\right] d\mathrm{S}(\mathbf{y}), \quad |\mathbf{x}| \to \infty, \qquad (2.6.1)$$

where the terms in square brackets are evaluated at the retarded time $t - |\mathbf{x}-\mathbf{y}|/c_o$, $p'_{ij} = (p-p_o)\delta_{ij} - \sigma_{ij}$ is the compressive stress tensor and the unit normal $\mathbf{n}$ on S is directed into the fluid. The first term on the right is the quadrupole noise, which has the same formal structure as when the body is absent. The surface integral is the dipole contribution.

In practice the length scale ℓ of the turbulence is comparable to some dimension of the body. The frequency of the hydrodynamic fluctuations $\sim v/\ell$, and the whole motion in the neighborhood of the body is therefore acoustically compact if $(v/\ell)\ell/c_o = v/c_o \ll 1$, i.e., provided the Mach number is small. The retarded time variations on S, which are of order $\mathbf{x}.\mathbf{y}/c_o|\mathbf{x}|$ when $|\mathbf{x}| \to \infty$ may then be neglected so that, with the origin in the neighborhood of the body, the first approximation to the surface integral yields the dipole sound field

$$\frac{x_i}{4\pi c_o |\mathbf{x}|^2} \frac{\partial F_i}{\partial t}(t - |\mathbf{x}|/c_o),$$

where $F_i(t) = \oint_S p'_{ij}(\mathbf{y},t) n_j d\mathrm{S}(\mathbf{y})$ is the net force exerted on the fluid by the rigid body. In this compact approximation the force can be calculated in terms of the vorticity $\boldsymbol{\omega}$ and

the velocity $\mathbf{v}$ from equation (2.5.4) (in which $dU_j/dt \equiv 0$ for a stationary body), and the acoustic pressure cast in the form

$$p(\mathbf{x},t) \approx \frac{-\rho_o x_i}{4\pi c_o|\mathbf{x}|^2}\frac{\partial}{\partial t}\left\{\int[(\boldsymbol{\omega}\wedge\mathbf{v}).\nabla Y_i]\,d^3\mathbf{y} - \nu\oint_S[\boldsymbol{\omega}\wedge\nabla Y_i.\mathbf{n}]\,dS(\mathbf{y})\right\}$$

$$\approx \frac{-\rho_o x_i}{4\pi c_o|\mathbf{x}|^2}\frac{\partial}{\partial t}\int(\boldsymbol{\omega}\wedge\mathbf{v})(\mathbf{y},t-|\mathbf{x}|/c_o).\nabla Y_i(\mathbf{y})d^3\mathbf{y}, \quad |\mathbf{x}|\to\infty, \qquad (2.6.2)$$

where [ ] denotes evaluation at $t-|\mathbf{x}|/c_o$, and $Y_i = y_i - \varphi_i^*(\mathbf{y})$ is the velocity potential of incompressible flow past the body having unit speed in the i-direction at large distances from S (the corresponding contribution to the radiation being equivalent to a dipole orientated in the i-direction). The approximation in the second line is applicable at high Reynolds numbers, $v\ell/\nu \gg 1$, when the "skin friction" contribution to the surface force is negligible.

The order of magnitude of $F \sim \rho_o v^2\ell^2$, and $\partial/\partial t \sim v/\ell$. The dipole generated acoustic pressure is therefore of order $(\ell/|\mathbf{x}|)\rho_o v^2 M$ $(M = v/c_o)$, with corresponding sound power $\Pi_a \sim \ell^2\rho_o v^3 M^3$ and acoustic efficiency $\Pi_a/(\ell^2\rho_o v^3) \sim O(M^3)$. For the direct quadrupole radiation, the acoustic pressure $\sim (\ell/|\mathbf{x}|)\rho_o v^2 M^2$, the same as in the absence of the body, and the efficiency is $\sim O(M^5)$. The radiation is accordingly dominated by the dipole when M is small, and as $M \to 0$ the acoustic power exceeds the quadrupole power by a factor $\sim 1/M^2 \gg 1$. Precisely how small M should be for this to be true depends on the details of the flow.

This increase in acoustic efficiency brought about by surface dipoles on an acoustically compact body occurs also for arbitrary, non-compact bodies when vorticity interacts with compact structural elements, such as edges, corners and protuberances. In the extreme case of a *flat*, rigid surface, whose dimension greatly exceeds the acoustic wavelength, the normal force exerted on an *incompressible* fluid vanishes identically. The integrated contribution from the dipoles is then null unless account is taken of retarded time differences, when their aggregate effect becomes the same as a higher order quadrupole that coincides with the *image* of the turbulence volume quadrupoles in the wall [20]; the overall efficiency is therefore $O(M^5)$, the same as for quadrupoles in free space.

Application of compact Green's functions. These results can also be obtained and extended by making use of the compact Green's function of §2.4. Consider vorticity convected past the body in low Mach number, homentropic mean flow (Figure 2.3).

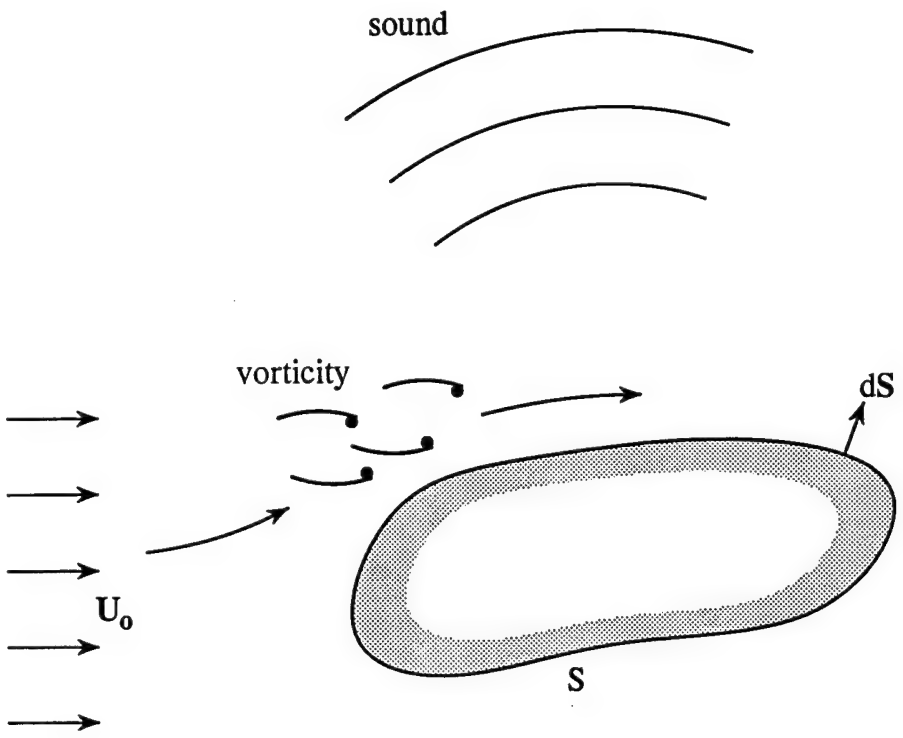

Figure 2.3. Turbulent flow past a stationary, rigid body.

The acoustic radiation will be determined by solving equation (2.3.16). The outgoing wave solution is given by *Kirchhoff's* formula [21]

$$B(\mathbf{x},t) = \oint_S \left\{ B(\mathbf{y},\tau)\frac{\partial G}{\partial y_j}(\mathbf{x},\mathbf{y},t-\tau) - \frac{\partial B}{\partial y_j}(\mathbf{y},\tau)G(\mathbf{x},\mathbf{y},t-\tau) \right\} n_j dS(\mathbf{y})d\tau + \int G(\mathbf{x},\mathbf{y},t-\tau)\Big(\mathrm{div}(\boldsymbol{\omega}\wedge\mathbf{v})(\mathbf{y},\tau)\Big)d^3\mathbf{y}d\tau, \tag{2.6.3}$$

where the retarded time integration with respect to τ is taken over $(-\infty,\infty)$.

The Green's function is chosen to have vanishing normal derivative on S, and the volume integral is transformed by the divergence theorem:

$$\int G\,\mathrm{div}(\boldsymbol{\omega}\wedge\mathbf{v})d^3\mathbf{y} = -\oint_S G(\boldsymbol{\omega}\wedge\mathbf{v})_j n_j dS - \int(\boldsymbol{\omega}\wedge\mathbf{v}).\nabla G d^3\mathbf{y}.$$

When viscous effects on S are assumed to be the same as for an incompressible fluid, Crocco's equation (2.3.7) may be approximated by

$$\partial\mathbf{v}/\partial t + \nabla B = -\boldsymbol{\omega}\wedge\mathbf{v} - \nu\,\mathrm{curl}\,\boldsymbol{\omega}$$

and (2.6.3) becomes

$$B(\mathbf{x},t) \approx -\int(\boldsymbol{\omega}\wedge\mathbf{v})_j(\mathbf{y},\tau)\frac{\partial G}{\partial y_j}(\mathbf{x},\mathbf{y},t-\tau)d^3\mathbf{y}d\tau + \nu\oint_S \boldsymbol{\omega}(\mathbf{y},\tau)\wedge\frac{\partial G}{\partial\mathbf{y}}(\mathbf{x},\mathbf{y},t-\tau).d\mathbf{S}(\mathbf{y})d\tau + \oint_S G(\mathbf{x},\mathbf{y},t-\tau)\frac{\partial v_j}{\partial\tau}(\mathbf{y},\tau)n_j dS(\mathbf{y})d\tau \tag{2.6.4}$$

In the absence of mean flow $B \equiv p/\rho_o$ in the acoustic far field. This remains true in the presence of flow at very low Mach number M_o, since in general the pressure as $|\mathbf{x}|\to\infty$ is calculated from

$$\frac{\partial p}{\partial t} = \rho_o\left(\frac{\partial}{\partial t} + \mathbf{U}_o.\nabla\right)B \quad\Longrightarrow\quad p(\mathbf{x},t) \approx \rho_o B(\mathbf{x},t)\Big(1+\mathrm{O}(M_o)\Big). \tag{2.6.5}$$

The last term on the right of (2.6.4) vanishes when S is rigid. Thus, when the G is approximated by the compact Green's function (2.4.13) we find, *correct to dipole order*,

$$\frac{p(\mathbf{x},t)}{\rho_o} \approx \frac{-x_i}{4\pi c_o|\mathbf{x}|^2}\frac{\partial}{\partial t}\left\{\int\left[(\boldsymbol{\omega}\wedge\mathbf{v}).\nabla Y_i\right]d^3\mathbf{y} - \nu\oint_S\left[\boldsymbol{\omega}\wedge\nabla Y_i.\mathbf{n}\right]d\mathbf{S}(\mathbf{y})\right\}$$

$$\approx \frac{-x_i}{4\pi c_o|\mathbf{x}|^2}\frac{\partial}{\partial t}\int\Big[(\boldsymbol{\omega}\wedge\mathbf{v}).\nabla Y_i\Big]d^3\mathbf{y}, \quad |\mathbf{x}|\to\infty,\ \frac{v\ell}{\nu}\gg 1, \tag{2.6.6}$$

where [ ] denotes evaluation at $t-|\mathbf{x}|/c_o$; in the second line the skin friction contribution has been discarded for high Reynolds number flow. These formulae are equivalent to Curle's approximations (2.6.2).

If the body also executes small amplitude vibrations at velocity $v(t)$, the compact Green's function used in (2.6.4) yields

$$p(\mathbf{x},t) \approx \frac{x_i}{4\pi c_o |\mathbf{x}|^2} \frac{\partial}{\partial t} \left[F_i + m_o \frac{dv_i}{dt} \right]_{t-|\mathbf{x}|/c_o}, \quad |\mathbf{x}| \to \infty, \tag{2.6.7}$$

where $\mathbf{F}$ is the force exerted on the fluid and m_o is the mass of fluid displaced by the body.

By writing $\mathbf{v} = \mathbf{U} + \mathbf{u}$ in (2.6.6), where $\mathbf{U}$ is the irrotational velocity component of the mean flow past the body, the velocity $\mathbf{u}$ is identified with the vorticity $\boldsymbol{\omega} = \text{curl}\, \mathbf{u}$. For streamlined bodies it frequently happens that $u \ll U$. No sound is generated when $\mathbf{u} = \mathbf{0}$ but, in contrast to sound production by the volume quadrupoles or when $\mathbf{U} = \mathbf{0}$, mean flow convection of vorticity past the body increases the amplitude of the sound from being proportional to u^2 to uU. This *linear* component of the radiation is furnished by the source $\text{div}(\boldsymbol{\omega} \wedge \mathbf{U})$. Furthermore, if $\mathbf{U} \to \mathbf{U}_o$ at large distances from the body, then $x_i \nabla Y_i . \boldsymbol{\omega} \wedge \mathbf{U} \equiv 0$ when $\mathbf{x}$ is parallel to $\mathbf{U}_o$ because $\mathbf{U}(\mathbf{y}) = U_{oi} \nabla Y_i$, so that the linear surface dipoles have no net component parallel to the incident mean stream $\mathbf{U}_o$.

For a bluff body the magnitude of the rotational velocity $\mathbf{u}$ in the wake is comparable to the mean flow speed, although for moderate Reynolds numbers the translational velocity of a typical vortical structure remains small until it is released into the flow. When this happens the core accelerates to a streamwise velocity close to that of the mean flow and a sound pulse is radiated. The periodic nature of these events for wires in a wind is responsible for Æolian tones [22 - 24]. The conclusion above that the intensity of the sound is strongest in directions at right angles to the mean flow, corresponds to dipole radiation produced by a fluctuating lift force, which reverses its direction as successive vortices are shed into the wake.

§2.7 Reciprocity applied to sources adjacent to a compliant wall

The generation of sound by turbulent flow over an inhomogeneous elastic surface involves the excitation of structural vibrations and their subsequent scattering. The general problem is amenable to simple analytical treatment only when convection by the mean flow is ignored, which is usually the case in underwater acoustics. The influence of small amplitude compliance can then be estimated by the following form of the reciprocal theorem [12], which we state in a form suitable for application to surfaces for which the compliant motion is *normal* to the undisturbed surface:

$$p(\mathbf{x},\omega)q^R(\omega) = -i\omega\zeta^R(\mathbf{y},\mathbf{x};\omega)F(\mathbf{y},\omega) \tag{2.7.1}$$

where $p(\mathbf{x},\omega)$ is the perturbation pressure at a point $\mathbf{x}$ in the fluid generated by a normal force $F(\mathbf{y},\omega)$ applied to the surface (directed *into* the surface) at $\mathbf{y}$, and $\zeta^R(\mathbf{y},\mathbf{x};\omega)$ is the normal displacement of the plate (directed into the fluid) at $\mathbf{y}$ produced by a point *volume* source of strength $q^R(\omega)$ at $\mathbf{x}$.

This formula is usually applied to the problems involving the interaction of turbulence "gusts" with an elastic surface in the vicinity of a structural inhomogeneity. By taking the volume source to have unit strength and the force to be the gust-generated *blocked surface pressure* p_s (i.e., the surface pressure that would be generated by the gust if the surface is regarded as *rigid*), the acoustic pressure for each frequency ω is determined by the equation

$$p(\mathbf{x},\omega) = -i\omega \oint_S p_s(\mathbf{y},\omega)\zeta^R(\mathbf{y},\mathbf{x},\omega)d\mathrm{S}(\mathbf{y}), \tag{2.7.2}$$

where $\zeta^R(\mathbf{y},\omega)$ is the flexural displacement at $\mathbf{y}$ produced by a unit volume source at $\mathbf{x}$. In real form, this becomes

$$p(\mathbf{x},t) = \frac{1}{2\pi}\frac{\partial}{\partial t}\oint_S \int_{-\infty}^{\infty} p_s(\mathbf{y},\tau)\zeta^R(\mathbf{y},\mathbf{x},t-\tau)d\mathrm{S}(\mathbf{y})d\tau. \tag{2.7.3}$$

3. SOUND GENERATED BY FLOW OVER A FLAT SURFACE

Intense surface pressure fluctuations beneath a turbulent boundary layer generate sound and structural vibrations. Sound is produced directly by aerodynamic sources within the fluid, and indirectly by the interaction of hydrodynamic pressures and the surface vibrations with discontinuities of the wall.

§3.1 Wall pressure wavenumber-frequency spectrum

The *blocked-pressure* is the pressure developed beneath a boundary layer on a hard wall, and is twice the pressure that a nominally identical flow would produce if the wall were absent. The response of a flexible wall to boundary layer forcing depends on both the temporal and spatial characteristics of the pressure. When the wall is locally plane and the fluctuations can be regarded as statistically stationary in time, the characteristics are expressed in terms of the wall-pressure wavenumber-frequency spectrum $\mathrm{P}(\mathbf{k},\omega)$ (the Fourier transform of the space-time correlation function of the wall pressure). By convention, coordinate axes (x_1, x_2, x_3) are taken with x_1 and x_3 respectively parallel and transverse to the mean flow, and with x_2 measured outwards from the wall (Figure 3.1a). Then

$$\mathrm{P}(\mathbf{k},\omega) = \frac{1}{(2\pi)^3}\int_{-\infty}^{\infty} \mathcal{R}(y_1, y_3, \tau)\mathrm{e}^{-i(\mathbf{k}.\mathbf{y}-\omega\tau)}dy_1 dy_3 d\tau, \quad \mathbf{k} = (k_1, 0, k_3), \tag{3.1.1}$$

where

$$\mathcal{R}(y_1, y_3, \tau) = \langle p_s(x_1, x_3, t)p_s(x_1 + y_1, x_3 + y_3, t + \tau)\rangle \tag{3.1.2}$$

is the wall pressure correlation function, $p_s(x_1, x_3, t)$ is the *fluctuating* component of the wall pressure, and the angle brackets $\langle\ \rangle$ denote an ensemble average. The wavenumber $\mathbf{k}$ is parallel to the wall, and (because $\mathcal{R}$ is real) $\mathrm{P}(-\mathbf{k}, -\omega) \equiv \mathrm{P}(\mathbf{k},\omega)$.

It is usually assumed that variations of $\mathcal{R}(y_1, y_3, \tau)$ and $\mathrm{P}(\mathbf{k},\omega)$ with x_1, x_3 are significant only over distances that are much larger than the length scales of the dominant turbulent motions, although these distances may not be large compared to the wavelengths of the boundary layer generated sound. When $\mathcal{R}(y_1, y_3, \tau)$ is independent of (x_1, x_3) and t, the wall pressure is *stationary random* in position and time, and

$$\langle p_s(\mathbf{k},\omega)p_s^*(\mathbf{k}',\omega')\rangle = \delta(\mathbf{k} - \mathbf{k}')\delta(\omega - \omega')\mathrm{P}(\mathbf{k},\omega), \tag{3.1.3}$$

where the asterisk denotes complex conjugate.

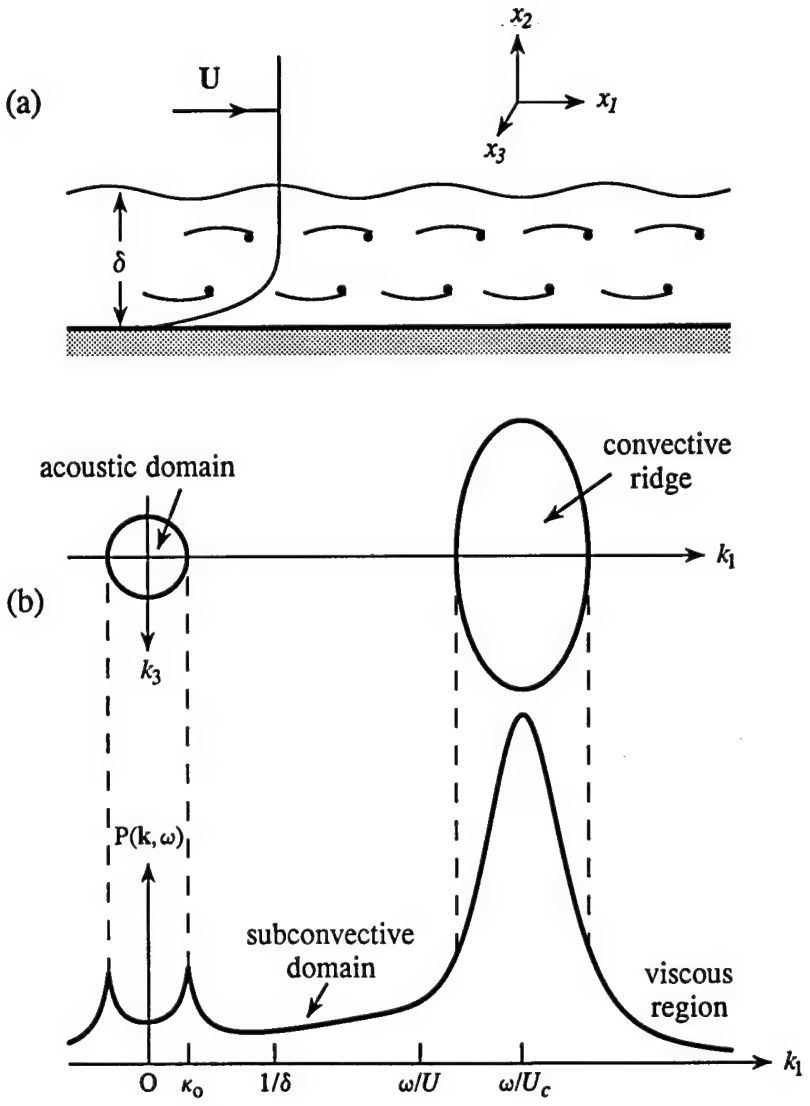

Figure 3.1. Turbulent boundary layer and wall pressure spectrum at low Mach number when $\omega\delta/U \gg 1$.

The wall *point pressure frequency spectrum* $\Phi_{pp}(\omega)$ is defined by

$$\langle p_s^2(x_1, x_3, t)\rangle = \int_{-\infty}^{\infty} \Phi_{pp}(\omega)\, d\omega, \quad \Phi_{pp}(\omega) = \int_{-\infty}^{\infty} \mathrm{P}(\mathbf{k}, \omega)\, dk_1 dk_3. \tag{3.1.4}$$

The root-mean-square wall pressure fluctuation p_{rms} is proportional to the *dynamic pressure* $\frac{1}{2}\rho_o U^2$ (ρ_o and U being the mean density and velocity of the free stream)

$$p_{rms} = \sqrt{\langle p_s^2(x_1, x_3, t)\rangle} = \sigma\, \frac{1}{2}\rho_o U^2; \tag{3.1.5}$$

for a smooth, hard wall at low subsonic velocities $\sigma \approx 0.01$ [25, 26].

The characteristic shape of the wavenumber-frequency spectrum at low Mach numbers is illustrated in Figure 3.1b for a fixed frequency satisfying $\omega\delta/U > 1$, where δ is the boundary layer thickness (the distance from the wall at which the mean flow velocity is $0.99U$). The strongest pressure fluctuations occur within the *convective ridge* centered on $k_1 = \omega/U_c$, $k_3 = 0$, where U_c is a convection velocity, and

$$\mathrm{P}(\mathbf{k}, \omega) \sim 10^3 \rho_o^2 v_*^6/\omega^3, \tag{3.1.6}$$

v_* being the *friction velocity.* The velocity U_c can be interpreted as the translational speed of the principal boundary layer eddies, and both experiment and numerical simulations indicate that $U_c \approx 0.5U - 0.7U$, with only a weak dependence on frequency ω.

At low subsonic Mach numbers, the phase velocity ω/k of surface pressures in the convective domain is subsonic and these pressures therefore decay rapidly with distance from the wall, and do not correspond to sound waves. However, convective pressures can generate sound (and structural vibrations) when the wall is rough or has other discontinuities at which convective energy is *scattered.* For a highly compliant elastomeric wall, in which the shear wave speed is comparable to U, the unsteady surface *shear stresses* that accompany the convective pressures may also cause significant structural excitation. For a typical homogeneous surface, the strongest coupling between the wall and flow is usually attributed to longer wavelength, "subconvective" pressures in the low-wavenumber region $|\kappa_o| < k \ll |\omega|/U_c$ where "resonant" forcing of the wall occurs because the phase velocity ω/k coincides with that of a vibrational mode of the wall. Here the spectral levels are usually 30 to 60 dB below the convective peak. In the acoustic domain $k < |\kappa_o|$, the phase velocity is supersonic, and wall pressure fluctuations are actually sound waves produced directly by boundary layer quadrupoles. The secondary circular ridge in Figure 3.1b at $k = |\kappa_o|$ is discussed at the end of §3.2.

§3.2 Smooth wall spectra at low Mach numbers

Theoretical models of $\mathrm{P}(\mathbf{k},\omega)$ generally assume the flow to be homentropic, of low Mach number over a flat, rigid wall with no mean pressure gradient. The steady growth of the boundary layer in the streamwise direction is usually ignored, and the mean flow velocity is taken to be parallel to the wall and dependent only on distance x_2 from the wall. A sufficient body of experimental data is available, derived principally from wind-tunnel experiments, to permit the formulation of empirical models of the convective domain, but reported properties of the subconvective and acoustic domains often vary significantly between different experiments.

The hydrodynamic domain. Chase [27] has devised the following model for $\mathrm{P}(\mathbf{k},\omega)$ at low Mach numbers in the hydrodynamic domain $k \gg |\kappa_o|$:

$$\begin{aligned} \frac{\mathrm{P}(\mathbf{k},\omega)}{\rho_o^2 v_*^3 \delta^3} &= \frac{1}{[(k_+\delta)^2 + 1/b^2]^{\frac{5}{2}}} \left(\mathrm{C_M}(k_1\delta)^2 + \mathrm{C_T}(k\delta)^2 \frac{(k_+\delta)^2 + 1/b^2}{(k\delta)^2 + 1/b^2} \right) \\ k_+^2 &= (\omega - U_c k_1)^2/(hv_*)^2 + k^2, \\ M &= U/c_o \ll 1, \quad k \gg |\omega|/c_o, \quad \omega\delta/U > 1. \end{aligned} \tag{3.2.1}$$

The adjustable coefficients in these expressions are fixed by comparison with experiment, and recommended values are

$$b \approx 0.75, \quad \mathrm{C_M} \approx 0.1553, \quad \mathrm{C_T} \approx 0.0047, \quad h \approx 3. \tag{3.2.2}$$

A simpler approximation which is applicable for $\omega\delta/U > 1$ in the immediate neighborhood of the convective ridge is due to Corcos [28]:

$$\begin{aligned} \mathrm{P}(\mathbf{k},\omega) &= \Phi_{pp}(\omega) \frac{\ell_1}{\pi[1 + \ell_1^2(k_1 - \omega/U_c)^2]} \frac{\ell_3}{\pi[1 + \ell_3^2 k_3^2]} \\ \ell_1 &\approx 9U_c/\omega, \quad \ell_3 \approx 1.4U_c/\omega, \end{aligned} \tag{3.2.3}$$

where ℓ_1 and ℓ_3 are turbulence correlation lengths in the x_1- and x_3-directions. The point pressure spectrum Φ_{pp}, based on data collated by Chase [27], may be approximated by

$$\frac{(U/\delta_*)\Phi_{pp}(\omega)}{(\rho_o v_*^2)^2} = \frac{(\omega\delta_*/U)^2}{[(\omega\delta_*/U)^2 + \alpha_p^2]^{\frac{3}{2}}}, \quad \alpha_p = 0.12. \tag{3.2.4}$$

In this formula $\delta_* = \int_0^\infty (1 - \bar{v}_1(x_2)/U)dx_2$ ($\sim \delta/8$) is the boundary layer displacement thickness, where $\bar{v}_1(x_2)$ is the mean velocity in the streamwise direction at distance x_2 from the wall.

Equations (3.2.1) imply that $\mathrm{P}(\mathbf{k},\omega)/\rho_o^2 v_*^3 \delta^3 \sim (k\delta)^2$ when $k\delta \ll 1$ (the *Kraichnan-Phillips* Theorem). In the interval $1 < k\delta \ll |\omega|\delta/U_c$ (where the term in $\mathrm{C_T}$ is still dominant in (3.2.1)) the spectrum is *wavenumber-white*, i.e.

$$\mathrm{P}(\mathbf{k},\omega)/\rho_o^2 v_*^3 \delta^3 \approx \mathrm{C_T} h^3 (v_*/U)^3/(\omega\delta/U)^3, \quad 1 < k\delta \ll |\omega|\delta/U_c. \tag{3.2.5}$$

This may be contrasted with a low wavenumber model due to Sevik [29], based on measurements of $\mathrm{P}(\mathrm{k},\omega)$ at $k = 0$ for both smooth and rough walls on buoyant bodies in water and in quiet wind tunnels:

$$\begin{aligned} \mathrm{P}(\mathbf{0},\omega)/\rho_o^2 v_*^3 \delta^3 &\approx 127 M^2 (v_*/U)/(\omega\delta/U)^{4.5}, \\ 24 \le |\omega|\delta/U &\le 240, \quad 0.01 \le M \le 0.15, \quad M = U/c_o. \end{aligned} \tag{3.2.6}$$

Sevik's formula explicitly involves fluid compressibility because of its dependence on Mach number M, and was originally proposed as a model for the acoustic domain. However, practically all published data suggest that the wall pressure spectrum is ultimately wavenumber white as $k\delta \to 0$, starting at values of k that are much greater than the acoustic wavenumber κ_o. If equation (3.2.6) is applied at subconvective wavenumbers ($1 \le k\delta \ll |\omega|\delta/U_c$) predictions of $\mathrm{P}(\mathbf{0},\omega)$ agree in magnitude with (3.2.5) at $\omega\delta/U \approx 24$ for M = 0.01. At higher Mach numbers, estimates based on Sevik's formula can be larger by up to 10 dB, although this is offset by a more rapid decrease with increasing frequency.

The acoustic domain. Consider the solution of Lighthill's equation expressed in Curle's form (2.2.6) for a boundary layer of infinitesimal Mach number, when S coincides with the plane of the wall. The surface integral in (2.2.6) represents the *reflection* of the quadrupole generated sound by the wall. When viscous shear stresses on the wall are ignored the reflection coefficient is unity, and the pressure $p_s = c_o^2(\rho - \rho_o)$ on the wall $x_2 = 0$ becomes

$$p_s(\mathbf{x},t) = \int \mathcal{F}(\mathbf{y}, t - |\mathbf{x}-\mathbf{y}|/c_o) \frac{d^3\mathbf{y}}{2\pi|\mathbf{x}-\mathbf{y}|}, \quad \mathbf{x} = (x_1, 0, x_3) \tag{3.2.7}$$

where $\mathcal{F}(\mathbf{x},t) \approx \partial^2(\rho_o v_i v_j)/\partial x_i \partial x_j$ for homentropic flow, and the integration is over the unsteady sources in the boundary layer.

When this expression is used in (3.1.1) to evaluate $\mathrm{P}(\mathbf{k},\omega)$, the resulting multiple integral diverges for $k = |\kappa_o|$, at the edge of the acoustic domain, if the boundary layer is assumed

to be of unlimited extent. The singularity is caused by the collective action of "grazing" acoustic waves, whose mean square decay like $1/|\mathbf{x}|^2$ with propagation distance over the wall is countered by the growth in the surface area of the boundary layer as $|\mathbf{x}| \to \infty$.

Chase [27] has extrapolated (3.2.1) into the acoustic domain, obtaining

$$\frac{\mathrm{P}(\mathbf{k},\omega)}{\rho_o^2 v_*^3 \delta^3} = \frac{1}{[(k_+\delta)^2 + 1/b^2]^{\frac{5}{2}}}\left[\frac{\mathrm{C_M}(k_1\delta)^2 k^2}{|k^2-\kappa_o^2| + \epsilon^2\kappa_o^2}\right.$$
$$\left. + \mathrm{C_T}(k\delta)^2 \frac{(k_+\delta)^2 + 1/b^2}{(k\delta)^2 + 1/b^2}\left(c_1 + \frac{c_2|k^2-\kappa_o^2|}{k^2} + \frac{c_3 k^2}{|k^2-\kappa_o^2| + \epsilon^2\kappa_o^2}\right)\right], \qquad (3.2.8)$$

where $c_1 = \frac{2}{3}$, $c_2 = c_3 = \frac{1}{6}$, and the values of the other coefficients are given in (3.2.2). The validity of this formula has not been confirmed by experiment; predictions in the acoustic domain are typically 20 dB smaller than those given by Sevik's formula (3.2.6) when $\omega\delta/U \approx 20 - 30$.

The value of ϵ (≈ 0.2) determines the magnitude of the spectral peak in Figure 3.1.1b at $k = |\kappa_o|$ when $M \ll 1$, although the existence of this theoretical maximum has not been confirmed experimentally. The value of ϵ is governed by the size of the boundary layer, the attenuation and refraction of surface propagating sound waves by the boundary layer, by diffraction when the wall has a finite radius of curvature, and by scattering at surface discontinuities and edges.

§3.3 Boundary layer generated sound

At low Mach numbers the wavelength of sound generated by the boundary layer greatly exceeds its thickness δ, and there exists a simple relation between the acoustic domain of $\mathrm{P}(\mathbf{k},\omega)$ and the frequency spectrum of the sound. When M is not small this relation is complicated by refraction, scattering and by sound generation by turbulence in the outer regions of the boundary layer at distances from the wall comparable to the acoustic wavelength.

Consider the sound radiated from a large region of the boundary layer of area $\mathcal{A}$, which may be assumed to be centered on the origin. At low Mach numbers the acoustic wavelengths are very much larger than the boundary layer thickness ($\kappa_o\delta \ll 1$), and the pressures at these wavenumbers are constant across the boundary layer; the acoustic pressure frequency spectrum $\Phi(\mathbf{x},\omega)$ of the boundary layer noise is then given by

$$\Phi(\mathbf{x},\omega) = \frac{2\mathcal{A}\kappa_o^2\cos^2\Theta}{|\mathbf{x}|^2}\mathrm{P}(\kappa_o\mathbf{x}/|\mathbf{x}|,\omega), \quad |\mathbf{x}| \to \infty, \quad \text{where} \quad \langle p^2(\mathbf{x},t)\rangle = \int_0^\infty \Phi(\mathbf{x},\omega)d\omega. \qquad (3.3.1)$$

where Θ is the angle between the radiation direction $\mathbf{x}$ and the normal to the wall (the x_2-axis).

There are no universally accepted measurements of the wall pressure spectrum in the acoustic domain for use in (3.3.1). Sevik's wavenumber-white approximation (3.2.6) yields

$$\frac{\Phi(\mathbf{x},\omega)}{\rho_o^2 v_*^3 \delta} \approx \frac{254 \mathcal{A} M^4 (v_*/U) \cos^2\Theta}{|\mathbf{x}|^2 (\omega\delta/U)^{\frac{5}{2}}}, \tag{3.3.2}$$

according to which the peak radiation direction is normal to the wall. A more complicated dependence on radiation direction is predicted by the Chase formula (3.2.8). Unless $\omega\delta/U$ is very large, predictions made with Sevik's formula are larger (by about 20 dB at $\omega\delta/U \approx 20$ for $M = 0.01$). Thus, equation (3.3.2) should probably be regarded as an upper bound for the quadrupole noise.

§3.4 Rough walls

The wall pressure wavenumber-frequency spectrum for flow over a rough wall whose characteristic roughness height R is much smaller than δ can be approximated by a smooth wall empirical formula provided the friction velocity is increased to compensate for the increased surface drag and turbulence production [30]. This procedure is satisfactory in the convective domain, but does not account for changes at low wavenumbers which are produced by scattering of convective pressures by roughness elements. In particular, it seems that when $\omega R/v_* > 5$, the aerodynamic sound generated by the boundary layer is dominated by this scattering.

To investigate the influence of surface roughness, let us assume that the motion is at low Mach number and of sufficiently high Reynolds number that viscous stresses can be disregarded; this will be the case if the roughness elements protrude beyond the viscous sublayer, i.e. for $Rv_*/\nu > 10$.

The roughness elements behave like point *dipoles*, the dipole strength being the unsteady drag on an element. If they are modeled as rigid hemispheres distributed randomly over the wall (Figure 3.2a) the following empirical spectrum is consistent with measurements by Hersh [31] of the noise generated by low Mach number flow of air from a sand roughened pipe (Figure 3.2b), provided R is identified with the mean roughness height:

$$\frac{\Phi_R(\mathbf{x},\omega)}{\rho_o^2 v_*^3 \delta} \approx \tau_o \frac{\mathcal{A}\cos^2\theta}{|\mathbf{x}|^2} \frac{R}{\delta} \frac{v_*^2}{c_o^2} \frac{(\omega R/v_*)^3}{[1+\beta(\omega R/v_*)^2]^{5.5}}, \tag{3.4.1}$$

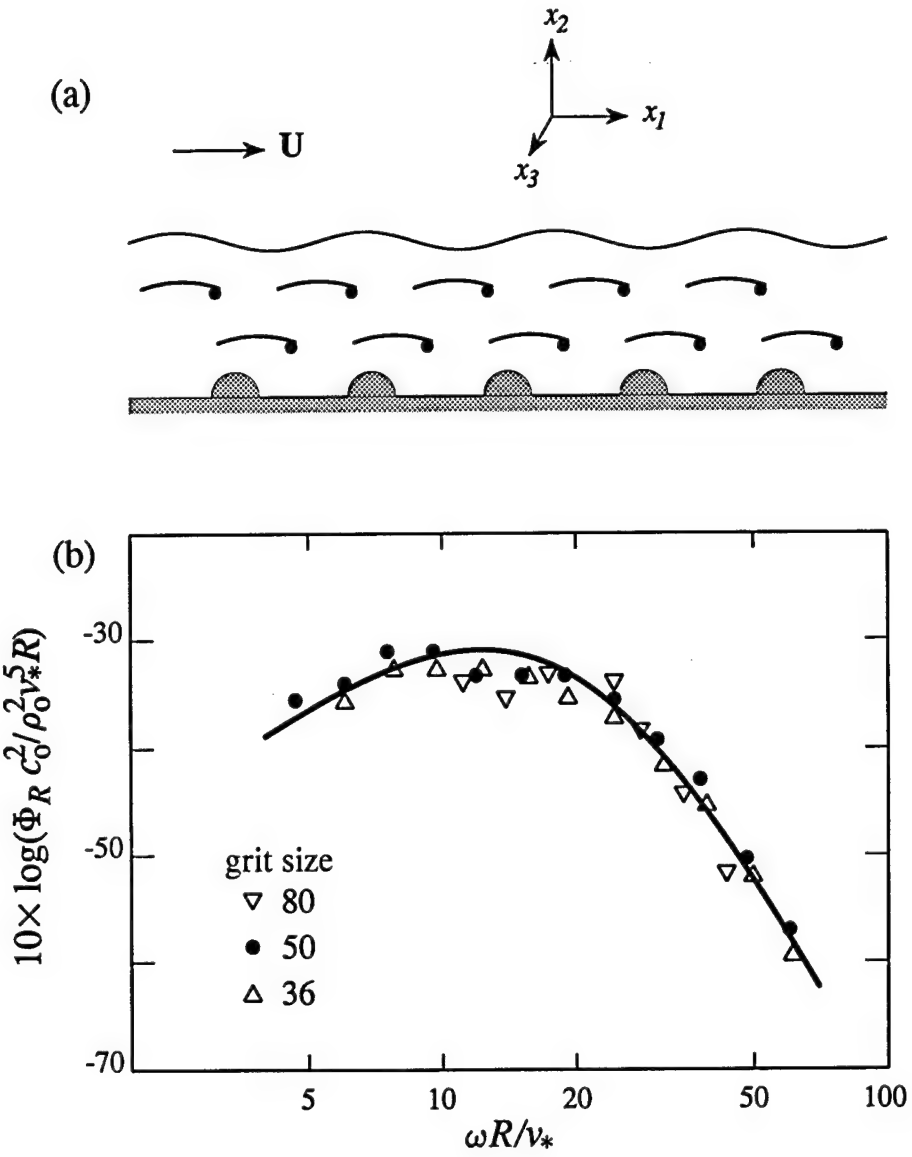

Figure 3.2. (a) Wall roughness modelled by rigid hemispheres.
(b) Roughness noise measured by Hersh [31].

where τ_o and β are empirical constants, and θ is the angle between the radiation direction $\mathbf{x}$ and the mean flow. The best fit to the *shape* of the experimental spectrum is obtained for $\beta = 0.0025$, as illustrated by the solid curve in Figure 3.2b, whose absolute position has been adjusted to overlie the data, since no directivity information is available from the Hersh experiments. This value of β and the exponent 5.5 of the denominator in (3.4.1) should be regarded as tentative. The "roughness" parameter τ_o depends on the spacing of the roughness elements, determined by the fraction α of the plane wall covered by hemispheres. When $\alpha \ll 1$, it appears that $\tau_o \approx (v_*/U_c)^2(\alpha/\pi)$.

§3.5 Homogeneous elastic walls

For a smooth, homogenous and compliant wall the boundary layer noise at very small Mach numbers is given by the following modification of equation (3.3.1)

$$\Phi(\mathbf{x},\omega) = \frac{\mathcal{A}\kappa_o^2 \cos^2\Theta}{2|\mathbf{x}|^2}|1+\mathrm{R}|^2\mathrm{P}(\kappa_o\mathbf{x}/|\mathbf{x}|,\omega), \quad |\mathbf{x}| \to \infty, \tag{3.5.1}$$

where R is the "reflection coefficient" for a plane acoustic wave of frequency ω specularly reflected at the wall into the radiation direction $\mathbf{x}$.

For example, when it is permissible to model the wall as a *vacuum backed*, thin elastic plate of bending stiffness B and mass m per unit area,

$$\mathrm{R} = \frac{(\omega/\omega_c)\cos\Theta\{(\omega/\omega_c)^2\sin^4\Theta - 1\} + i\epsilon}{(\omega/\omega_c)\cos\Theta\{(\omega/\omega_c)^2\sin^4\Theta - 1\} - i\epsilon}, \tag{3.5.2}$$

where $\omega_c = c_o^2\sqrt{m/\mathrm{B}}$ is the coincidence frequency (above which the phase speed of *bending waves* on the plate *in vacuo* exceeds the speed of sound c_o), and ϵ is a fluid loading parameter given by

$$\epsilon = \frac{\rho_o c_1}{\rho_s c_o}\left(\frac{1-2\sigma}{12(1-\sigma)^2}\right)^{\frac{1}{2}} \equiv \frac{\rho_o}{\rho_s}\left(\frac{\mathrm{E}}{12\rho_s c_o^2(1-\sigma^2)}\right)^{\frac{1}{2}}, \tag{3.5.3}$$

where σ, ρ_s, c_1, E are respectively the Poisson's ratio, mass density, P-wave speed, and Young's modulus of the material of the plate [32]. For a steel plate in water $\epsilon \approx 0.135$; for aluminum in water $\epsilon \approx 0.391$. For an aluminum or steel plate of thickness h *in water* the coincidence frequency $\omega_c \approx 0.95c_o/h$.

§3.6 Sound generated by a surface irregularity

Consider low Mach number turbulent flow past a surface irregularity, such as the hemispherical boss in Figure 3.3a attached to a plane surface $x_2 = 0$. The acoustic radiation can be calculated from (2.6.4) when the vorticity and velocity distributions are known. The compact Green's function depends on the wall properties:

Rigid wall

$$G(\mathbf{x},\mathbf{y},t-\tau) = \frac{1}{4\pi|\mathbf{X}-\mathbf{Y}|}\delta\big(t-\tau-|\mathbf{X}-\mathbf{Y}|/c_o\big)+\frac{1}{4\pi|\mathbf{X}-\bar{\mathbf{Y}}|}\delta\big(t-\tau-|\mathbf{X}-\bar{\mathbf{Y}}|/c_o\big); \quad (3.6.1)$$

Elastic wall

$$\begin{aligned} G(\mathbf{x},\mathbf{y},t-\tau) &= \frac{1}{4\pi|\mathbf{X}-\mathbf{Y}|}\delta\big(t-\tau-|\mathbf{X}-\mathbf{Y}|/c_o\big) \\ &\quad + \frac{1}{8\pi^2|\mathbf{X}-\bar{\mathbf{Y}}|}\int_{-\infty}^{\infty} \mathrm{R}(\omega)\exp\big(-i\omega(t-\tau-|\mathbf{X}-\bar{\mathbf{Y}}|/c_o)\big)\,d\omega. \quad (3.6.2) \end{aligned}$$

In these formulae

$$\mathbf{Y} = (Y_1, y_2, Y_3), \quad \bar{\mathbf{Y}} = (Y_1, -y_2, Y_3),$$

where, for $j = 1$ and 3, Y_j is the velocity potential of irrotational flow at unit speed past the surface irregularity in directions parallel to the wall. $\mathrm{R}(\omega)$ is the wall reflection coefficient, defined as in §3.5. For a rigid wall $\mathrm{R} = 1$, and (3.6.2) reduces to the hard wall case (3.6.1). For a vacuum-backed thin plate, R is given by (3.5.2).

The radiation is of dipole type, and can be expressed in terms of the unsteady drag force $D_i(t)$ exerted on the irregularity (c.f. (2.6.7)). If the coordinate origin is taken within the irregularity we find, as $|\mathbf{x}| \to \infty$:

$$\begin{aligned} p(\mathbf{x},t) &\approx \frac{-x_i}{2\pi c_o|\mathbf{x}|^2}\left[\frac{dD_i(t)}{dt}\right]_{t-|\mathbf{x}|/c_o} \quad \text{for a rigid wall;} \\ &\approx \frac{-x_i}{4\pi c_o|\mathbf{x}|^2}\left[\frac{\partial}{\partial t}\int_{-\infty}^{\infty} D_i(\omega)\{1+\mathrm{R}(\omega)\}\mathrm{e}^{-i\omega t}\,d\omega\right]_{t-|\mathbf{x}|/c_o} \\ &= \frac{-x_i}{4\pi c_o|\mathbf{x}|^2}\left[\frac{dD_i(t)}{dt}+\frac{\partial}{\partial t}\int_{-\infty}^{\infty} D_i(\omega)\mathrm{R}(\omega)\mathrm{e}^{-i\omega t}\,d\omega\right]_{t-|\mathbf{x}|/c_o} \quad \text{for an elastic wall,} \quad (3.6.3) \end{aligned}$$

where $D_i(\omega) = (1/2\pi)\int_{-\infty}^{\infty} D_i(t)\mathrm{e}^{i\omega t}\,dt$. In the elastic case this formula assumes the mass of the irregularity is small compared to the mass of the area of the plate that it covers (so that it has a negligible influence on flexural motions of the plate)

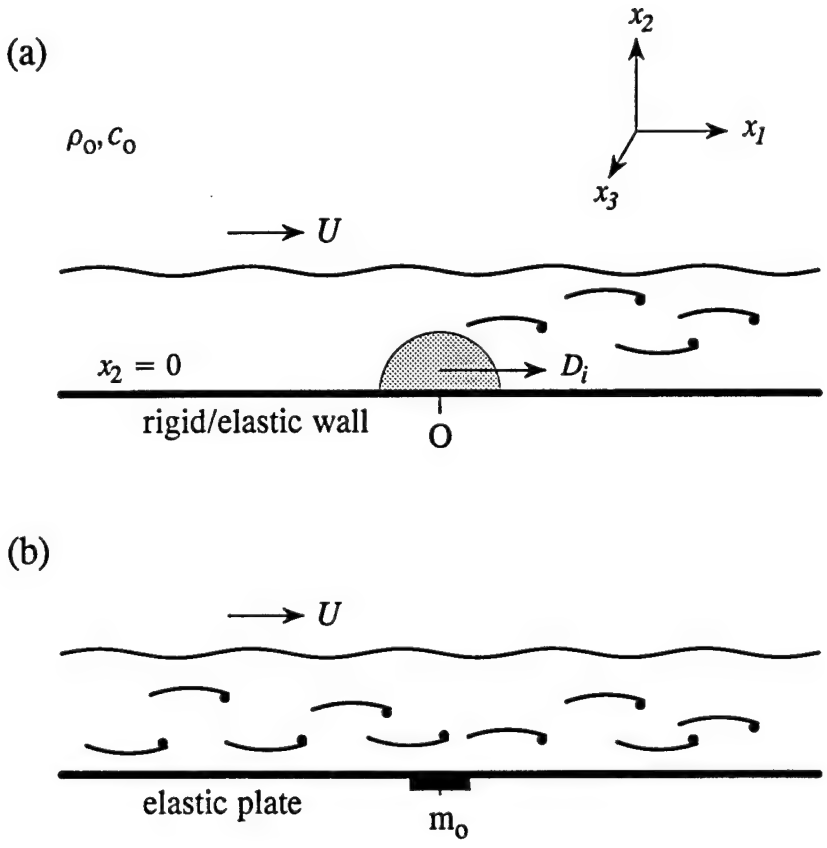

Figure 3.3. (a) The strength of the dipole radiation from a small surface irregularity is determined by the drag force D_i.
(b) Aerodynamically smooth plate with mass load.

§3.7 Pinned elastic plate

Consider a thin, homogeneous, vacuum-backed elastic plate of bending stiffness B and mass density m per unit area loaded with a point mass m_o at $\mathbf{x} = \mathbf{0}$ (Figure 3.3b), such that the surface of the plate exposed to flow is aerodynamically smooth. Green's function is given by [33]

$$G(\mathbf{x},\mathbf{y},t-\tau) = G_o(\mathbf{x},\mathbf{y},t-\tau) \;-\; \frac{\mathrm{m}_o\cos\Theta}{2(2\pi)^4 c_o|\mathbf{x}|}\iint_{-\infty}^{\infty}\frac{\omega^3\{1-\mathrm{R}(\omega)\}\mathrm{e}^{i(\mathbf{k}.\mathbf{y}+\gamma(k)y_2-\omega[t])}\,d^2\mathbf{k}d\omega}{\gamma(k)\mathcal{Z}(\omega)\mathcal{D}(k,\omega)}, \tag{3.7.1}$$

where $G_o(\mathbf{x},\mathbf{y},t-\tau)$ is defined by (3.6.2) with $\mathbf{Y} = \bar{\mathbf{Y}} \equiv \mathbf{y}$ (for a smooth wall). In the integral, $[t] = t-\tau-|\mathbf{x}|/c_o$ denotes retarded time, and

$$\begin{aligned}
\gamma(k) &= \mathrm{sgn}(\omega)\sqrt{\kappa_o^2-k^2}, \qquad +i\sqrt{k^2-\kappa_o^2} \text{ according as } k \lesseqgtr |\kappa_o|;\\
\mathcal{D}(k,\omega) &= \mathrm{B}k^4 - m\omega^2 - \frac{i\rho_o\omega^2}{\gamma(k)};\\
\mathcal{Z}(\omega) &= 1-\frac{\mathrm{m}_o K_o^2}{2\pi m}\int_0^\infty \frac{\lambda\,d\lambda}{[(1-i\eta)\lambda^4 - 1 - (\epsilon/\mu)/\sqrt{\lambda^2-\mu^2}]};\\
K_o &= \sqrt{\frac{m\omega^2}{\mathrm{B}}} \text{ the vacuum bending wavenumber}, \quad \mu = \sqrt{\frac{|\omega|}{\omega_c}},
\end{aligned} \tag{3.7.2}$$

and η is a loss factor for the plate ($\gtreqless 0$ according as $\omega \gtreqless 0$). When $\omega > 0$ the square root in the integral for $\mathcal{Z}(\omega)$ is *negative* imaginary when $\lambda^2 < \mu^2$; the value of $\mathcal{Z}(\omega)$ for $\omega < 0$ is given by

$$\mathcal{Z}(\omega) = \mathcal{Z}^*(-\omega),$$

where the asterisk denotes complex conjugate.

In the limit $\mathrm{m}_o \to \infty$ the plate is "pinned" at $\mathbf{x} = \mathbf{0}$, and cannot execute flexural motions (although *bending* still occurs there). This might be taken to model the effect of an isolated rivet; if the "rivet head" is not flush with the surface exposed to the flow equation (3.7.1) is modified by taking G_o to be defined exactly as in (3.6.2), with $\mathbf{Y}$, $\bar{\mathbf{Y}}$ determined by the shape of the rivet head. In this case there are two components of the sound generated at the rivet, corresponding respectively to the drag dipole (3.6.3) and the pinning contribution given by the integral term in (3.7.1).

When the radiation is expressed in terms of the blocked pressure p_s we make use of the

reciprocal theorem formula (2.7.3), in which

$$\frac{\partial \zeta^R}{\partial t} = \left(\frac{\partial G}{\partial y_2}\right)_{y_2=0}.$$

The contribution to the far field sound from mass load m_o (i.e., from the final term in (3.7.1)) can then be expressed in the form

$$p(\mathbf{x},t) \approx \frac{-im_o \cos\Theta}{8\pi^2 c_o |\mathbf{x}|} \int\int_{-\infty}^{\infty} \frac{\omega^3 \{1-\mathrm{R}(\omega)\} p_s(\mathbf{k},\omega) \mathrm{e}^{-i\omega(t-|\mathbf{x}|/c_o)}}{\mathcal{Z}(\omega)\mathcal{D}(k,\omega)} d^2\mathbf{k}d\omega, \quad |\mathbf{x}| \to \infty. \quad (3.7.3)$$

This integral will have significant contributions from two distinct wavenumber regions: (i) from the convective range of wavenumbers ($k_1 \sim \omega/U_c$, $k_3 \sim 0$) that defines the dominant wall pressure fluctuations, and (ii) from the vicinity of the region where $\mathcal{D}(k,\omega) = 0$, which corresponds to the sound radiated when bending waves generated by subconvective wall pressures over the whole plate are scattered by the mass load. The actual contribution in case (ii) will be determined by the size of the boundary layer flow and the magnitude of the loss factor η.

When $m_o \to \infty$ (plate pinned at $\mathbf{x} = \mathbf{0}$), the acoustic pressure is independent of m_o, and can be written

$$p(\mathbf{x},t) \approx \frac{im\cos\Theta}{4\pi(\omega_c h/c_o)} \frac{h}{|\mathbf{x}|} \int\int_{-\infty}^{\infty} \frac{\omega|\omega|\{1-\mathrm{R}(\omega)\} p_s(\mathbf{k},\omega) \mathrm{e}^{-i\omega(t-|\mathbf{x}|/c_o)}}{\mathcal{I}(\omega)\mathcal{D}(k,\omega)} d^2\mathbf{k}d\omega, \quad |\mathbf{x}| \to \infty, \quad (3.7.4)$$

where

$$\mathcal{I}(\omega) = \int_0^{\infty} \frac{\lambda\, d\lambda}{[(1-i\eta)\lambda^4 - 1 - (\epsilon/\mu)/\sqrt{\lambda^2-\mu^2}]}$$

§3.8 Forward and backward facing steps

Wall surface irregularities in the form of forward or backward facing steps produce drag fluctuations that are equivalent to localized aeroacoustic dipole sources. To fix ideas, consider the forward facing step of height h illustrated schematically in Figure 3.4. Take the coordinate origin at the foot O of the step, with the mean flow locally in the x_1-direction. The sound radiated by low Mach number turbulent flow over the step is calculated using the Green's function (3.6.1) when the surface is rigid. When the step is formed by two overlapping, identical plates, the step noise is determined by (3.6.2), where $\mathrm{R}(\omega)$ is the reflection coefficient for a plane wave incident on an infinite homogeneous plate. Because the wall is

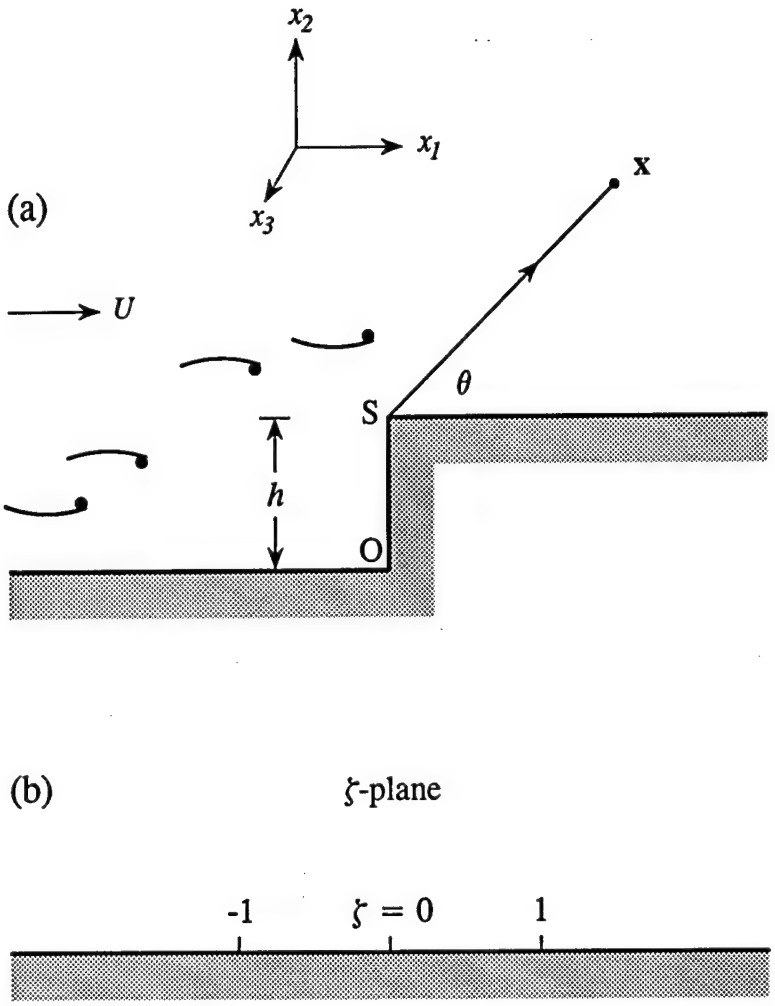

Figure 3.4. (a) Forward facing step. (b) The ζ-plane.

uniform in the x_3-direction we have $Y_3 = y_3$; the function Y_1 is determined by conformal mapping of the complex region $z = y_1 + iy_2$ "above" the step onto the upper half $\mathrm{Im}\,\zeta > 0$ of the ζ-plane by means of the formula

$$\frac{z}{h} = \frac{1}{\pi}\left\{\sqrt{\zeta^2-1} \mp \ln\left(\zeta + \sqrt{\zeta^2-1}\right)\right\} + \frac{i}{2}(1 \pm 1), \quad \mathrm{Im}\,\zeta \geq 0, \tag{3.8.1}$$

where the upper/lower signs are to be taken respectively for forward/backward facing steps. The foot of the step O maps into the point $\zeta = \mp 1$, and the top S maps into $\zeta = \pm 1$. Then

$$Y_1(\mathbf{y}) = \mathrm{Re}\left(\frac{h\zeta}{\pi}\right). \tag{3.8.2}$$

When the step height h is small compared to the dominant turbulence length scale we can take

$$Y_1(\mathbf{y}) = y_1 \mp \frac{h}{2\pi i}\int_{-\infty}^{\infty} \frac{e^{i(ky_1+\gamma(k)y_2)}}{\gamma(k)}\,dk \;=\; y_1 \mp \frac{ih}{2\pi}\,\mathrm{H}_0^{(1)}(\kappa_o\sqrt{y_1^2+y_2^2}), \tag{3.8.3}$$

The Green's function can be used if the vorticity and velocity distributions are known. If, however, the unsteady drag $D_1(x_3,t)$, per unit span (x_3-direction) can be found by alternative means, (3.6.3) gives the radiation in the form,

$$\begin{aligned} p(\mathbf{x},t) \;&\approx\; \frac{-\cos\theta}{4\pi c_o|\mathbf{x}|}\frac{d}{dt}\int_{span} dy_3 \int_{-\infty}^{\infty} D_1(y_3,\omega)\{1+\mathrm{R}(\omega)\}\mathrm{e}^{-i\omega[t]}\,d\omega, \\ &=\; \frac{-\cos\theta}{4\pi c_o|\mathbf{x}|}\frac{d}{dt}\int_{span}\left\{D_1(y_3,[t]) + \int_{-\infty}^{\infty} D_1(y_3,\omega)\mathrm{R}(\omega)\mathrm{e}^{-i\omega[t]}\,d\omega\right\} dy_3, \quad |\mathbf{x}| \to \infty, \end{aligned} \tag{3.8.4}$$

where θ is the angle between the radiation direction $\mathbf{x}$ and the flow direction (x_1-axis), and $[t] = t - \sqrt{x_1^2 + x_2^2 + (x_3-y_3)^2}/c_o$. $\mathrm{R} \equiv 1$ for a rigid wall, and then

$$p(\mathbf{x},t) \approx \frac{-\cos\theta}{2\pi c_o|\mathbf{x}|}\frac{d}{dt}\int_{span} D_1(y_3,[t])\,dy_3, \quad |\mathbf{x}| \to \infty. \tag{3.8.5}$$

§3.9 Rib-stiffened elastic wall

Suppose the wall can be modeled as an aerodynamically smooth, vacuum-backed, thin elastic plate with a narrow rib-stiffener along the x_3-axis (Figure 3.5). The sound radiated from the rib can be calculated from the reciprocal theorem formula (2.7.3) in terms of the blocked wall pressure p_s.

When the dominant wall pressure fluctuations have length scales larger than the width of the rib, the far field acoustic pressure at $\mathbf{x}$ can be expressed in the general form [34]

$$p(\mathbf{x},t) \approx \frac{\pi m}{c_o|\mathbf{x}|}\frac{\partial}{\partial t}\sum_{j=0}^{3}\iint_{-\infty}^{\infty}\frac{\omega^2\{1-\mathrm{R}(\omega)\}\alpha_j(n_1,\omega)(-k/K_o)^j p_s(k,\kappa_o n_3,\omega)\mathrm{e}^{-i\omega(t-|\mathbf{x}|/c_o)}dkd\omega}{K_o\mathcal{D}\left(\sqrt{k^2+\kappa_o^2 n_3^2},\omega\right)}. \tag{3.9.1}$$

In this formula $p_s(k,\kappa_o n_3,\omega)$ is the Fourier transform of the blocked wall pressure, $\mathrm{R}(\omega)$ is the reflection coefficient (3.5.2), and $\mathbf{n} \equiv (n_1,n_2,n_3) = \mathbf{x}/|\mathbf{x}|$ is the unit vector in the radiation direction.

The coefficients $\alpha_j(n_1,\omega)$ are dimensionless and depend on the way in which the plate is attached to the rib. When the plate is *clamped* to the rib (so that $\zeta = 0$ and $\partial\zeta/\partial x_1 = 0$ at $x_1 = 0$, ζ = plate flexural displacement) we have [34]

$$\alpha_0 = \frac{\Psi_2+\Psi_1 n_1\mu}{\Psi_1^2-\Psi_0\Psi_1}, \quad \alpha_1 = \frac{-[\Psi_1+\Psi_0 n_1\mu]}{\Psi_1^2-\Psi_0\Psi_1}, \quad \alpha_2=\alpha_3=0, \tag{3.9.2}$$

where

$$\Psi_j = \int_{-\infty}^{\infty}\frac{\lambda^j\,d\lambda}{(1-i\eta)\Lambda^4-1-(\epsilon/\mu)/\sqrt{\Lambda^2-\mu^2}}, \quad \Lambda^2=\lambda^2+\mu^2 n_3^2. \tag{3.9.3}$$

For $\omega > 0$ we take $\sqrt{\Lambda^2-\mu^2} > 0$ when $|\lambda| > \mu\sqrt{1-n_3^2}$, and $\sqrt{\Lambda^2-\mu^2} = -i\sqrt{\mu^2-\Lambda^2}$ for $|\lambda| < \mu\sqrt{1-n_3^2}$. For $\omega < 0$ the α_j are determined from the formula

$$\alpha_j(n_1,-\omega) = (-1)^j\alpha_j^*(n_1,\omega).$$

To calculate the acoustic pressure frequency spectrum (defined as in the second of equations (3.3.1)) for a rib of wetted span L we use the result

$$\langle p_s(k_1,k_3,\omega)p_s^*(k_1',k_3,\omega')\rangle \approx \frac{L}{2\pi}\delta(\omega-\omega')\delta(k_1-k_1')\mathrm{P}(k_1,k_3,\omega), \quad L \gg \delta. \tag{3.9.4}$$

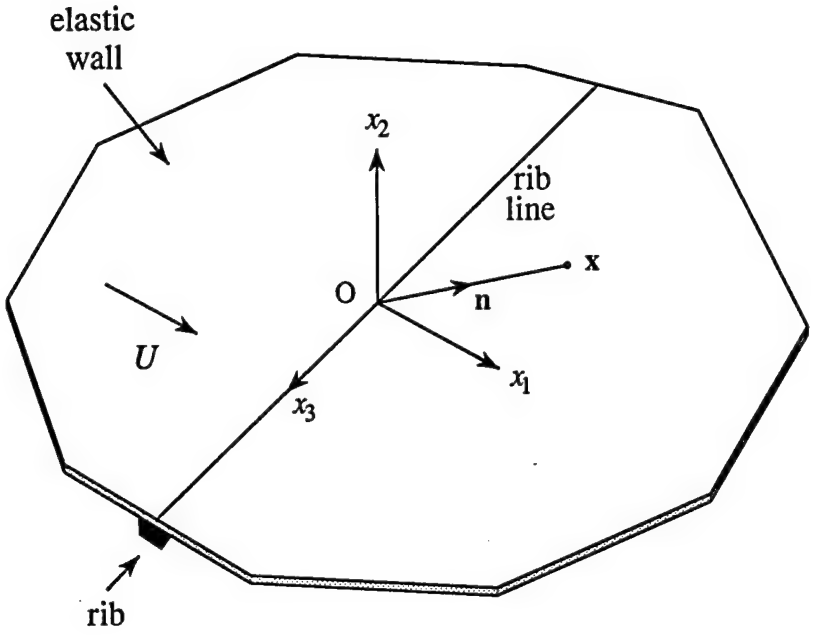

Figure 3.5. Rib-stiffened wall.

Then (3.9.1) supplies

$$\Phi(\mathbf{x},\omega) \approx \frac{\pi L m^2 \omega^5 |1-\mathrm{R}(\omega)|^2}{\omega_c |\mathbf{x}|^2} \int_{-\infty}^{\infty} \frac{\mathrm{P}(k,\kappa_o n_3,\omega) \left|\sum_j \alpha_j(n_1,\omega)(-k/K_o)^j\right|^2 dk}{\left|\mathcal{D}\left(\sqrt{k^2+\kappa_o^2 n_3^2},\omega\right)\right|^2},$$

$$|\mathbf{x}| \to \infty, \quad \omega > 0. \tag{3.9.5}$$

The remarks following equation (3.7.3) concerning the dominant contributions to the integral in (3.7.3) also apply to equations (3.9.1) and (3.9.5), namely, that the integrals will tend to be dominated by contributions from (i) from the convective region $k_1 \sim \omega/U_c$, and (ii) resonant wall modes where $\mathcal{D}(\sqrt{k^2+\kappa_o^2 n_3^2},\omega) \ll 1$, the latter being controlled by the boundary layer size and the loss factor η.

§3.10 Flow-excited panel radiation

The method of §3.9 is easily extended to the case illustrated in Figure 3.6, in which an elastic plate is divided into *equal* strip-like panels transverse to the mean flow direction [34], the ribs being located at $x_1 = Nd$, $-\infty < N < \infty$. The acoustic pressure may now be expressed in the form

$$p(\mathbf{x},t) \approx \frac{2\pi^2 m}{c_o d|\mathbf{x}|}\frac{\partial}{\partial t}\sum_{N=-\infty}^{\infty}\sum_{j=0}^{3}\int_{-\infty}^{\infty}\frac{\omega^2\{1-\mathrm{R}(\omega)\}(-1)^j\alpha_j(n_1,\omega)}{K_o\mathcal{D}\left(\sqrt{(\kappa_o n_1+2N\pi/d)^2+\kappa_o^2 n_3^2},\omega\right)}\left(\frac{\kappa_o n_1+2N\pi/d}{K_o}\right)^j$$

$$\times\ p_s\left(\kappa_o n_1+\frac{2N\pi}{d},\kappa_o n_3,\omega\right)\mathrm{e}^{-i\omega(t-|\mathbf{x}|/c_o)}d\omega, \quad |\mathbf{x}|\to\infty. \tag{3.10.1}$$

For *clamped* panel edges the coefficients α_j are given by equations (3.9.2), but with Ψ_j defined by

$$\Psi_j = \frac{2\pi}{K_o d}\sum_{N=-\infty}^{\infty}\frac{\lambda_N^j}{(1-i\eta)\Lambda_N^4 - 1 - (\epsilon/\mu)/\sqrt{\Lambda_N^2-\mu^2}} \tag{3.10.2}$$

where

$$\lambda_N = 2N\pi/K_o d - \mu n_1, \quad \Lambda_N^2 = \lambda_N^2 + \mu^2 n_3^2.$$

The formulae (3.10.1) and (3.10.2) are exact within the approximation of linear, thin plate theory, and with the neglect of mean flow convection of sound. However, correspondingly simple formulae are not available for panels of finite dimensions, such as the rectangular panels relevant in underwater acoustics. In this case the reciprocal formula (2.7.3) gives a formally exact procedure for calculating the radiation in terms of the wall pressure fluctuations, and the flexural displacement $\zeta^R(\mathbf{x},\mathbf{y},\omega)$ of an arbitrary point $\mathbf{y}$ of the panel produced by a time harmonic volume source of unit strength placed at the far field point $\mathbf{x}$. This reduces the problem to the solution of a well defined diffraction problem, which must be solved numerically.

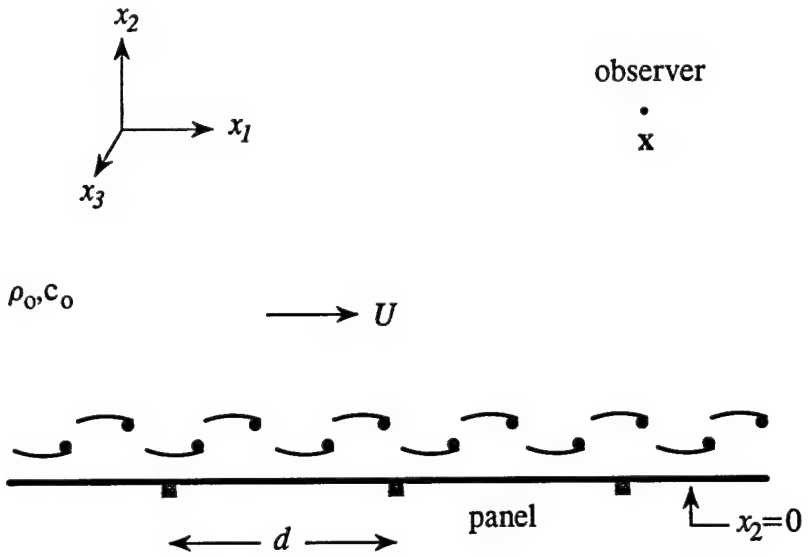

Figure 3.6. Periodically rib-stiffened wall.

4. SOUND GENERATED AT THE EDGE OF A LARGE SURFACE

In underwater applications free stream turbulence inflow on a *leading* edge is not usually an important source of sound, except possibly when the impinging vorticity is shed from a neighboring upstream solid boundary or control surface. The contribution from trailing edges also tends to be small because the upwash velocity generated by inflow turbulence is largely canceled by shedding from the edge. Nevertheless, experiments at high Reynolds numbers [35 - 37] indicate that a trailing edge can be an important source of high frequency "self-noise", attributable to relatively small scale turbulence, generated by the natural instability of the boundary layers on the airfoil, interacting with the trailing edge. At lower Reynolds numbers (smaller than about 2×10^5 when based on airfoil chord), quasi-periodic shedding of vorticity can occur, especially when the trailing edge is blunt, causing the airfoil to "sing" at a frequency $\omega \approx U/h$, where h is the airfoil thickness near the edge and U the mean stream velocity [30].

§4.1 Edge noise Green's functions

At very small Mach numbers the wavelength of the sound produced by the interaction of unsteady flow with the edge is always very much larger than the "hydrodynamic wavelength", which is effectively the distance between the edge and those components of the turbulence that interact effectively with the edge. This makes it possible to express the edge noise in terms of a compact Green's function, defined such that the source point $\mathbf{y}$ is very much closer to the edge than a characteristic acoustic wavelength. We give expressions for the frequency domain compact Green's function $G(\mathbf{x}, \mathbf{y}, ; \omega)$ for the semi-infinite configurations illustrated in Figure 4.1:

i. Rigid half-plane [11] (Figure 4.1a):

The plane occupies $x_1 < 0,\ x_2 = 0$

$$G(\mathbf{x}, \mathbf{y}; \omega) = G_0(\mathbf{x}, \mathbf{y}; \omega) + G_1(\mathbf{x}, \mathbf{y}; \omega) + \ldots, \tag{4.1.1}$$

where, for $|\mathbf{x} - y_3\mathbf{i}_3| \to \infty$ and $\kappa_o\sqrt{y_1^2 + y_2^2} \ll 1$,

$$G_0(\mathbf{x}, \mathbf{y}; \omega) = \frac{-1}{4\pi|\mathbf{x} - y_3\mathbf{i}_3|} e^{i\kappa_o|\mathbf{x} - y_3\mathbf{i}_3|}, \quad G_1(\mathbf{x}, \mathbf{y}; \omega) = \frac{-1}{\pi\sqrt{2\pi i}} \frac{\sqrt{\kappa_o}\varphi^*(\mathbf{x})\varphi^*(\mathbf{y})}{|\mathbf{x} - y_3\mathbf{i}_3|^{3/2}} e^{i\kappa_o|\mathbf{x} - y_3\mathbf{i}_3|}. \tag{4.1.2}$$

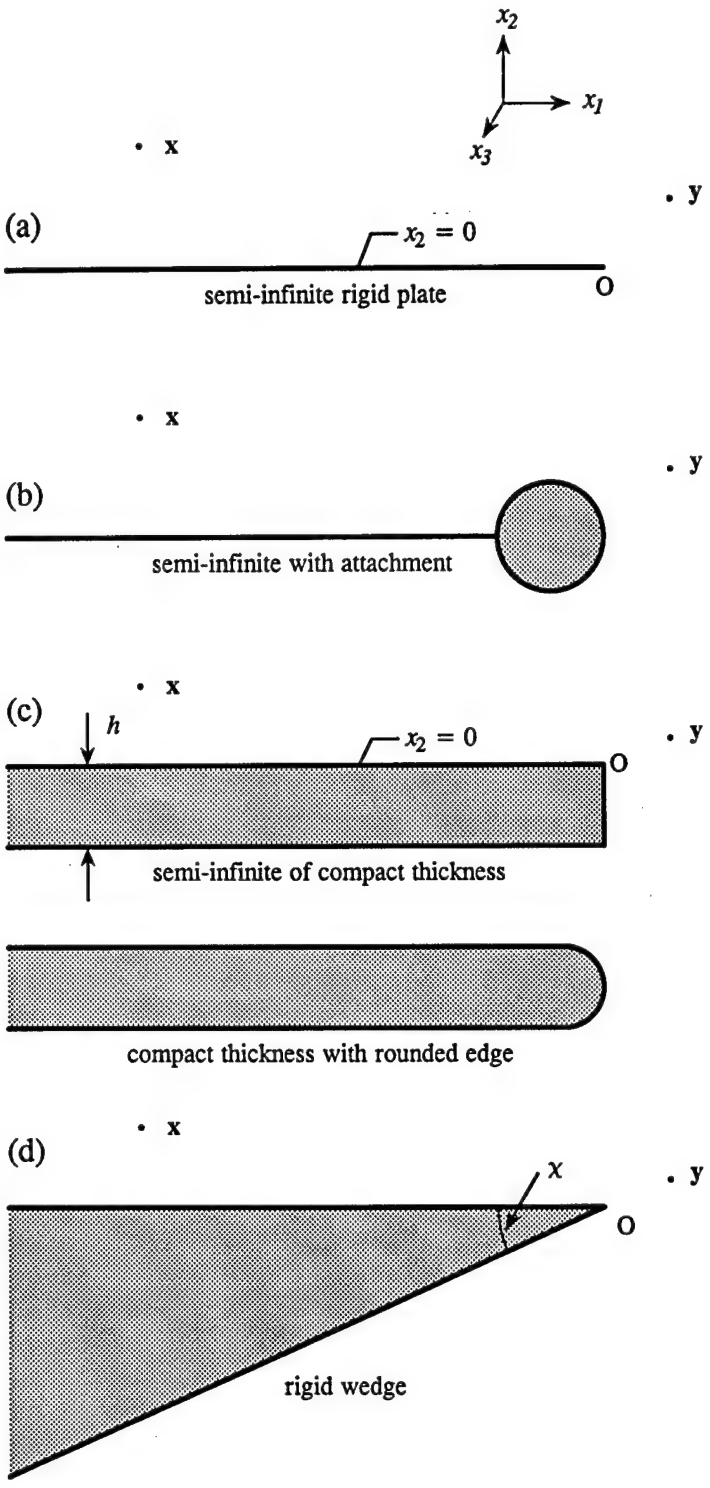

Figure 4.1. Edge scattering configurations.

$\mathbf{i}_3$ is a unit vector parallel to the x_3-axis (the edge), and

$$\varphi^*(\mathbf{x}) = \sqrt{r}\sin(\theta/2) \tag{4.1.3}$$

is a velocity potential of incompressible flow around the edge (in the anticlockwise direction) expressed in terms of polar coordinates $(x_1, x_2) = r(\cos\theta, \sin\theta)$. The component G_0 of G is the radiation from a point source at $\mathbf{y}$ when scattering is neglected. G_1 is the first correction due to the presence of the half-plane, and may also be expressed in the integral form

$$\begin{aligned} G_1(\mathbf{x},\mathbf{y};\omega) &= \frac{\mathrm{sgn}(x_2)\mathrm{sgn}(y_2)}{16\pi^3}\int_{-\infty}^{\infty}\frac{\mathrm{e}^{i\{ky_1+k_1x_1+k_3(x_3-y_3)+\bar\gamma|y_2|+\gamma|x_2|\}}dkdk_1dk_3}{\sqrt{\bar\kappa_o+k}\sqrt{\bar\kappa_o+k_1}(k+k_1+i0)} \\ &\approx \frac{-\varphi^*(\mathbf{y})\mathrm{sgn}(x_2)\mathrm{e}^{\frac{i\pi}{4}}}{4\pi^{\frac{5}{2}}}\iint_{-\infty}^{\infty}\frac{\mathrm{e}^{i\{k_1x_1+\gamma|x_2|+k_3(x_3-y_3)\}}}{\sqrt{\bar\kappa_o+k_1}}\,dk_1dk_3, \quad \kappa_o\sqrt{y_1^2+y_2^2}\ll 1, \end{aligned} \tag{4.1.4}$$

where

$$\gamma = \sqrt{\kappa_o^2-k_1^2-k_3^2}, \quad \bar\gamma = \sqrt{\kappa_o^2-k^2-k_3^2}, \quad \bar\kappa_o = \sqrt{\kappa_o^2-k_3^2}$$

are either real with sign $\mathrm{sgn}(\omega)$ or positive imaginary.

The component G_1 of the compact Green's function reduces to a particularly simple form for two-dimensional problems involving sources with no dependence on the spanwise coordinate x_3. The dependence of G_1 on x_3, y_3 is eliminated by integrating over $-\infty < y_3 < \infty$, using the method of stationary phase for $\kappa_o\sqrt{x_1^2+x_2^2}\to\infty$. When the result is multiplied by $(-1/2\pi)\mathrm{e}^{-i\omega(t-\tau)}$ and integrated over all frequencies, we find

$$G_1(\mathbf{x},\mathbf{y},t-\tau) \approx \frac{\varphi^*(\mathbf{x})\varphi^*(\mathbf{y})}{\pi|\mathbf{x}|}\delta(t-\tau-|\mathbf{x}|/c_o), \quad |\mathbf{x}|\to\infty, \tag{4.1.5}$$

where $\mathbf{x} = (x_1, x_2)$, $\mathbf{y} = (y_1, y_2)$ in two-dimensions. The two-dimensional counterpart of G_0 is independent of $\mathbf{y}$ and is therefore of use only in applications involving monopole sources, which are uninfluenced by the edge to first order.

ii. Rigid half-plane with attachment (Figure 4.1b):

The representations (4.1.1) - (4.1.4) remain valid when the edge of the half plane supports a rigid, "attachment" whose cross-section is acoustically compact and length scale of variation in the spanwise (x_3) direction is compact, provided the potential $\varphi^*(\mathbf{y}) \equiv \varphi^*(y_1, y_2)$ is replaced by $\Phi^*(\mathbf{y}) \equiv \Phi^*(y_1, y_2, y_3)$ which describes potential flow around the irregular edge, such that

$$\Phi^*(y_1, y_2, y_3) \to \varphi^*(y_1, y_2), \quad \text{as } \sqrt{y_1^2+y_2^2}\to\infty.$$

iii. Rigid half-plane of compact thickness (Figure 4.1c):

Formulae (4.1.1) - (4.1.4) can be used provided the wall thickness h is acoustically compact and $\varphi^*(\mathbf{y})$ is re-defined as in Case ii. For example, for the square-edged, thick half-plane of Figure 4.1c (where the negative x_1-axis is assumed to lie in the upper surface, with the origin at the edge) we find by conformal transformation

$$\Phi^*(\mathbf{y}) = -\sqrt{\frac{h}{\pi}}\,\mathrm{Re}\,\zeta$$

$$\frac{z}{h} = f(\zeta) \equiv -\frac{1}{\pi}\Big\{\zeta\sqrt{\zeta^2-1} - \ln(\zeta+\sqrt{\zeta^2-1})\Big\} - i, \tag{4.1.6}$$

where the transformation in the second line maps the fluid region in Figure 4.1c onto the upper half ($\mathrm{Im}\,\zeta > 0$) of the ζ-plane, where $\sqrt{\zeta^2-1}$ is taken to have positive imaginary part.

iv. Rigid wedge (Figure 4.1d):

The dominant term in the compact Green's function for a rigid wedge of interior angle χ can be expressed in the following manner, analogous to $G_1(\mathbf{x},\mathbf{y};\omega)$ of (4.1.2):

$$G(\mathbf{x},\mathbf{y};\omega) \approx \frac{-1}{\pi(2i)^\nu\Gamma(\nu)}\frac{\kappa_o^\nu\varphi^*(\mathbf{x})\varphi^*(\mathbf{y})}{|\mathbf{x}-y_3\mathbf{i}_3|^{1+\nu}}\mathrm{e}^{i\kappa_o|\mathbf{x}-y_3\mathbf{i}_3|}, \quad |\mathbf{x}-y_3\mathbf{i}_3|\to\infty, \quad \nu=\frac{\pi}{2\pi-\chi}, \tag{4.1.7}$$

where $\mathbf{i}_3$ is a unit vector in the x_3-direction (parallel to the edge), and

$$\varphi^*(\mathbf{x}) = \mathrm{Re}\big(z^\nu\mathrm{e}^{-i\nu\pi}\big), \quad z = x_1+ix_2, \tag{4.1.8}$$

is a velocity potential of incompressible flow around the edge (in the anticlockwise direction). When the wedge is rounded, or has an acoustically compact attachment, of the type considered for the half plane, the potential $\varphi^*(\mathbf{y}) \equiv \varphi^*(y_1,y_2)$ must be replaced by $\Phi^*(\mathbf{y}) \equiv \Phi^*(y_1,y_2,y_3)$ which describes potential flow around the irregular edge, with the asymptotic property

$$\Phi^*(y_1,y_2,y_3) \to \mathrm{Re}\big(z'^\nu\mathrm{e}^{-i\nu\pi}\big), \quad z'=y_1+iy_2, \quad \text{as } \sqrt{y_1^2+y_2^2}\to\infty. \tag{4.1.9}$$

For the half-plane, the component G_0 of G represents the radiation from a point source at $\mathbf{y}$ when scattering is neglected; G_1 is the first correction due to presence of the half-plane. Thus, for the Reynolds stress fluctuation $(\rho_o v_i v_j)(\mathbf{x},\omega)$ near the edge, the edge generated acoustic pressure is given by

$$p(\mathbf{x},\omega) \approx \frac{\sqrt{\kappa_o}}{\pi\sqrt{2\pi i}}\int(\rho_o v_i v_j)(\mathbf{y},\omega)\frac{\partial^2\varphi^*(\mathbf{y})}{\partial y_i\partial y_j}\frac{\varphi^*(\mathbf{x})}{|\mathbf{x}-y_3\mathbf{i}_3|^{3/2}}\exp\left(i\kappa_o|\mathbf{x}-y_3\mathbf{i}_3|\right)d^3\mathbf{y}, \ |\mathbf{x}-y_3\mathbf{i}_3|\to\infty.$$

In the time domain $p(\mathbf{x},t) = \int_{-\infty}^{\infty} p(\mathbf{x},\omega)\mathrm{e}^{-i\omega t}d\omega$, but it is not necessary to evaluate the integral to estimate the acoustic efficiency. For an eddy of dimension ℓ and frequency v/ℓ, distance ℓ_0 from the edge, we find

$$p(\mathbf{x},t) \sim \frac{\ell}{|\mathbf{x}|}\left(\frac{\ell}{\ell_0}\right)^{\frac{3}{2}} \rho_o v^2 \sqrt{M}\sin^{\frac{1}{2}}\psi \sin(\tfrac{1}{2}\theta), \quad M \sim v/c_o \ll 1, \quad |\mathbf{x}| \to \infty,$$

where ψ is the angle between the observer direction and the edge of the plate. The acoustic pressure is a maximum in the upstream directions $\theta \approx \pm\pi$,

Thus, the acoustic efficiency $\sim (\ell/\ell_0)^3 M^2$, which is larger than the efficiency of turbulence near a compact solid by a factor $1/M$. For the case of turbulence in a boundary layer flow over the edge, for example, the edge-generated sound power is the same as the direct acoustic power produced by turbulence quadrupoles (of efficiency $\sim M^5$) in a region of the boundary layer extending a distance $\ell_0/M^3 \gg \ell_0$ upstream of the edge. In water this distance can be so large that *all* of the noise can be considered to be generated at the edge. The frequency of the edge noise will also tend to be higher by a factor $\sim U/v$, where U and v are the mean and fluctuating velocity components, because the frequency of the quadrupole sound $\sim v/\delta$, where δ is of the order of the boundary layer thickness, whereas for edge noise the frequency $\sim U/\delta$ is set by the rate at which the turbulence is swept past the edge, where $\partial^2\varphi^*/\partial y_i \partial y_j$ is large.

§4.2 General representation of trailing edge noise [38 - 41]

Consider turbulent flow past the trailing edge of the upper wall ($x_2 = 0$) of a non-compact surface, which may be regarded as any one of the surfaces in Figure 4.1. The main stream outside the boundary layer has low subsonic speed U in the x_1-direction (as indicated in Figure 4.2 for a thin half-plane). The details of the boundary layer turbulence are unknown, but it will be assumed that during the interaction with the edge the statistical properties of the impinging turbulence are the same as those several boundary layer thicknesses upstream. This permits the edge noise to be expressed in terms of the boundary layer wall pressure in the upstream region, which may regarded as uninfluenced by the proximity of the edge.

The calculation of the noise can be formulated as a scattering problem, in which the pressure p_I, say, that would be produced by the same turbulent flow if the surface were removed, is scattered by the edge. The scattered pressure p' includes both acoustic and hydrodynamic components, the latter accounting for the modification of the near field

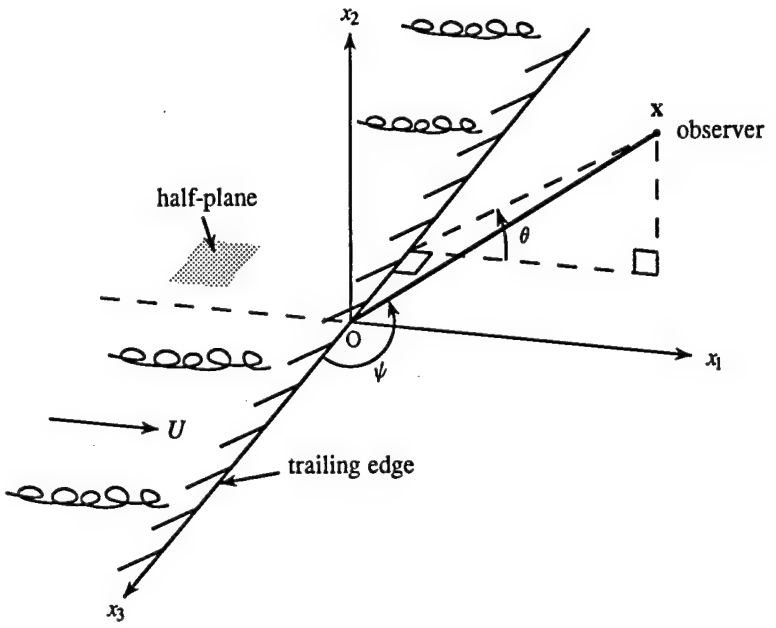

Figure 4.2. Coordinates for trailing edge noise.

pressure by the surface. The condition that the normal velocity vanishes on the surface will be taken in the high Reynolds number approximation

$$\partial p_{\mathrm{I}}/\partial x_n + \partial p'/\partial x_n = 0, \quad \text{on S}, \tag{4.2.1}$$

where S denotes the entire surface (including the "upper", "lower" and "edge region"). We assume that in turbulence-free regions pressure fluctuations of frequency ω satisfy the Helmholtz equation

$$(\nabla^2 + \kappa_o^2)p = 0. \tag{4.2.2}$$

No explicit account is taken of the boundary layer turbulence, except insofar as it is responsible for the pressure p_{I}; in particular $p'(\mathbf{x},\omega)$ is assumed to be a solution of (4.2.2) everywhere, so that the scattering of sound by the shear flow is ignored. This approximation is not valid at very high frequencies when the acoustic wavelength is comparable to the thickness of the boundary layer [42 - 44].

Because of its definition, the pressure $p_{\mathrm{I}}(\mathbf{x},\omega)$ must be an outgoing solution of Helmholtz's equation in $x_2 \leq 0$, in the region "below" the boundary layer sources, and is equal to *half* the boundary layer blocked pressure p_s on $x_2 = +0$ (c.f. equation (3.2.7)). Hence,

$$p_{\mathrm{I}}(\mathbf{x},\omega) = \frac{1}{2}\iint_{-\infty}^{\infty} p_s(\mathbf{k},\omega)\mathrm{e}^{i(\mathbf{k}.\mathbf{x}-\gamma(k)x_2)}dk_1dk_3, \quad x_2 \leq 0, \tag{4.2.3}$$

where $\gamma(k)$ is defined as in (4.1.4). The problem of determining p' now reduces to a consideration of the scattering of each Fourier component $\frac{1}{2}p_s(\mathbf{k},\omega)\mathrm{e}^{i(\mathbf{k}.\mathbf{x}-\gamma(k)x_2)}$ of p_{I} by S.

The scattered pressure p' is an outgoing disturbance both above and below S, and has the following general representation in terms of the Kirchhoff formula

$$p'(\mathbf{x},\omega) = -\oint_{\mathrm{S}} \frac{\partial p_{\mathrm{I}}}{\partial y_n}(y_1,0,y_3,\omega)G(\mathbf{x},\mathbf{y};\omega)d\mathrm{S}(\mathbf{y}), \tag{4.2.4}$$

provided Green's function is chosen to have vanishing normal derivative on S, and y_n is normal to S and directed into the fluid. At low Mach numbers the distances of those turbulence eddies from the edge that are responsible for the edge noise are always very much smaller than the acoustic wavelength, so that $G(\mathbf{x},\mathbf{y};\omega)$ may be approximated by the generalized form of the compact Green's function (4.1.2), for which $\varphi^*(\mathbf{y})$ is replaced by $\Phi^*(\mathbf{y})$ (as described in §4.1ii, iii).

When the result of this calculation is integrated over all frequencies, the pressure in the acoustic far field is found to be given by

$$p(\mathbf{x},t) \approx \frac{\sin^{\frac{1}{2}}\psi \sin(\frac{1}{2}\theta)}{|\mathbf{x}|\sqrt{2\pi i c_o}} \iint_{-\infty}^{\infty} \sqrt{\omega}\mathcal{I}(k_1) p_s\left(k_1, \frac{\kappa_o x_3}{|\mathbf{x}|}, \omega\right) \mathrm{e}^{-i\omega(t-|\mathbf{x}|/c_o)} dk_1 d\omega, \quad |\mathbf{x}| \to \infty. \tag{4.2.5}$$

where $\theta = \arcsin(x_2/\sqrt{x_1^2+x_2^2})$, and ψ is the angle between the observer direction and the edge (the x_3-axis, see Figure 4.2 for the thin half-plane). The peak acoustic pressures are radiated in the "forward" directions $\theta = \pm\pi$. The influence of edge geometry is governed by the complex valued function $\mathcal{I}(k_1)$ which is defined by

$$\begin{aligned} \mathcal{I}(k_1) &= \text{c.c.} \left(i \oint_C \frac{dw(z)}{dz} \mathrm{e}^{-ik_1 z} dz \right), \qquad k_1 > 0, \quad z = y_1 + iy_2; \\ \mathcal{I}(k_1) &= \text{c.c.} \left\{ \mathcal{I}(-k_1) \right\}, \qquad k_1 < 0 \end{aligned} \tag{4.2.6}$$

where $w(z)$ is the analytic function whose real part is $\Phi^*(\mathbf{y})$, "c.c." denotes complex conjugate, and the integration is taken in the *anticlockwise* sense around the contour C formed by the surface profile of S in the y_1y_2-plane . If a spanwise section of the edge of length L is wetted by the turbulent flow, the relation (3.9.4) may now be used to express the acoustic pressure frequency spectrum in the form

$$\Phi(\mathbf{x},\omega) \approx \frac{\omega L \sin^2(\theta/2)\sin\psi}{2\pi^2 c_o |\mathbf{x}|^2} \int_{-\infty}^{\infty} |\mathcal{I}(k_1)|^2 \mathrm{P}(k_1, \kappa_o \cos\psi, \omega)\, dk_1, \quad |\mathbf{x}| \to \infty, \tag{4.2.7}$$

This formula is applied using measured values of the wall pressure spectrum $\mathrm{P}(\mathbf{k},\omega)$. In practice, most estimates and comparisons with experiment are based on a measurement of the surface pressure frequency spectrum $\Phi_{pp}(\omega)$ at a single point, which is then used in an empirical model of $\mathrm{P}(\mathbf{k},\omega)$ which depends linearly on $\Phi_{pp}(\omega)$. The simplest is the Corcos model (3.2.3), which represents the behavior of $\mathrm{P}(\mathbf{k},\omega)$ at low Mach numbers when $\omega\delta_*/U > 0.1$ ($\delta_* \approx \delta/8$) in the immediate vicinity of the convective ridge (Figure 3.1), where the spectrum has a large maximum. Because of the dominant contribution from this region, the integral (4.2.7) may often be approximated by setting $k_1 = \omega/U_c$ in $\mathcal{I}(k_1)$, i.e.

$$\Phi(\mathbf{x},\omega) \approx \frac{\omega L \sin^2(\theta/2)\sin\psi}{2\pi^2 c_o |\mathbf{x}|^2} \left|\mathcal{I}\left(\frac{\omega}{U_c}\right)\right|^2 \int_{-\infty}^{\infty} \mathrm{P}(k_1, \kappa_o \cos\psi, \omega)\, dk_1, \quad |\mathbf{x}| \to \infty, \tag{4.2.8}$$

§4.3 Influence of surface geometry on edge noise

The details of edge geometry become important at high frequencies, when the turbulence length scale is comparable to the radius of curvature of the edge. The following examples illustrate the trends to be expected for three different edge types:

Thin half-plane This is the canonical case (a) of Figure 4.1, for which

$$w(z) = -i\sqrt{z}, \qquad \mathcal{I}(k_1) = -\sqrt{\frac{\pi}{k_1}}\, e^{\frac{i\pi}{4}}, \quad k_1 > 0. \tag{4.3.1}$$

Square-edge The first of case (c) in Figure 4.1; compact wall thickness h:

$$w(z) = -\sqrt{\frac{h}{\pi}}\zeta, \qquad |\mathcal{I}(k_1)| \approx \sqrt{\frac{\pi}{k_1}}\frac{0.71}{(k_1h)^{\frac{1}{6}}}\,\frac{\{1+0.25k_1h+(k_1h)^2\}}{1+(k_1h)^2}, \quad k_1h > 0.1, \tag{4.3.2}$$

where $\zeta(z)$ is defined in (4.1.6)

Rounded edge Probably the simplest case amenable to analytical treatment is shown in Figure 4.3b. The boundary of the rounded edge is mapped onto the real ζ-axis, and the fluid is mapped into $\mathrm{Im}\,\zeta > 0$ by

$$\frac{z}{h} = \frac{f(\zeta)+\alpha f(\zeta/\beta)}{1+\alpha}, \quad \text{and} \quad w(z) = -\sqrt{\frac{h(1+\alpha/\beta^2)}{\pi(1+\alpha)}}\zeta, \tag{4.3.3}$$

where $f(\zeta)$ is given in (4.1.6), and α and β are numerical coefficients. For the case shown in Figure 4.3b, $\alpha = 0.0013$, $\beta = 0.02$, the mean radius of curvature of the edge $\sim 1.14h$, and

$$|\mathcal{I}(k_1)| \approx \sqrt{\frac{\pi}{k_1}}\,\exp\left(-\frac{k_1h}{4} - \frac{(k_1h)^2}{20.25}\right), \quad k_1 > 0. \tag{4.3.4}$$

Half-plane with cylindrical attachment (Figure 4.3a). The semi-infinite plane ($x_1 < 0$, $x_2 = 0$) is smoothly connected at its edge to a circular cylinder of diameter D on the underside ($x_2 = -0$):

$$w(z) = -\sqrt{2\pi D}\zeta, \qquad |\mathcal{I}(k_1)| \approx \sqrt{\frac{\pi}{k_1}}\, e^{-\alpha k_1 D}, \quad k_1 > 0, \quad \alpha = \left(\frac{3}{2\pi}\right)^2 \tag{4.3.5}$$

where the fluid region is mapped onto the upper half of the ζ-plane by

$$\frac{z}{D} = \frac{\pi\zeta}{1+\zeta\ln\left(1-\frac{1}{\zeta}\right)}. \tag{4.3.6}$$

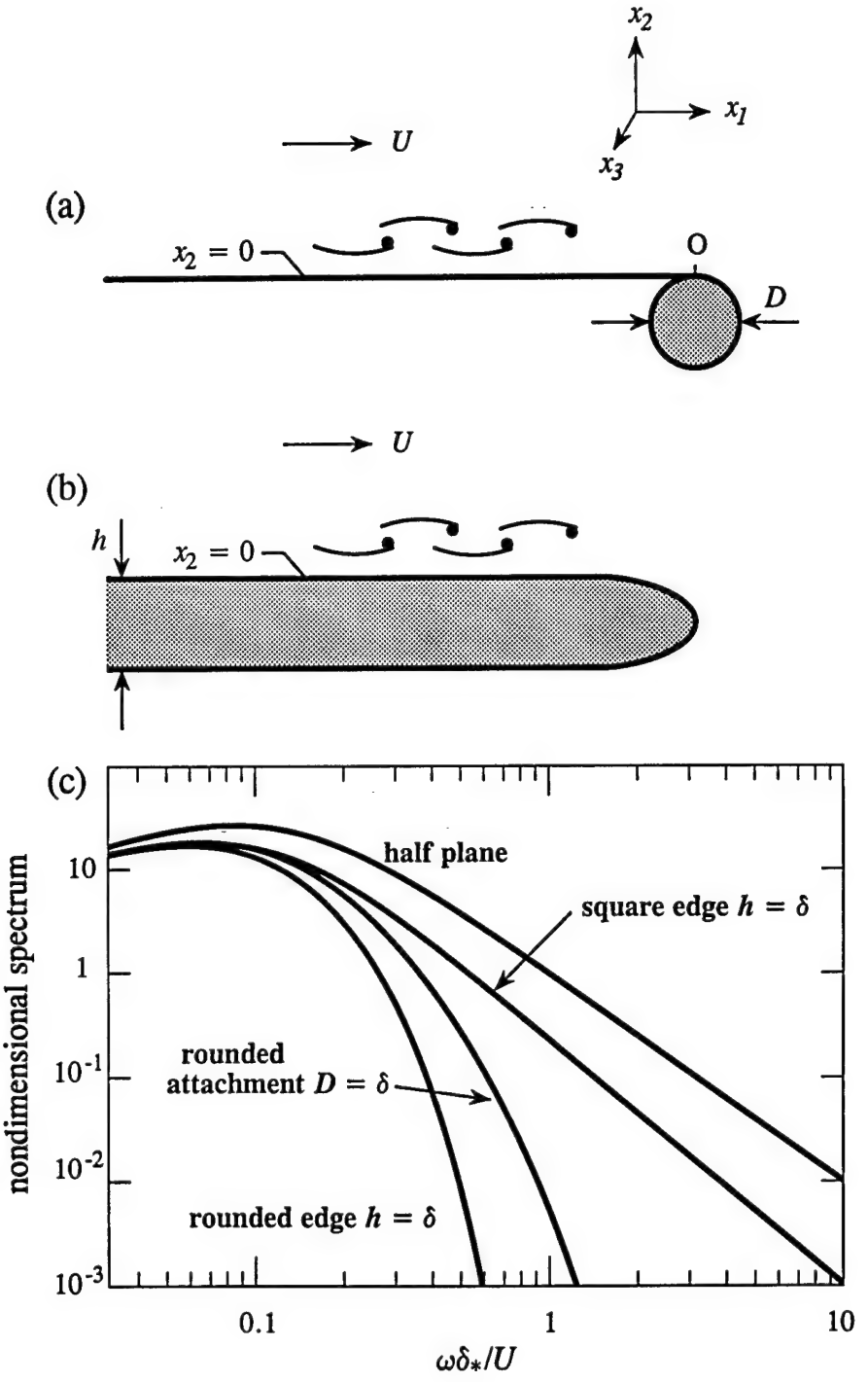

Figure 4.3. Predicted edge noise spectrum $(U/\delta_*)\Phi(\mathbf{x},\omega)/[a_o(\rho_o v_*^2)^2 M(L\delta_*/|\mathbf{x}|^2)\sin\psi\sin^2(\theta/2)]$ for the half-plane; for square edge of thickness $h = \delta$; for a half-plane with rounded attachment of diameter $D = \delta$; and for a rounded edge of thickness $h = \delta$.

When the Corcos model (3.2.3), (3.2.4) is used, the acoustic pressure frequency spectrum (4.2.8) can be expressed in the non-dimensional form

$$\frac{(U/\delta_*)\Phi(\mathbf{x},\omega)}{(\rho_o v_*^2)^2} \approx M\left(\frac{L\delta_*}{|\mathbf{x}|^2}\right)\sin\psi\sin^2\left(\frac{\theta}{2}\right)\left(\frac{\omega}{\pi U_c}\right)\left|\mathcal{I}\left(\frac{\omega}{U_c}\right)\right|^2 \frac{a_o(\omega\delta_*/U)}{[\alpha_p^2+(\omega\delta_*/U)^2]^{\frac{3}{2}}}, \quad a_0 = 0.035, \tag{4.3.7}$$

where $M = U/c_o$ is the Mach number of the main stream. In particular, for the half-plane

$$\frac{(U/\delta_*)\Phi(\mathbf{x},\omega)}{(\rho_o v_*^2)^2} \approx M\left(\frac{L\delta_*}{|\mathbf{x}|^2}\right)\sin\psi\sin^2\left(\frac{\theta}{2}\right)\frac{a_o(\omega\delta_*/U)}{[\alpha_p^2+(\omega\delta_*/U)^2]^{\frac{3}{2}}}. \tag{4.3.8}$$

The general expression (4.3.7) for arbitrary edge geometry reduces to this result when the hydrodynamic length scale U_c/ω is much larger than the characteristic dimension of the edge.

The predicted forms of the acoustic pressure spectra are compared in Figure 4.3 for the above cases in the particular case in which $h = D = \delta$, where δ is the turbulent boundary layer thickness for flow over the upper surface.

The surface pressure. The surface pressure on the upper surface of a thin *half-plane* determined by the scattering theory of §4.2 can be cast in the form

$$p(x_1,\pm 0,x_3,\omega) = \frac{1}{2}\iint_{-\infty}^{\infty} p_s(\mathbf{k},\omega)\left[1\pm\operatorname{erf}\left(e^{-\frac{i\pi}{4}}|x_1|^{\frac{1}{2}}\sqrt{(\kappa_o^2-k_3^2)^{1/2}+k_1}\,\right)\right]e^{i\mathbf{k}.\mathbf{x}}\,d^2\mathbf{k}, \quad x_1<0, \tag{4.3.9}$$

where $\mathbf{k} = (k_1, k_3)$ and the $\pm$ sign is taken on the upper/lower surface $x_2 = \pm 0$. The argument of the error function has positive real part for all real values of k_1, so that the error function ≈ 1 as $x_1 \to -\infty$. Thus, $p \to 0$ on the lower surface ($x_2 = -0$) far upstream of the edge, whereas $p \to p_s \equiv 2p_I$ on the surface $x_2 = +0$ exposed to the turbulent stream. This occurs at distances upstream of the edge exceeding the characteristic eddy dimension, and represents a pressure doubling by "specular reflection" of the incident pressure p_I by the plane, rigid surface. Thus, if the impinging boundary layer turbulence is assumed to convect as a frozen pattern over the edge, measurements of the upstream wall pressure p_s (or, rather, of its wavenumber-frequency spectrum) can be used to predict the edge noise spectrum.

§4.4 Noise from flow over a right-angled wedge

Consider the edge noise generated by turbulent boundary layer flow off the upper surface $x_2 = +0$ of the rigid, right angled wedge bounded by the planes $x_1 < 0,\ x_2 = 0$ and $x_1 = 0,\ x_2 < 0$. We regard the turbulence as frozen during its convection past the edge, and determine the sound generated for the two wedges illustrated in Figure 4.4: (a) with a sharp, and (b) with a rounded edge.

For a wedge of arbitrary interior angle χ, we find by the method of §4.2, using Green's function (4.1.7), with $\varphi^*(\mathbf{y})$ replaced by $\Phi^*(\mathbf{y})$ for a rounded edge geometry, that the acoustic pressure is given by

$$p(\mathbf{x},t) \approx \frac{\varphi^*(\mathbf{x})}{(2ic_o)^\nu \Gamma(\nu)|\mathbf{x}|^{1+\nu}} \iint_{-\infty}^{\infty} \omega^\nu \mathcal{I}(k_1) p_s\left(k_1, \frac{\kappa_o x_3}{|\mathbf{x}|}, \omega\right) \mathrm{e}^{-i\omega(t-|\mathbf{x}|/c_o)} dk_1 d\omega, \quad |\mathbf{x}| \to \infty, \tag{4.4.1}$$

where $\nu = \pi/(2\pi - \chi)$, and $\mathcal{I}(k_1)$ is defined as in (4.2.6) with the path of integration in the z-plane being over the profile of the wedge in the y_1y_2-plane in the anticlockwise sense. The corresponding frequency pressure spectrum for a wetted span of length L is

$$\begin{aligned}\Phi(\mathbf{x},\omega) &\approx \frac{L}{\pi}\left(\frac{\cos\nu(\theta-\pi)}{\Gamma(\nu)|\mathbf{x}|}\right)^2 \left(\frac{\omega\sin\psi}{2c_o}\right)^{2\nu} \int_{-\infty}^{\infty} |\mathcal{I}(k_1)|^2 \mathrm{P}(k_1, \kappa_o\cos\psi, \omega)\, dk_1 \\ &\approx \frac{L}{\pi}\left(\frac{\cos\nu(\theta-\pi)}{\Gamma(\nu)|\mathbf{x}|}\right)^2 \left(\frac{\omega\sin\psi}{2c_o}\right)^{2\nu} \left|\mathcal{I}\left(\frac{\omega}{U_c}\right)\right|^2 \int_{-\infty}^{\infty} \mathrm{P}(k_1, \kappa_o\cos\psi, \omega)\, dk_1 \quad |\mathbf{x}| \to \infty.\end{aligned} \tag{4.4.2}$$

For a sharp cornered wedge

$$w = z^\nu \mathrm{e}^{-i\nu\pi}, \qquad \mathcal{I}(k_1) = \frac{-2\nu\sin(\nu\pi)\Gamma(\nu)\mathrm{e}^{i\frac{\nu\pi}{2}}}{(k_1+i0)^\nu}. \tag{4.4.3}$$

Hence, for the

Sharp right-angled corner (Figure 4.4a): $\nu = \frac{2}{3}$, and

$$w(z) = z^{\frac{2}{3}}\mathrm{e}^{-\frac{2\pi i}{3}}, \qquad \mathcal{I}(k_1) = \frac{-2\Gamma(\frac{2}{3})\mathrm{e}^{i\frac{\pi}{3}}}{\sqrt{3}(k+i0)^{\frac{2}{3}}}. \tag{4.4.4}$$

The Corcos model (3.2.4) then yields

$$\frac{(U/\delta_*)\Phi(\mathbf{x},\omega)}{(\rho_o v_*^2)^2} \approx M^{\frac{4}{3}}\left(\frac{\delta_* L}{|\mathbf{x}|^2}\right)\cos^2\left(\frac{2}{3}(\theta-\pi)\right)\sin^{\frac{4}{3}}\psi\, \frac{a_o'(\omega\delta_*/U)}{[\alpha_o^2+(\omega\delta_*/U)^2]^{\frac{3}{2}}}, \quad |\mathbf{x}| \to \infty, \tag{4.4.5}$$

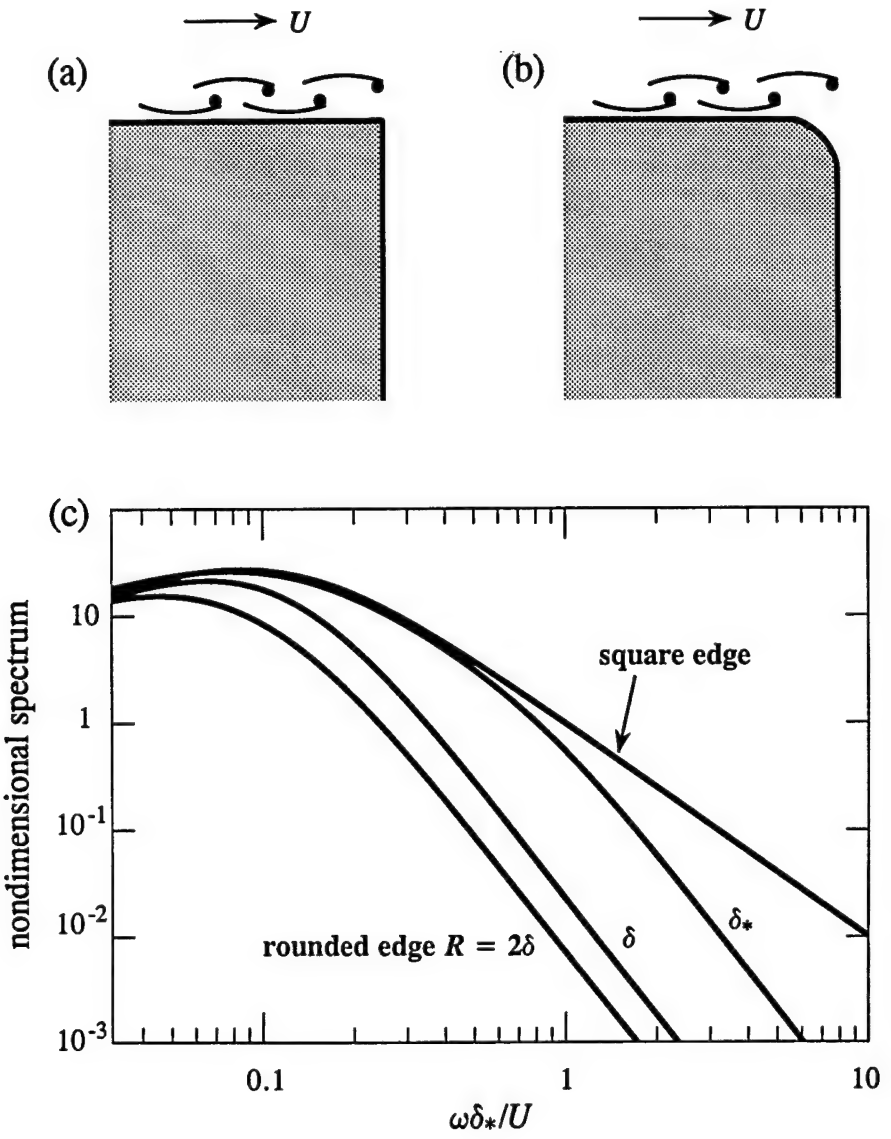

Figure 4.4. Predicted noise spectrum $(U/\delta_*)\Phi(\mathbf{x},\omega)/[a_o'(\rho_o v_*^2)^2 M^{\frac{4}{3}}(L\delta_*/|\mathbf{x}|^2)\sin^{\frac{4}{3}}\psi\cos^2(\frac{2}{3}(\theta-\pi))]$ for square-edged and rounded right-angled wedges; R is the mean radius of curvature of the rounded edge.

where $a_o' = 0.033$. This approximation is strictly applicable when both faces of the wedge are large compared to the acoustic wavelength.

Rounded right-angled corner: An estimate of the influence of rounding can be obtained from the case illustrated in Figure 4.4b, for which

$$w(z) = -\left(\frac{16R}{3\pi}\right)^{\frac{2}{3}}\zeta, \quad |\mathcal{I}(k_1)| = \frac{2\Gamma(\frac{2}{3})}{\sqrt{3}|k_1|^{\frac{2}{3}}}\mathcal{F}(k_1R), \tag{4.4.6}$$

where R is the mean radius of curvature of the edge, and $\zeta(z)$ and $\mathcal{F}(k_1R)$ are defined by

$$\frac{z}{R} = \frac{-8i}{3\pi}\left(\zeta^{\frac{3}{2}} + (1+\zeta)^{\frac{3}{2}}\right), \quad \mathcal{F}(k_1R) \approx \left(\frac{1.18 - 0.126\xi + 2.3\xi^2 + 0.5\xi^3}{(1+0.16\xi+0.1\xi^2+\xi^3)(1+\xi)}\right), \quad \xi = (k_1R)^{\frac{2}{3}}. \tag{4.4.7}$$

The first of equations (4.4.7) maps the upper half of the ζ-plane onto the profile in the plane $z = x_1 + ix_2$ of the fluid region bounded by the rounded wedge, with the real ζ-axis corresponding to the wedge profile. The acoustic pressure spectrum $\Phi(\mathbf{x},\omega)$ for this case is obtained by multiplying the sharp-cornered expression (4.4.5) by $\mathcal{F}^2(\omega R/U_c)$.

Figure 4.4c compares the edge noise spectra for these two cases. For the rounded edge $\Phi(\mathbf{x},\omega)$ does not decrease exponentially fast at high frequencies, but $\Phi(\mathbf{x},\omega) \sim O(1/\omega^{\frac{10}{3}})$. This is because the edge rounding in the model of Figure 4.4b has a continuous slope, but the *curvature* is discontinuous at each end of the rounded sections.

§4.5 Influence of mean flow direction

When the mean flow over the trailing edge is inclined at an angle β ($< 90°$) to the x_1-axis (see Figure 4.2) the edge noise spectrum continues to be given by the general formula (4.2.5). To derive the analog of equation (4.2.7) for the acoustic pressure spectrum we must make use of the following corrected form of the relation (3.9.4)

$$\langle p_s(k_1,k_3,\omega)p_s^*(k_1',k_3,\omega')\rangle \approx \frac{L}{2\pi\cos\beta}\delta(\omega-\omega')\delta(k_1-k_1')\mathrm{P}'(k_1,k_3,\omega), \quad L \gg \delta. \tag{4.5.1}$$

where L is the transverse width of the turbulent stream (so that the wetted edge of the airfoil has length $L/\cos\beta$), and $\mathrm{P}'(k_1,k_3,\omega)$ here denotes the blocked pressure spectrum defined with respect to the x-coordinate system. This system is inclined at angle β to the mean flow. Let $\mathrm{P}(K_1,K_3,\omega)$ denote the wall pressure spectrum defined relative to a coordinate system in which the K_1-axis is parallel to the mean flow, then

$$\mathrm{P}'(k_1,\kappa_o\cos\psi,\omega) \approx \mathrm{P}(k_1\cos\beta, k_1\sin\beta,\omega), \quad M \to 0, \tag{4.5.2}$$

and (4.2.7) becomes

$$\Phi(\mathbf{x},\omega) \approx \frac{\omega L \sin^2(\theta/2)\sin\psi}{2\pi^2 c_o \cos\beta|\mathbf{x}|^2}\int_{-\infty}^{\infty}|\mathcal{I}(k_1)|^2\mathrm{P}(k_1\cos\beta,k_1\sin\beta,\omega)\,dk_1, \quad |\mathbf{x}|\to\infty,$$

$$\approx \frac{\omega L \sin^2(\theta/2)\sin\psi}{2\pi^2 c_o \cos^2\beta|\mathbf{x}|^2}\left|\mathcal{I}\left(\frac{\omega}{U_c\cos\beta}\right)\right|^2\int_{-\infty}^{\infty}\mathrm{P}\left(k_1,\frac{\omega\tan\beta}{U_c},\omega\right)\,dk_1. \qquad (4.5.3)$$

The Corcos approximation (4.3.7) then reduces to

$$\frac{(U/\delta_*)\Phi(\mathbf{x},\omega)}{(\rho_o v_*^2)^2} \approx M\left(\frac{L\delta_*}{|\mathbf{x}|^2}\right)\frac{\sin\psi\sin^2\left(\frac{\theta}{2}\right)}{\cos\beta}\left(\frac{\omega}{\pi U_c\cos\beta}\right)\left|\mathcal{I}\left(\frac{\omega}{U_c\cos\beta}\right)\right|^2$$

$$\times\frac{a_o(\omega\delta_*/U)}{[\alpha_o^2+(\omega\delta_*/U)^2]^{\frac{3}{2}}[1+(1.4)^2\tan^2\beta]}, \quad a_0=0.035. \qquad (4.5.4)$$

5. BLADES AND BLADE TIPS

The efficiency of aerodynamic sound generation by lifting surfaces of compact chord is the same as for an acoustically rigid, compact body ($\propto M^3$). The amplitude of the self-noise generated by a short section of the trailing edge generally depends on the orientation of the section relative to the mean flow (§4.5). The importance of this can be worked out exactly for surfaces of elliptic planform, and approximately for any slowly varying planform. In particular, the influence of blade tip contributions can be estimated.

§5.1 Green's functions

We consider Green's functions for a sequence of three thin airfoils of increasingly complex planform, but of acoustically compact *chord.*

The strip airfoil:

Let the airfoil have constant chord $2a$ and infinite span (Figure 5.1a). Take coordinate axes as in the Figure, with the origin on the midspan and the x_1, x_2, x_3-axes respectively in the direction of the mean flow, the mean lift and the span. The time and frequency domain compact Green's functions are defined as in (2.4.13) and (2.4.14) with

$$X_1 = x_1, \quad X_2 = \mathrm{Re}\Big\{ -i\sqrt{z^2 - a^2}\Big\}, \quad X_3 = x_3, \quad \text{where} \quad z = x_1 + ix_2 \tag{5.1.1}$$

Airfoil with slowly varying chord:

The definition (5.1.1) is applicable also when the chord varies *slowly* with x_3, i.e., when

$$a \equiv a(x_3), \quad \frac{da}{dx_3} \ll 1.$$

Elliptic airfoil:

Let the planform be the ellipse (Figure 5.1b)

$$f(x_1, x_3) \equiv \frac{x_1^2}{a^2} + \frac{x_3^2}{c^2} - 1 = 0, \tag{5.1.2}$$

then

$$\begin{aligned} X_1 &= x_1, \quad X_2 = x_2 - \varphi^*(\mathbf{x}), \quad X_3 = x_3, \\ \varphi^*(\mathbf{x}) &= \frac{-x_2}{\Psi(0)}\left[\frac{a}{\sqrt{\Lambda}} - \Psi\left(\frac{\sqrt{\Lambda}}{a}\right)\right], \\ \Psi(x) &= \int_x^\infty \frac{(1+\alpha^2+\mu^2)d\mu}{\sqrt{1+\mu^2}\sqrt{\alpha^2+\mu^2}[\alpha + \sqrt{1+\mu^2}\sqrt{\alpha^2+\mu^2}]}, \quad \alpha = \frac{c}{a}, \end{aligned} \tag{5.1.3}$$

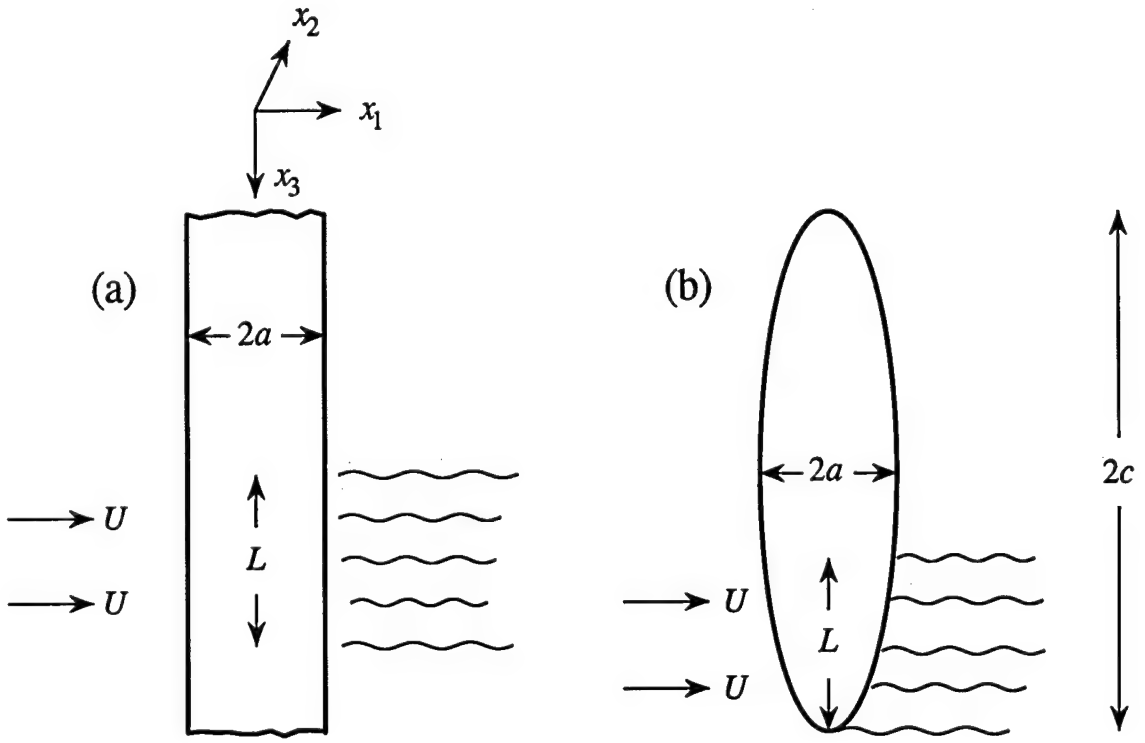

Figure 5.1. (a) Strip airfoil of chord $2a$; (b) Elliptic airfoil of aspect ratio c/a.

and $\Lambda(\mathbf{x})$ is the positive root of [45]

$$\frac{x_1^2}{a^2+\Lambda}+\frac{x_2^2}{\Lambda}+\frac{x_3^2}{c^2+\Lambda}=1. \tag{5.1.4}$$

Near the airfoil $\Lambda(\mathbf{x}) \to +0$, and

$$\Lambda \approx \frac{f(x_1,x_3)\mathrm{H}\big(f(x_1,x_3)\big)}{x_1^2/a^4+x_3^2/c^4}+\frac{x_2^2}{|f(x_1,x_3)|}, \tag{5.1.5}$$

$$X_2 \approx \frac{x_2}{\Psi(0)}\left[\frac{a}{\sqrt{\Lambda}}+\frac{\sqrt{\Lambda}}{2a}\left(1+\frac{1}{\alpha^2}\right)\right]. \tag{5.1.6}$$

where H is the Heaviside step function.

§5.2 Trailing edge self-noise

Consider low Mach number mean flow at speed U in the x_1-direction. The self-noise generated at the trailing edge can be expressed in the form (4.2.4). In the acoustic far field the analog of (4.2.5) becomes

$$p(\mathbf{x},t) \approx \frac{-\cos\Theta}{8\pi c_o|\mathbf{x}|}\iint_{-\infty}^{\infty}\omega\gamma(k)\mathcal{I}(\mathbf{k})p_s(\mathbf{k},\omega)\mathrm{e}^{-i\omega(t-|\mathbf{x}|/c_o)}dk_1dk_3d\omega, \quad |\mathbf{x}|\to\infty. \tag{5.2.1}$$

In this formula $\mathbf{k}=(k_1,0,k_3)$, γ is defined as in (4.1.4), $\Theta=\arccos(x_2/|\mathbf{x}|)$ is the angle between the airfoil normal (x_2-axis) and the radiation direction, and

$$\mathcal{I}(\mathbf{k})=\int\big[X_2(\mathbf{y})\big]_-^+\mathrm{e}^{i\{k_1y_1+(k_3-\kappa_o\cos\psi)y_3\}}d\mathrm{S}(\mathbf{y}), \tag{5.2.2}$$

where ψ is the angle between the spanwise direction (x_3-axis) and $\mathbf{x}$, and the integration is over the upper surface ($x_2=+0$) of the airfoil. The function $X_2(\mathbf{y})$ exhibits the following discontinuous behavior across the airfoils:

$$\begin{aligned}\big[X_2(\mathbf{y})\big]_-^+ &= X_2(y_1,+0,y_3)-X_2(y_1,-0,y_3) \\ &= 2\sqrt{a^2-x_1^2}, && \text{strip airfoil;} \\ &= 2\sqrt{a(x_3)^2-x_1^2}, && \text{slowly varying chord;} \\ &= \frac{2a}{\Psi(0)}\sqrt{1-\frac{x_1^2}{a^2}-\frac{x_3^2}{c^2}}, && \text{elliptic airfoil.}\end{aligned} \tag{5.2.3, 5.2.4}$$

When the slowly varying chord approximation is applied to the elliptic airfoil we make the substitution

$$a(x_3) \to a\sqrt{1-\frac{x_3^2}{c^2}},$$

in which case

$$\left[X_2(\mathbf{y})\right]_-^+ \approx 2a\sqrt{1-\frac{x_1^2}{a^2}-\frac{x_3^2}{c^2}},$$

which agrees with the exact expression in (5.2.4) provided $\Psi(0) \approx 1$. Figure 5.2 shows that this is an excellent approximation when the aspect ratio $\alpha = c/a$ of the elliptic airfoil exceeds about 5.

To evaluate the integral (5.2.2) only the contribution from the vicinity of the trailing edge $x_1 = a(x_3)$ must be retained. For the strip airfoil, and turbulence length scales that are much smaller than the airfoil chord ($ka \gg 1$), we write

$$\begin{aligned}\mathcal{I}(\mathbf{k}) &= 2\int \sqrt{a^2-y_1^2}\, e^{i\{k_1 y_1 + (k_3-\kappa_o\cos\psi)y_3\}} dS(\mathbf{y}) \\ &\sim 4\pi\sqrt{2a}\,\delta(k_3-\kappa_o\cos\psi)\int_{-\infty}^{a}\sqrt{a-y_1}\, e^{ik_1y_1}dy_1 = -2\pi\sqrt{2\pi a}\,\delta(k_3-\kappa_o\cos\psi)\frac{e^{i(k_1a+\frac{\pi}{4})}}{k_1^{3/2}}\end{aligned} \tag{5.2.5}$$

Using this in (5.2.1) and calculating the acoustic pressure frequency spectrum $\Phi(\mathbf{x},\omega)$ for the wetted section of the trailing edge of span L shown in Figure 5.1a, we find (using (3.9.4)), for the

Strip airfoil:

$$\begin{aligned}\Phi(\mathbf{x},\omega) &\approx \frac{aL}{8|\mathbf{x}|^2}\frac{\omega^2\cos^2\Theta}{c_o^2}\int_{-\infty}^{\infty}\frac{P(k_1,\kappa_o\cos\psi,\omega)\,dk_1}{|k_1|} \\ &\approx 0.027\,\frac{aLM^2\cos^2\Theta\Phi_{pp}(\omega)}{|\mathbf{x}|^2}, \quad M\equiv\frac{U}{c_o}\ll 1, \quad \omega a/U\gg 1, \quad |\mathbf{x}|\to\infty,\end{aligned} \tag{5.2.6}$$

where the Corcos formula (3.2.3) has been used to obtain the second line.

The integral (5.2.2) defining $\mathcal{I}(\mathbf{k})$ for the elliptic airfoil is evaluated by first expanding $[X_2(\mathbf{y})]_-^+$ about the trailing edge $y_1 = a\sqrt{1-y_2^3/c^2}$, as in (5.2.5), by writing

$$\sqrt{1-\frac{y_1^2}{a^2}-\frac{y_3^2}{c^2}} \sim \sqrt{2}\left(1-\frac{y_3^2}{c^2}\right)^{\frac{1}{4}}\sqrt{\left(1-\frac{y_3^2}{c^2}\right)^{\frac{1}{2}}-\frac{y_1}{a}},$$

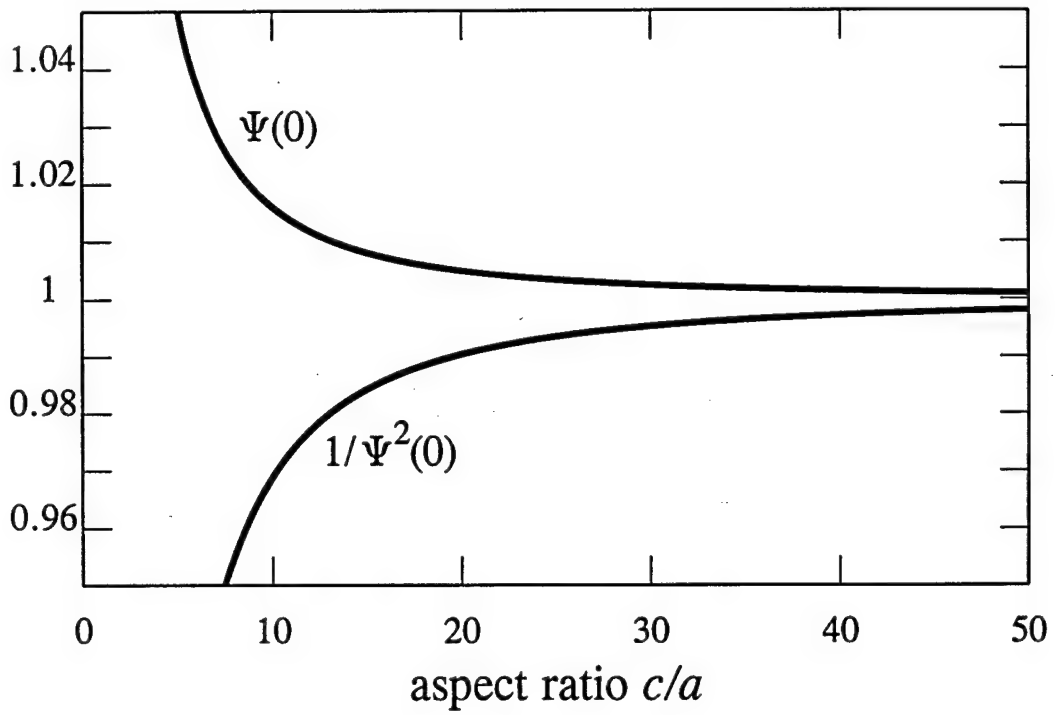

Figure 5.2. Dependence of $\Psi(0)$ and $1/\Psi^2(0)$ on aspect ratio c/a.

and performing the y_1-integration over the range $-\infty < y_1 < a\sqrt{1-y_2^3/c^2}$. Let us suppose, as indicated in Figure 5.1b, that a section of the trailing edge of length L *inboard of the blade tip* is wetted by the flow, and examine the contribution to the radiation from the tip region. Then

$$\mathcal{I}(\mathbf{k}) \approx \frac{-\sqrt{2\pi i a}}{\Psi(0)k_1^{3/2}} \int_{c-L}^{c} \left(1-\frac{y_3^2}{c^2}\right)^{\frac{1}{4}} \exp\left\{i\left(k_1 a\sqrt{1-\frac{y_3^2}{c^2}} + (k_3-\kappa_o\cos\psi)y_3\right)\right\} dy_3.$$

When the turbulence scales are much smaller than the airfoil chord ($ka \gg 1$), the principal contributions to this integral are from the neighborhood of that value of y_3 where the phase of the exponential is stationary. Geometrically, this corresponds to the condition that the vector $(k_1, 0, k_3 - \kappa_o\cos\psi)$ be parallel to the normal to the elliptic trailing edge, and yields

$$\mathcal{I}(\mathbf{k}) \approx \frac{-2\pi a^2 c \exp\left\{i\sqrt{k_1^2a^2+(k_3-\kappa_o\cos\psi)^2c^2}\right\}}{\Psi(0)[k_1^2a^2+(k_3-\kappa_o\cos\psi)^2c^2]} \mathrm{H}\left(\frac{k_3-\kappa_o\cos\psi}{k_1} - \frac{a(1-L/c)}{\sqrt{Lc}\sqrt{2-L/c}}\right). \tag{5.2.7}$$

H is the Heaviside step function, whose argument is positive provided the point on the trailing edge where $(k_1, 0, k_3 - \kappa_o\cos\psi)$ is normal to the edge lies within the interval $c - L < x_3 < c$ wetted by the flow. It may be verified that this result reduces to (5.2.5) when $c/a \to \infty$.

Hence, evaluating the acoustic pressure frequency spectrum in the usual way (making use of (3.1.3)), and noting that $\kappa_o \ll k$, we find for the

Elliptic airfoil:

$$\Phi(\mathbf{x},\omega) \approx \frac{a^4c^2\omega^2\cos^2\Theta}{8\Psi^2(0)c_o^2|\mathbf{x}|^2} \int_{-\infty}^{\infty} \frac{k^2\mathrm{P}(\mathbf{k},\omega)}{(k_1^2a^2+k_3^2c^2)^2} \mathrm{H}\left(\frac{k_3}{k_1} - \frac{a(1-L/c)}{\sqrt{Lc}\sqrt{2-L/c}}\right) dk_1 dk_3, \quad |\mathbf{x}| \to \infty. \tag{5.2.8}$$

Using the Corcos approximation (3.2.3), this result can be expressed in the form

$$\Phi(\mathbf{x},\omega) \approx \Phi_o(\mathbf{x},\omega)\mathcal{K}\left(\frac{c}{a},\frac{c}{L}\right), \quad \Phi_o(\mathbf{x},\omega) \equiv 0.027\,\frac{aLM^2\cos^2\Theta\Phi_{pp}(\omega)}{|\mathbf{x}|^2}$$

$$\mathcal{K}\left(\frac{c}{a},\frac{c}{L}\right) = \frac{1}{\Psi^2(0)}\frac{c}{a}\frac{c}{L}\int_{\mu_o}^{\infty} \frac{(1+\mu^2)\,d\mu}{(1+(1.4)^2\mu^2)(1+c^2\mu^2/a^2)^2}, \quad \mu_o = \frac{a}{c}\frac{(c/L-1)}{\sqrt{2c/L-1}}. \tag{5.2.9}$$

Thus, $\mathcal{K}(c/a, c/L)$ represents the ratio $\Phi(\mathbf{x},\omega)/\Phi_o(\mathbf{x},\omega)$ of the edge noise spectrum to that of the sound generated by a trailing edge section of span L of a strip airfoil of chord $2a$. This is plotted in Figure 5.3 as a function of the fractional span of the wetted tip L/c for three

different aspect ratios c/a. The contribution from the tip region is 6 dB or more below that from an inboard section of the airfoil of chord $2a$ and equal span when $L/c < 0.1$. According to (5.2.9), $\mathcal{K} \sim \pi/4\Psi^2(0) \approx \pi/4$ provided $a \ll c$ and $L = c$,, i.e., the maximum edge noise from the elliptic airfoil is always about 1 dB smaller than that from an airfoil of uniform chord a of the same span. Note that, since $\Psi^2(0) \approx 1$ for $c/a > 5$, these conclusions remain true when the calculation is based on the slowly varying chord approximation.

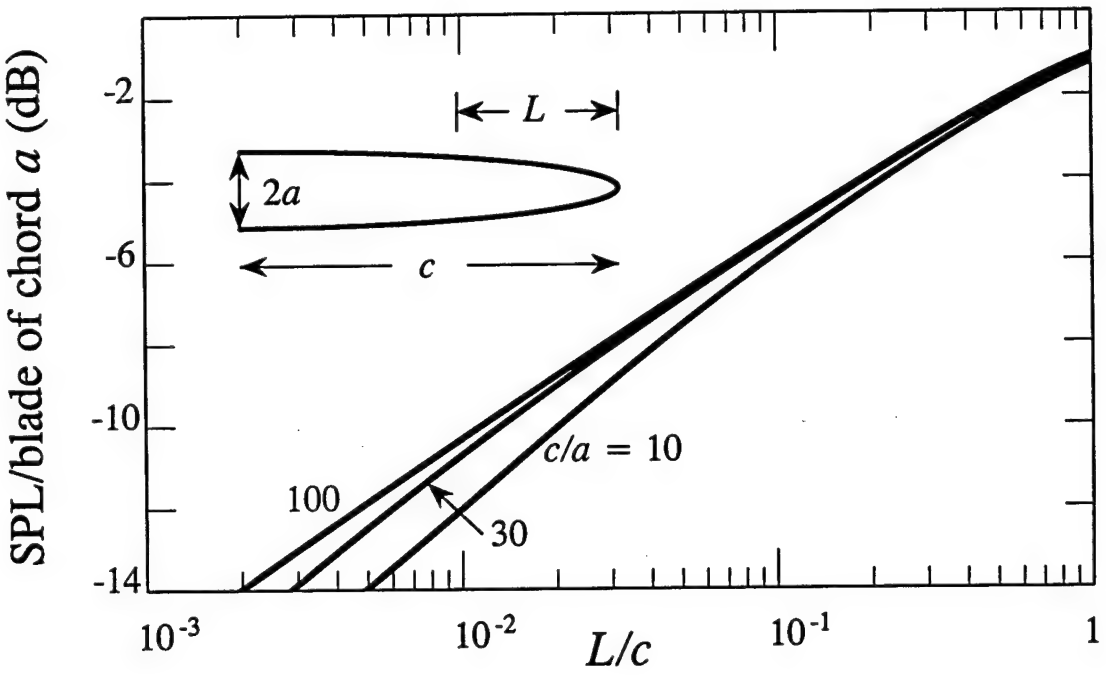

Figure 5.3. Edge noise produced by a tip region of length L of an elliptic airfoil of maximum chord $2a$ relative to that produced by the same flow over a spanwise section of length L of a strip airfoil of chord $2a$.

6. SLOTS AND FLAP SIDE-EDGES

The side edges of part span trailing edge flaps are important contributors to trailing edge noise [46 - 51]. In typical underwater applications the streamwise "slot" between an undeployed flap and the neighboring fixed section of a trailing edge is large enough to be an important additional source of noise. This case can be handled analytically by modelling the trailing edge region by a rigid half-plane (as for conventional trailing edge noise, §4) and the slot as a rectangular cut-out, as indicated in Figure 6.1a. In a first approximation the influence of flap deployment *on the generation of sound* can be estimated by assuming the width $2s$ of the slot to increase with distance towards the trailing edge.

§6.1 Green's function: non-compact airfoil chord

The slot is assumed to be acoustically compact and to occupy the region $-\ell < x_1 < 0$, $x_2 = 0$, $|x_3| < s$ of the rigid half-plane $x_1 < 0$, $x_2 = 0$. For an observer at $\mathbf{x}$ in the acoustic far field, the compact Green's function is written

$$G(\mathbf{x},\mathbf{y};\omega) = G_0(\mathbf{x},\mathbf{y};\omega) + G_1(\mathbf{x},\mathbf{y};\omega) + G_s(\mathbf{x},\mathbf{y};\omega), \tag{6.1.1}$$

where G_0, G_1 are defined as in (4.1.2) for the rigid half-plane, and G_s is the correction produced by the slot.

The functional form of G_s depends on the *minimum distance* Δ of the source point $\mathbf{y}$ from the slot, i.e., on the magnitude of Δ/s:

For $\Delta \sim s$:

$$G_s(\mathbf{x},\mathbf{y};\omega) \approx -\frac{\sin^{\frac{1}{2}}\psi \sin(\theta/2)\sqrt{\kappa_o \ell}\, e^{i\kappa_o|\mathbf{x}|}}{\pi\sqrt{2\pi i}|\mathbf{x}|}\,\beta(y_1)\mathrm{Re}\left\{\ln\left[\frac{z}{s}+\sqrt{\frac{z^2}{s^2}-1}\right]\right\}, \quad z = y_3 + iy_2; \tag{6.1.2}$$

For $\Delta \gg s$:

$$\begin{aligned} G_s(\mathbf{x},\mathbf{y};\omega) &\approx \frac{2\sin^{\frac{1}{2}}\psi \sin(\theta/2)\sqrt{\kappa_o \ell}\, e^{i\kappa_o|\mathbf{x}|}}{\pi^2\sqrt{2\pi i}|\mathbf{x}|}\int_{-\ell}^{0}\frac{\beta(\xi)}{R(\xi,\mathbf{y})}\tan^{-1}\left(\frac{\alpha}{\sqrt{1+\alpha^2}}\right)d\xi \\ &\equiv \frac{-\mathrm{sgn}(y_2)\sin^{\frac{1}{2}}\psi \sin(\theta/2)\sqrt{\kappa_o \ell}\, e^{i\kappa_o|\mathbf{x}|}}{8\pi^3\sqrt{2\pi i}|\mathbf{x}|} \\ &\quad \times \int_{-\ell}^{0}\beta(\xi)d\xi\int_{-\infty}^{\infty}\frac{e^{i[k\xi+k_1y_1+k_3y_3+\gamma|y_2|]}dkdk_1dk_3}{\sqrt{\bar\kappa_o+k}\sqrt{\bar\kappa_o+k_1}(k+k_1+i0)}; \end{aligned} \tag{6.1.3}$$

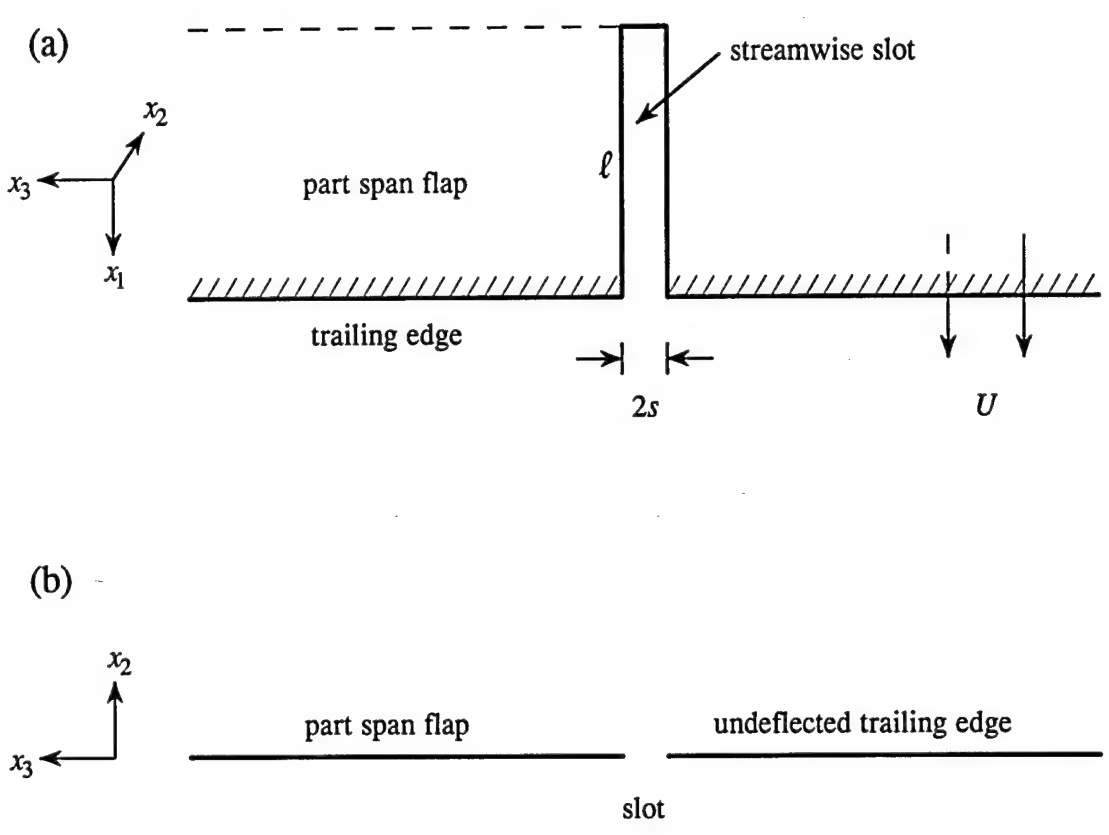

Figure 6.1. (a) Model of a trailing edge, streamwise slot;
(b) View of the slotted half-plane from downstream.

where

$$(y_1, y_2) = r(\cos\theta_o, \sin\theta_o), \qquad \alpha = \sqrt{\frac{2r|\xi|}{R(R+R_1)}}\sin\frac{\theta_o}{2},$$

$$R = \sqrt{(y_1-\xi)^2+y_2^2+y_3^2},\ R_1 = \sqrt{(r+|\xi|)^2+y_3^2},$$

and γ and $\bar{\kappa}_o$ are defined as in (4.1.4). The derivation of these formulae is discussed in §6.3.

The angles ψ and θ specify the far field observer direction $\mathbf{x}$, as in Figure 4.2. The dimensionless function $\beta(x_1)$ defines a rectilinear source distribution to which the slot is acoustically equivalent when irradiated by a (reciprocal) point source placed at $\mathbf{x}$. This function is tabulated in Table 6.1 and plotted in Figure 6.2 for four different values of the slot aspect ratio $2s/\ell$.

$2s/\ell \rightarrow$	0.025	0.05	0.075	0.1
x_1/ℓ	$\beta(x_1)$			
-1.0	0.310	0.360	0.390	0.420
-0.9	0.234	0.282	0.310	0.344
-0.8	0.204	0.240	0.268	0.291
-0.7	0.184	0.216	0.239	0.259
-0.6	0.167	0.195	0.216	0.234
-0.5	0.151	0.177	0.196	0.212
-0.4	0.136	0.159	0.176	0.190
-0.3	0.119	0.139	0.155	0.168
-0.2	0.100	0.118	0.132	0.143
-0.1	0.077	0.090	0.103	0.113
0.0	0.000	0.000	0.000	0.000

Table 6.1

The approximation (6.1.2) is applicable for source distributions in the immediate neighborhood of the slot whose length scale in the x_3-direction is comparable to the slot width $2s$, whereas (6.1.3) should be used when the bulk of the source distribution is spread over a much larger spanwise domain which, nevertheless, is well within the acoustic near field of the slot.

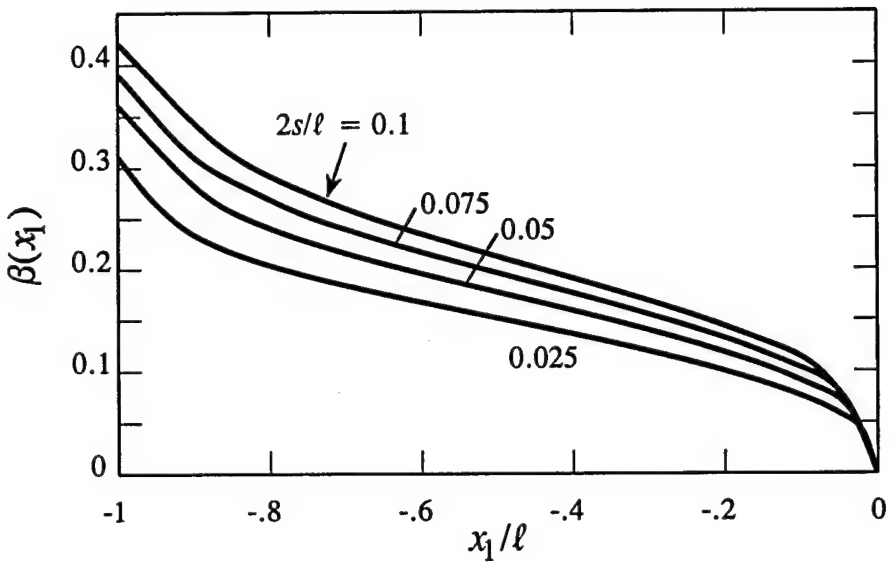

Figure 6.2. Dependence of the Green's function source strength $\beta(x_1)$ on the slot aspect ratio $2s/\ell$.

§6.2 Green's function: compact chord

For a thin airfoil whose chord at the slot is $2a \gg \ell$ (Figure 6.3) the compact Green's function in the absence of the slot is given by (2.4.14), when the coordinate origin is at midchord. When the origin is shifted to the trailing edge, with the x_1-axis along the axis of symmetry of the slot, the analogs of equations (6.1.2), (6.1.3) are found to be:

For $\Delta \sim s$:

$$G_s(\mathbf{x},\mathbf{y};\omega) \approx \frac{i\cos\Theta\sqrt{2\kappa_o^2 a\ell}e^{i\kappa_o|\mathbf{x}|}}{4\pi|\mathbf{x}|}\beta(y_1)\mathrm{Re}\left\{\ln\left[\frac{z}{s}+\sqrt{\frac{z^2}{s^2}-1}\right]\right\}, \quad z = y_3 + iy_2; \quad (6.2.1)$$

For $\Delta \gg s$:

$$\begin{aligned} G_s(\mathbf{x},\mathbf{y};\omega) &\approx \frac{-i\cos\Theta\sqrt{2\kappa_o^2 a\ell}e^{i\kappa_o|\mathbf{x}|}}{2\pi^2|\mathbf{x}|}\int_{-\ell}^{0}\frac{\beta(\xi)}{R(\xi,\mathbf{y})}\tan^{-1}\left(\frac{\alpha}{\sqrt{1+\alpha^2}}\right)d\xi \\ &\equiv \frac{i\mathrm{sgn}(y_2)\cos\Theta\sqrt{2\kappa_o^2 a\ell}e^{i\kappa_o|\mathbf{x}|}}{32\pi^3|\mathbf{x}|} \\ &\quad\times\int_{-\ell}^{0}\beta(\xi)d\xi\int_{-\infty}^{\infty}\frac{e^{i(k\xi+k_1y_1+k_3y_3)-|y_2|\sqrt{k_1^2+k_3^2}}dkdk_1dk_3}{\sqrt{k+i0}\sqrt{k_1+i0}(k+k_1+i0)}; \quad (6.2.2) \end{aligned}$$

where $\Theta = \cos^{-1}(x_2/|\mathbf{x}|)$ is the angle between the radiation direction and the upward normal to the airfoil (the x_2-axis).

§6.3 Derivation of Green's function

We use the method of [49] making use of the reciprocal theorem, in which $G(\mathbf{x},\mathbf{y};\omega) \equiv G(\mathbf{y},\mathbf{x};\omega)$ is first calculated as a function of $\mathbf{y}$ in the neighborhood of the slot when a unit point source is placed at the far field point $\mathbf{x}$ (defined as in (2.4.2)). Details are given below for an airfoil of non-compact chord, but the procedure is readily modified for the case of compact chord discussed in §6.2.

The length ℓ of the slot is assumed to be small compared to the acoustic wavelength. Thus, when scattering by the slot is ignored, the potential in the neighborhood of the slot produced by an acoustic source at the far field point $\mathbf{x}$ is given by (4.1.1). In the immediate vicinity of the slot the motion induced through the slot is locally two-dimensional and can be approximated by

$$G = \mathcal{A} + \mathcal{B}\,\mathrm{Re}\Big\{\ln[z/s+\sqrt{z^2/s^2-1}]\Big\}, \quad z = y_3 + iy_2, \quad (6.3.1)$$

where $\mathcal{A} \equiv \mathcal{A}(\mathbf{x};\omega)$ is independent of $\mathbf{y}$, and $\mathcal{B} \equiv \mathcal{B}(\mathbf{x},y_1;\omega)$ determines the local volume flux through the slot (which varies with y_1 along its length) induced by the incident potential (4.1.1).

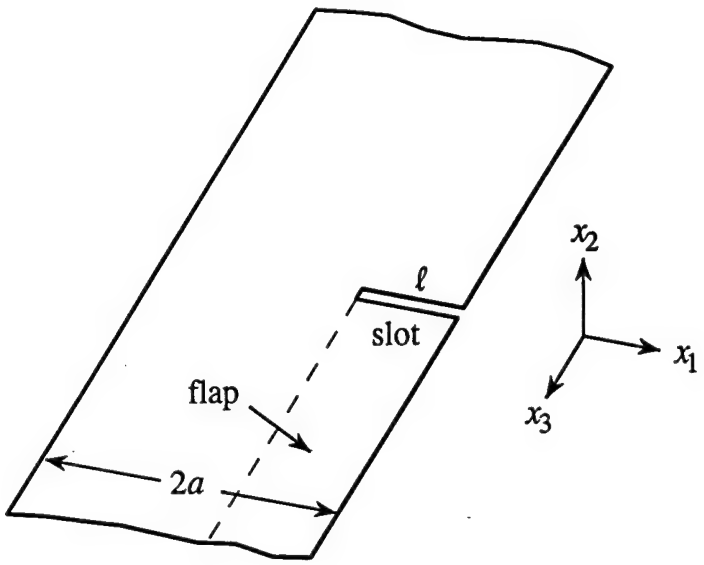

Figure 6.3. Trailing edge slot in airfoil of compact chord.

At large distances ($\gg s$) from the slot the influence of the induced motion through the slot is equivalent to that produced by a line source of variable strength $\sigma(x_1)$, say, per unit length distributed over $-\ell < x_1 < 0$ on the upper surface $x_2 = +0$, together with that produced by an equal and opposite distribution ($-\sigma(x_1)$ per unit length) on the underside $x_2 = -0$. At distances from the slot that greatly exceed s but are well within an acoustic wavelength, the net field can therefore be cast in the Macdonald's form [52, 53 (§8.4.2)]

$$G = G_0 + G_1 - \frac{2}{\pi^2}\int_{-\ell}^{0} \frac{\sigma(\xi)}{R(\xi, \mathrm{y})} \tan^{-1}\left(\frac{\alpha}{\sqrt{1+\alpha^2}}\right) d\xi, \tag{6.3.2}$$

where R and α are defined as in (6.1.3).

It follows from a comparison of (6.3.1) and (6.3.2) that, since $\kappa_o y_3 \ll 1$,

$$\mathcal{A} = G_0 \approx \frac{-e^{i\kappa_o|\mathbf{x}|}}{4\pi|\mathbf{x}|}. \tag{6.3.3}$$

To determine $\mathcal{B}$ and σ we introduce a length h which is assumed to be large compared to s, yet small compared to the length scale of variation of $\mathcal{B}$ and σ along the axis of the slot. Then, for each fixed value of y_1 in the interval $-\ell < y_1 < 0$ we find from (6.3.1), (6.3.2)

$$\begin{aligned} G &\sim \mathcal{A} + \mathcal{B}\ln\left|\frac{2z}{s}\right|, \quad |z|/s \to \infty \\ &\sim G_0 + G_1 + \frac{\sigma(y_1)}{\pi}\ln\left|\frac{z}{h}\right| + \frac{1}{2\pi}\int_{-\ell}^{0} \frac{\sigma(\xi)}{|y_1-\xi|}\left[1 - \frac{4}{\pi}\tan^{-1}\left(\frac{\alpha}{\sqrt{1+\alpha^2}}\right)\right] d\xi - \frac{1}{2\pi}\int_{-\ell}^{0} \frac{\sigma(\xi)d\xi}{|y_1-\xi|}, \\ & \qquad |z|/h \to 0, \quad \alpha = \sqrt{\frac{2\xi y_1}{|y_1-\xi|(|y_1-\xi| - y_1 - \xi)}}, \end{aligned} \tag{6.3.4}$$

where the principal value notation implies that the interval $y_1 - h/2 < \xi < y_1 + h/2$ is to be excluded in the final integral. Hence $\mathcal{B} = \sigma/\pi$, and by setting

$$\mathcal{B} \equiv \frac{\sigma}{\pi} = \frac{-\sin\frac{1}{2}\psi \sin(\theta/2)\sqrt{\kappa_o \ell} e^{i\kappa_o|\mathbf{x}|}}{\pi\sqrt{2\pi i}|\mathbf{x}|}\beta(\xi), \tag{6.3.5}$$

it follows that β is the solution of the integral equation

$$\beta(\xi)\ln\left(\frac{2h}{s}\right) + \frac{1}{2}\int_{-\ell}^{0} \frac{\beta(\eta)d\eta}{|\xi-\eta|} - \frac{1}{2}\int_{-\ell}^{0} \frac{\beta(\eta)}{|\xi-\eta|}\left[1 - \frac{4}{\pi}\tan^{-1}\left(\frac{\alpha}{\sqrt{1+\alpha^2}}\right)\right] d\eta = \sqrt{\frac{|\xi|}{\ell}}, \quad -\ell < \xi < 0. \tag{6.3.6}$$

This can be solved by collocation (Figure 6.2); the solution is stable provided $h/2s \geq 1$.

§6.4 Boundary layer generated slot noise

The sound generated by turbulent flow in the x_1-direction over the slot can be calculated by the method of §4.2, by using the formulae (4.2.3) and (4.2.4) to express the radiated sound in terms of the blocked pressure p_s. Because the dominant boundary layer pressures have surface wavenumbers (k_1, k_3) in the convective region centered on $(\omega/U_c, 0)$, the characteristic length scale of the source field in the spanwise direction greatly exceeds the slot width $2s$. It

is therefore appropriate to calculate the slot noise by using one of the "outer" forms (6.1.3), (6.2.2) of G_s.

For an airfoil of non-compact chord, equations (6.1.3) and (4.2.4) yield the far field acoustic pressure in the form

$$p(\mathbf{x},t) \approx \frac{\sin^{\frac{1}{2}}\psi \sin(\theta/2)}{\sqrt{2\pi i}|\mathbf{x}|} \iint_{-\infty}^{\infty} d^2\mathbf{k}d\omega \int_{-\ell}^{0} \sqrt{\kappa_o \ell} p_s(\mathbf{k},\omega)\beta(\xi)\mathrm{erf}\left(e^{-\frac{i\pi}{4}}|\xi|^{\frac{1}{2}}\sqrt{\bar{\kappa}_o + k_1}\right) e^{i(k_1\xi - \omega[t])}d\xi, \tag{6.4.1}$$

where $[t] = t - |\mathbf{x}|/c_o$ is the retarded time. Forming the acoustic pressure frequency spectrum in the usual way (using (3.1.3)) we find

$$\begin{aligned}\Phi(\mathbf{x},\omega) &\approx \frac{\omega\ell \sin\psi \sin^2(\theta/2)}{\pi c_o|\mathbf{x}|^2} \int_{-\infty}^{\infty} \mathrm{P}(\mathbf{k},\omega) \left|\int_{-\ell}^{0} \beta(\xi)\mathrm{erf}\left(e^{-\frac{i\pi}{4}}|\xi|^{\frac{1}{2}}\sqrt{\bar{\kappa}_o + k_1}\right) e^{ik_1\xi}d\xi\right|^2 d^2\mathbf{k} \\ &\approx \frac{\omega\ell \sin\psi \sin^2(\theta/2)}{\pi c_o|\mathbf{x}|^2}\Phi_{pp}(\omega) \left|\int_{-\ell}^{0} \beta(\xi)\mathrm{erf}\left(e^{-\frac{i\pi}{4}}|\xi|^{\frac{1}{2}}\sqrt{\frac{\omega}{U_c}}\right) e^{i\omega\xi/U_c}d\xi\right|^2, \quad \omega > 0,\end{aligned} \tag{6.4.2}$$

where $\Phi_{pp}(\omega)$ is the blocked pressure frequency spectrum.

Using the Chase [27] approximation (3.2.4) this result can be written

$$\frac{(U/\delta_*)\Phi(\mathbf{x},\omega)}{(\rho_o v_*^2)^2} \approx M\frac{\ell^2}{|\mathbf{x}|^2}\sin\psi\sin^2\left(\frac{\theta}{2}\right)\frac{\mathcal{F}(\omega)(\omega\delta_*/U)^2}{[\alpha_p^2 + (\omega\delta_*/U)^2]^{\frac{3}{2}}}, \tag{6.4.3}$$

where

$$\mathcal{F}(\omega) = \left(\frac{\omega\ell}{U}\right)\frac{1}{\ell^2}\left|\int_{-\ell}^{0}\beta(\xi)\mathrm{erf}\left(e^{-\frac{i\pi}{4}}|\xi|^{\frac{1}{2}}\sqrt{\frac{\omega}{U_c}}\right)e^{i\omega\xi/U_c}d\xi\right|^2 \tag{6.4.4}$$

is a dimensionless function of the frequency. The asymptotic formula for the behavior of the error function as $\omega\ell/U_c \to \infty$ [54] supplies

$$\mathcal{F}(\omega) \sim \mathcal{F}_\infty = \frac{\pi U_c}{20U\ell}\left|\int_{-\ell}^{0}\frac{\beta(\xi)d\xi}{\sqrt{|\xi|}}\right|^2, \quad \frac{\omega\ell}{U_c} \to \infty. \tag{6.4.5}$$

Thus, $\Phi(\mathbf{x},\omega)$ decreases like ω^{-1} at high frequencies, whereas the trailing edge noise generated by the same flow decreases at least as fast as ω^{-2} (see (4.3.7)).

The situation is illustrated in Figure 6.4a for a slot of aspect ratio $2s/\ell = 0.05$, and for $\ell/\delta = 10$, where $\delta \sim 8\delta_*$ is the boundary layer thickness. The dashed curve is the spectrum

$$(U/\delta_*)\Phi(\mathbf{x},\omega)/[a_o(\rho_o v_*^2)^2 M(\ell\delta_*/|\mathbf{x}|^2)\sin\psi\sin^2(\theta/2)] \text{ (dB)}$$

of the sound generated by a section of the *trailing edge* whose spanwise length equals the slot length ℓ. The "slot noise" is the spectrum $(U/\delta_*)\Phi(\mathbf{x},\omega)/[a_o(\rho_o v_*^2)^2 M(\ell\delta_*/|\mathbf{x}|^2)\sin\psi\sin^2(\theta/2)]$

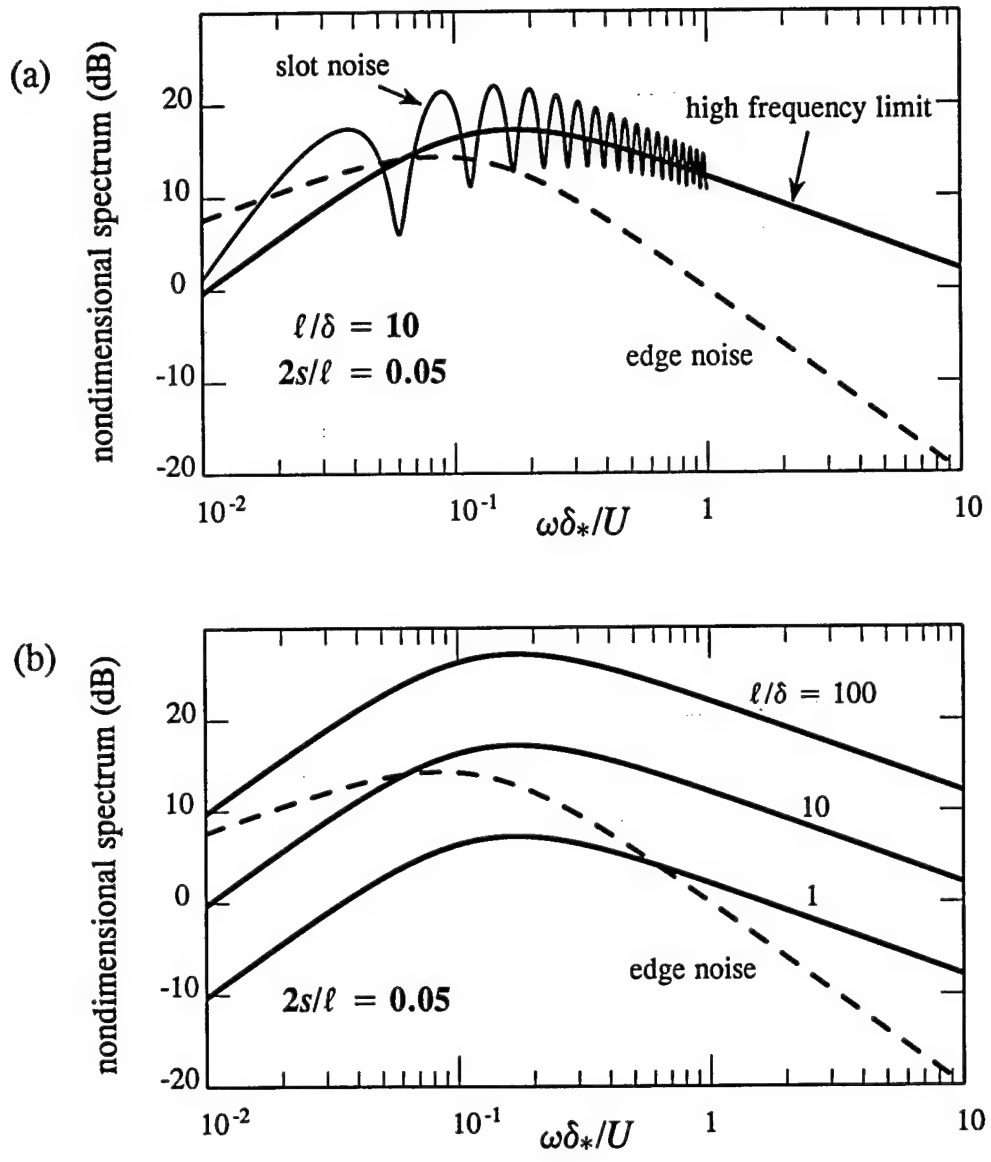

Figure 6.4. (a) Comparison of slot noise and the trailing edge noise generated by a section of the edge of span ℓ. (b) Dependence of slot noise on ℓ/δ.

determined by (6.4.3) for $U_c = 0.7U$. At very high frequencies the amplitude of the slot noise fluctuations (caused by the frequency dependence of $\mathcal{F}(\omega)$) decrease, and the high frequency limit shown in the figure is the prediction of (6.4.3) when $\mathcal{F}(\omega)$ is replaced by $\mathcal{F}_\infty$.

Evidently the high frequency approximation provides a good overall representation of the strength of the slot noise for all frequencies, and it has been used in Figure 6.4b to illustrate the dependence of slot noise on ℓ/δ.

§6.5 Side-edge flap noise

To investigate the sound generated by the side-edge vortex formed when a part-span flap is deployed at a finite angle of attack (Figure 6.5a), it is necessary to modify the slot geometry. The distance between the adjacent sides of the flap and the undeflected trailing edge now increases as the trailing edges are approached; in a first approximation, the influence of flap deflection at the side-edge can therefore be modeled by taking the slot width $2s$ *for an undeflected flap* to vary along the slot. The simplest case is that in which flap deployment consists of a simple rotation through a *small* angle ϑ about the flap leading edge, as illustrated in Figure 6.5a. In this case flap deployment is approximated by the method of §§6.1 - 6.3 by assuming the slot semi-width $s \equiv s(y_1)$ to increase with y_1 (Figure 6.5b) according to

$$s(y_1) = s_o\Big[1 + (y_1/\ell + 1)\Big(\sqrt{1 + (\vartheta\ell/2s_o)^2} - 1\Big)\Big], \quad -\ell < y_1 < 0, \tag{6.5.1}$$

where $2s_o$ is the slot width in the undeflected state ($\vartheta = 0$).

The compact Green's function is given by the formulae of §§6.1, 6.2, except that explicit account is now be taken of the dependence s on y_1. Equation (6.3.6) for the source strength β is unchanged provided s is replaced by $s(\xi)$. The effect of this modification on the functional form of $\beta(x_1)$ is illustrated in Figure 6.6 when $2s_o/\ell = 0.05$ for $\vartheta = 0°,\ 5°,\ 10°$. The magnitude of $\beta(x_1)$ is seen to be determined principally by the *local* slot width $2s$: $\beta(x_1)$ differs significantly from its value in the undeflected state only towards the trailing edge.

To estimate the side-edge noise generated by the flap lift vortex Γ, which begins to form near the forward part of the side-edge (Figure 6.7), assume the mean position of the vortex lies along the line $x_1 > -\ell$, $x_2 \approx \vartheta(y_1 + \ell)$, $x_3 = s_o$, where $\vartheta \ll 1$ and the x_1-axis is taken to be parallel to the flap edge. For small ϑ the component of the unsteady flow velocity

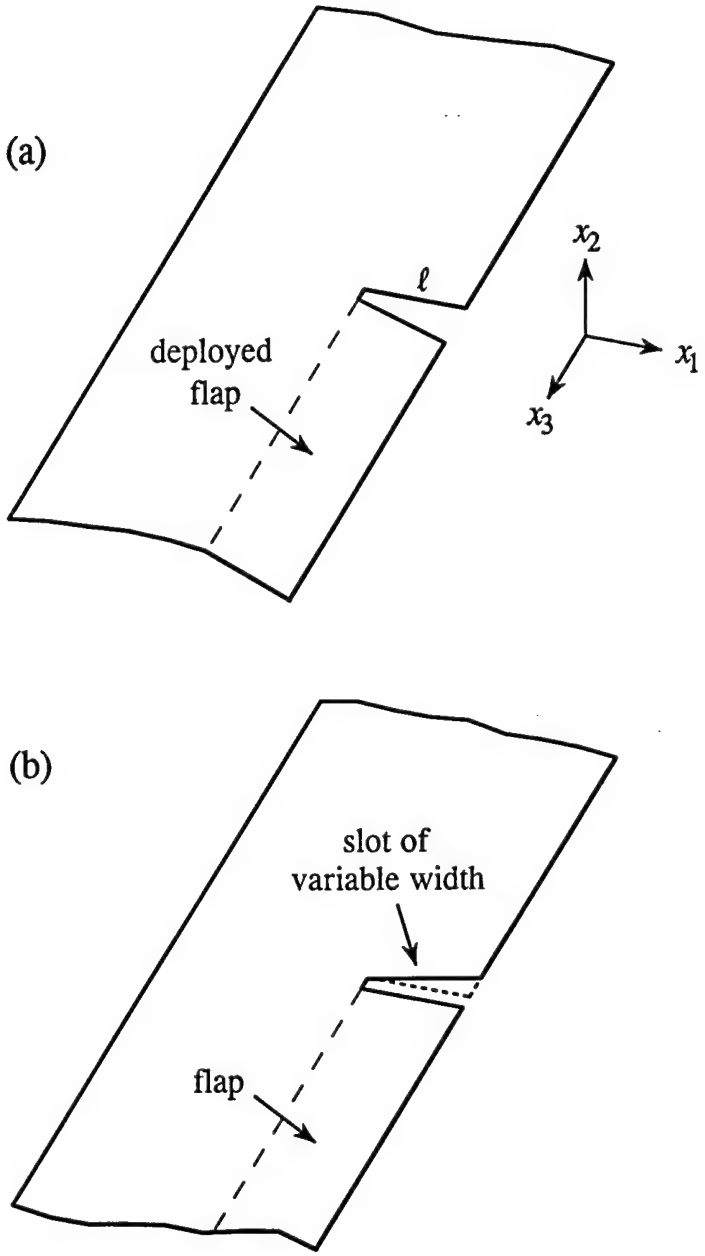

Figure 6.5. Modelling flap deployment by a side-edge slot of variable width.

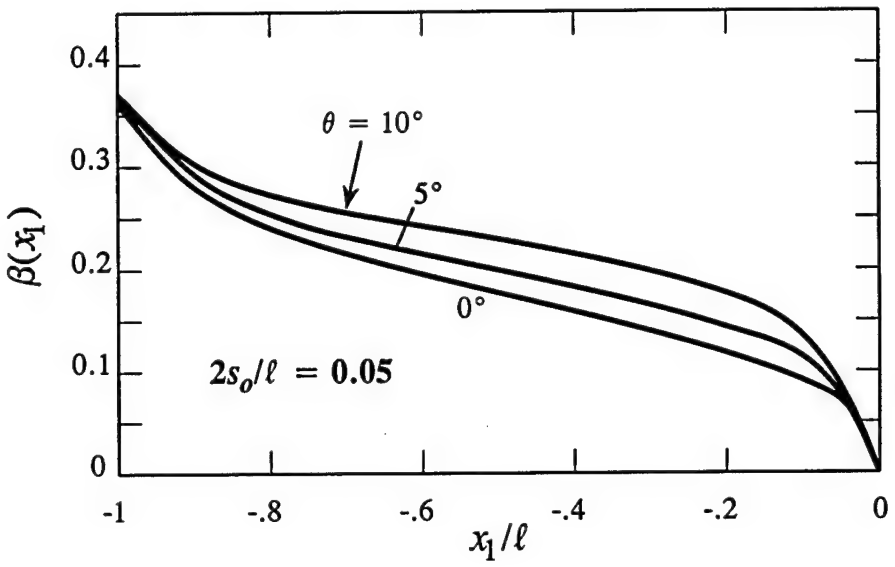

Figure 6.6. Dependence of $\beta(x_1)$ on ϑ when $2s_o/\ell = 0.05$.

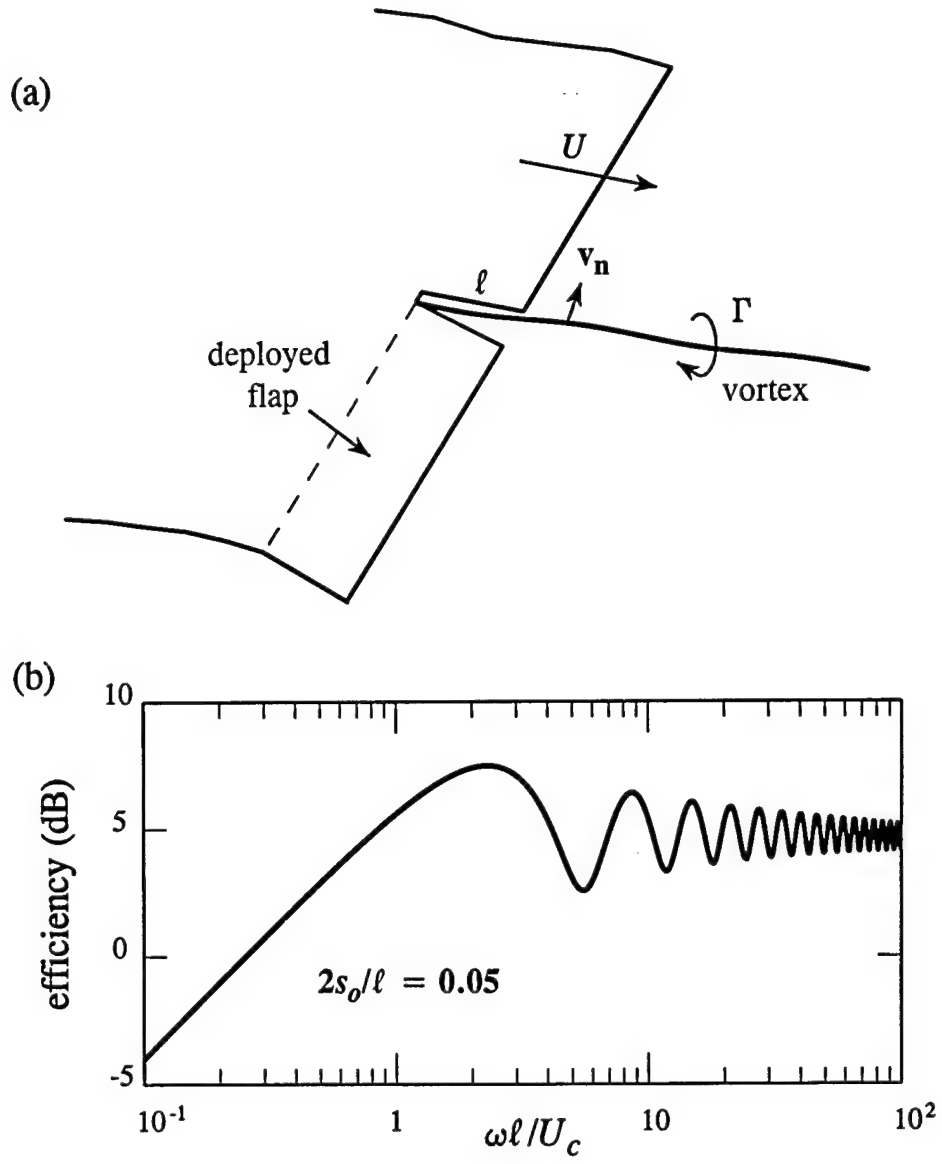

Figure 6.7. (a) Modelling side-edge vortex noise; (b) The efficiency factor $10 \times \log_{10} \mathcal{E}$.

normal to the vortex axis is taken in the form

$$\mathbf{v}_n \equiv \mathbf{v}_n(t - x_1/U_c) \equiv (0, v_2, v_3) = \int_{-\infty}^{\infty} \mathbf{v}_n(\omega) \mathrm{e}^{i\omega(x_1/U_c - t)} d\omega \tag{6.5.2}$$

where U_c is a suitable convection velocity associated with the propagation of disturbances along the vortex core. Using the general solution (2.6.4) (with $\nu = 0$ and $v_j n_j = 0$ on S), with G_s given by (6.1.2) for an airfoil of non-compact chord, the sound generated by the interaction of the vortex with the side-edge is found to be given by

$$p(\mathbf{x}, t) \approx \frac{\rho_o \Gamma \sin^{\frac{1}{2}} \psi \sin(\theta/2)}{2\pi\sqrt{2\pi i}|\mathbf{x}|\sqrt{\vartheta}} \int_{-\infty}^{\infty} d\omega \int_{-\ell}^{0} \frac{\beta(y_1)\sqrt{\kappa_o \ell}\{v_3(\omega) - v_2(\omega)\}\mathrm{e}^{i\omega(x_1/U_c - [t])} dy_1}{\sqrt{s(y_1)(y_1 + \ell)}}, \quad \vartheta \ll 1, \tag{6.5.3}$$

where $[t] = t - |\mathbf{x}|/c_o$ is the retarded time.

Let $\mathbf{v}_n(t - x_1/U_c)$ be a stationary random function, and let $\Phi_{23}(\omega) > 0$ be the frequency spectrum defined by

$$\Big\langle \big(v_3(\omega) - v_2(\omega)\big)\big(v_3^*(\omega') - v_2^*(\omega')\big) \Big\rangle = U^2 \delta(\omega - \omega') \Phi_{23}(\omega), \tag{6.5.4}$$

where the asterisk denotes complex conjugate. The side-edge noise frequency spectrum can then be written

$$\Phi(\mathbf{x}, \omega) \approx \frac{M_c \rho_o^2 U^2 \Gamma^2 \sin\psi \sin^2(\theta/2)}{4\pi^3 |\mathbf{x}|^2} \left(\frac{\ell}{s_o \vartheta}\right) \Phi_{23}(\omega) \mathcal{E}(\omega\ell/U_c), \quad |\mathbf{x}| \to \infty, \ \omega > 0, \tag{6.5.5}$$

where $M_c = U_c/c_o$, and the dimensionless *efficiency factor* $\mathcal{E}(\omega\ell/U_c)$ is given by

$$\mathcal{E} = \frac{\omega\ell}{U_c} \left| \int_{-\ell}^{0} \frac{\beta(y_1) \mathrm{e}^{i\omega y_1/U_c}}{[1 + (y_1/\ell + 1)(\sqrt{1 + (\vartheta\ell/2s_o)^2} - 1)]} \frac{dy_1}{\sqrt{\ell(y_1 + \ell)}} \right|^2. \tag{6.5.6}$$

$\mathcal{E}(\omega\ell/U_c)$ turns out be effectively independent of the flap angle ϑ (at least for $\vartheta \leq 10°$), and is plotted in Figure 6.7 for $2s_o/\ell = 0.05$.

In a rough approximation the vortex strength $\Gamma \sim U\ell\vartheta$, and

$$\Phi(\mathbf{x}, \omega) \approx \frac{M_c \rho_o^2 U^4 \ell^2 \sin\psi \sin^2(\theta/2)}{2\pi^3 |\mathbf{x}|^2} \left(\frac{\ell\vartheta}{2s_o}\right) \Phi_{23}(\omega) \mathcal{E}(\omega\ell/U_c), \quad |\mathbf{x}| \to \infty, \tag{6.5.7}$$

wherein $\ell\vartheta/2s_o$ is the ratio of flap deflection at the trailing edge to the undeflected slot width. Further predictions from this formula require a quantitative knowledge of the frequency spectrum $\Phi_{23}(\omega)$.

In addition, however, the side-edge vortex also produces sound by interacting with the trailing edges of the flap and the neighboring undeflected airfoil, determined by the component G_1 of the composite Green's function (6.1.1) (see (4.1.2)). This can be significant only at lower frequencies, when the length scale of the associated unsteady hydrodynamic pressures are large enough to affect these edges. The principal source term in (2.6.4) may now be approximated by $\boldsymbol{\omega} \wedge \mathbf{v} = (0, -u_3\Gamma, 0)\delta(y_2)\delta(y_3)$, produced by spanwise oscillations of the vortex core. In this case we find

$$p(\mathbf{x},t) \approx \frac{-\rho_o\Gamma\sqrt{M_c}\sin^{\frac{1}{2}}\psi\sin(\theta/2)}{2\sqrt{2}\pi|\mathbf{x}|}\, u_3(t-|\mathbf{x}|/c_o), \quad |\mathbf{x}|\to\infty, \tag{6.5.8}$$

where u_3 is defined in (6.5.2).

Hence, forming the acoustic pressure frequency spectrum as before:

$$\begin{aligned}\Phi(\mathbf{x},\omega) &\approx \frac{M_c\rho_o^2U^2\Gamma^2\sin\psi\sin^2(\theta/2)}{4\pi^2|\mathbf{x}|^2}\,\Phi_3(\omega)\\ &\approx \frac{\vartheta^2M_c\rho_o^2U^4\ell^2\sin\psi\sin^2(\theta/2)}{4\pi^2|\mathbf{x}|^2}\,\Phi_3(\omega), \quad |\mathbf{x}|\to\infty,\end{aligned} \tag{6.5.9}$$

where $\langle u_3(\omega)u_3^*(\omega')\rangle = U^2\delta(\omega-\omega')\Phi_3(\omega)$. For small deflections ϑ it appears that this will be small compared to the side-edge generated sound (6.5.7).

The results (6.5.7) and (6.5.9) represent the sound produced by perturbed motions of the vortex Γ without taking account of contributions from any other vorticity that may be produced at the surfaces of the flap and airfoil by that motion. The importance of these additional sources of sound is not known, and can only be determined from a more detailed knowledge of the hydrodynamic flow in the neighborhood of the side edge.

REFERENCES

1. Lighthill, M. J. 1952 Proc. Roy. Soc. Lond. A211, 564 - 587. On sound generated aerodynamically. Part I: General theory.
2. Lighthill, M. J. 1954 Proc. Roy. Soc. Lond. A222, 1 - 32. On sound generated aerodynamically. Part II: Turbulence as a source of sound.
3. Hinze, J. O. 1975 Turbulence (Second edition). New York: McGraw-Hill.
4. Batchelor, G. K. 1953 The theory of homogeneous turbulence. Cambridge University Press.
5. Morfey, C. L. 1973 J. Sound Vib. 31, 391 - 397. Amplification of aerodynamic noise by convected flow inhomogeneities.
6. Crighton, D. G., and J. E. Ffowcs Williams 1969 J. Fluid Mech. 36, 585 - 603. Sound generation by turbulent two-phase flow.
7. Ffowcs Williams, J. E. and Hawkings, D. L. 1969 Phil. Trans. Roy. Soc. A264, 321 - 342. Sound generation by turbulence and surfaces in arbitrary motion.
8. Curle, N. 1955 Proc. Roy. Soc. Lond. A231, 505 - 514. The influence of solid boundaries upon aerodynamic sound.
9. Batchelor, G. K. 1967 An Introduction to Fluid Dynamics. Cambridge University Press.
10. Powell, A. 1961 Vortex sound. Rept. No. 61 - 70, Department of Engineering, University of California, Los Angeles.
11. Howe, M. S. 1975 J. Fluid Mech. 71, 625 - 673. Contributions to the theory of aerodynamic sound, with application to excess jet noise and the theory of the flute.
12. Rayleigh, Lord 1894 The Theory of Sound, two volumes. London: Macmillan. (Reprinted by Dover Publications, New York, 1945).
13. van Dyke, M. 1964 Perturbation methods in Fluid Mechanics. New York: Academic Press.
14. Crow, S. C. 1970 Studies in Appl. Math. 49, 21 - 44. Aerodynamic sound emission as a singular perturbation problem.
15. Lesser, M. B. and Crighton, D. G. 1976 Physical Acoustics 11, 69 - 149. Physical acoustics and the method of matched asymptotic expansions.
16. Wu, J. C. 1981 AIAA J. 19, 432 - 441. Theory for aerodynamic force and moment in viscous flows.
17. Howe, M. S. 1989 J. Fluid Mech. 206, 131 - 153. On unsteady surface forces, and sound produced by the normal chopping of a rectilinear vortex.

18. Howe, M. S. 1991 Proc. Roy. Soc. Lond. A433, 573 - 598. On the estimation of the sound produced by complex fluid-structure interactions, with application to a vortex interacting with a shrouded rotor in a duct.

19. Howe, M. S. 1995 Q. J. Mech. appl. Math. 48, 401 - 426. On the force and moment exerted on a body in an incompressible fluid, with application to rigid bodies and bubbles at high and low Reynolds numbers.

20. Powell, A. 1960 J. Acoust. Soc. Am. 32, 962 - 990. Aerodynamic noise and the plane boundary.

21. Pierce, A. D. 1989 Acoustics, An introduction to its principles and applications. American Institute of Physics.

22. Powell, A. 1963 AGARD Rept. 466. Mechanisms of aerodynamic sound production.

23. Blokhintzev, D. 1946 J. Acoust. Soc. Am. 18, 322 - 334. The propagation of sound in an inhomogeneous moving medium I.

24. Phillips, O. M. 1956 J. Fluid Mech. 1, 607 - 624. The intensity of Aeolian tones.

25. Schewe, G. 1983 On the structure and resolution of wall pressure fluctuations associated with turbulent boundary layer flow. J. Fluid Mech. 134, 311 - 328.

26. Lauchle, G. C. and Daniels, M. 1987 Phys. Fluids 30, 3019 - 3024. Wall pressure fluctuations in turbulent pipe flow.

27. Chase, D. M. 1980 J. Sound Vib. 70, 29 - 67. Modeling the wavevector-frequency spectrum of turbulent boundary layer wall pressure.

28. Corcos, G. M. 1964 J. Fluid Mech. 18, 353 - 378. The structure of the turbulent pressure field in boundary layer flows.

29. Sevik, M. M. 1986 Topics in hydroacoustics. In Proc. IUTAM Symposium Aero- and Hydroacoustics, Lyon, July 3-6, 1985. Berlin: Springer-Verlag.

30. Blake, W. K. 1986 Mechanics of flow-induced sound and vibration, Vol. 2: Complex flow-structure interactions. New York: Academic Press.

31. Hersh, A. S. 1983 AIAA Paper No.87 - 2663. Surface roughness generated flow noise.

32. Cremer, L. and M. Heckl, E. E. Ungar 1988 Structure-borne Sound (2nd ed). New York: Springer-Verlag.

33. Howe, M. S. 1997 Acoustics of Fluid-Structure Interactions. Cambridge University Press (in press).

34. Howe, M. S. and Shah, P. L. 1996 J. Acoust. Soc. Am. 99, 3401 - 3411. Influence of mean flow on boundary layer generated interior noise.

35. Blake, W. K. and Gershfeld, J. L. 1989 In Lecture Notes in Engineering 46 (Ed. M. Gad-el-Hak), Frontiers in Experimental Fluid Mechanics: The aeroacoustics of trailing edges.

36. Brooks, T. F., Pope, D. S. and Marcolini, M. A. 1989 NASA Ref. Pub. No. 1218. Airfoil self-noise and prediction.

37. Crighton, D. G. 1991 airframe noise. Chapter 7 of Aeroacoustics of Flight Vehicles: Theory and Practice (Vol. 1). NASA Ref. Pub. No. 1258.

38. Chase, D. M. 1972 J. Acoust. Soc. Am. 52, 1011 - 1023. Sound radiated by turbulent flow off a rigid hal-plane as obtained from a wavevector spectrum of hydrodynamic pressure.

39. Chandiramani, K. L. 1974 J. Acoust. Soc. Am. 55, 19 - 29. diffraction of evanescent waves, with applications to aerodynamically scattered sound and radiation from unbaffled plates.

40. Chase, D. M. 1975 AIAA J. 13, 1041 - 1047. Noise radiated from an edge in turbulent flow.

41. Amiet, R. K. 1976 J. Sound Vib. 47, 387 - 393. Noise due to turbulent flow past a trailing edge.

42. Olsen, W. and Boldman, D. 1979 AIAA Paper 79-1524. Trailing edge noise data with comparison to theory.

43. Goldstein, M. E. 1979 J. Fluid Mech. 91, 601- 632. Scattering and distortion of the unsteady motion on transversely sheared mean flows.

44. Howe, M. S. 1981 J. Sound Vib. 75, 239 - 250. The displacement-thickness theory of trailing edge noise.

45. Lamb, Horace 1932 Hydrodynamics (6th. ed.). Cambridge University Press.

46. Ahtye, W. F., Miller, W. R. and Meecham, W. C. 1979 AIAA Paper 79-0667. wing and flap noise measured by near and far field cross-correlation techniques.

47. Kendall, J. M. and Ahtye, W. F. 1980 AIAA Paper 80-0035. Noise generation by a lifting wing/flap combination at Reynolds numbers to 2.8×10^6.

48. Hardin, J. C. 1980 AIAA J. 18, 549 - 552. Noise radiation from the side edges of flaps.

49. Howe, M. S. 1982 J. Sound Vib. 80, 555 - 573. On the generation of side-edge flap noise.

50. Hardin, J. C., Martin, J. E. 1997 AIAA J. 35, 810 - 815. Flap side-edge noise: acoustic analysis of Sen's model.

51. Sen, R. 1997 AIAA J. 35, 441 - 449. Vortex-oscillation model of airfoil side-edge noise.

52. Macdonald, H. M. 1915 Proc. Lond. Math. Soc. 14, 410 - 427. A class of diffraction problems.

53. Bowman, J. J., Senior, T. B. A. and Uslenghi, P. L. E. 1987 Electromagnetic and acoustic scattering by simple shapes (revised printing). New York: Hemisphere.

54. Abramowitz, M. and Stegun, I. A. 1970 (eds.) Handbook of Mathematical Functions (Ninth corrected printing), US Dept. of Commerce, Nat. Bur. Stands. Appl. Math. Ser. No.55.

PRINCIPAL SYMBOLS

δ	boundary layer thickness
δ_*	displacement thickness
η	shear coefficient of viscosity
κ_o	acoustic wavenumber ω/c_o
φ_i^*	incompressible velocity potential satisfying (2.4.7)
μ	$\sqrt{\lvert\omega\rvert/\omega_c}$
ν	kinematic viscosity
π_{ij}	momentum flux tensor
$\Phi(\mathbf{x},\omega)$	acoustic pressure frequency spectrum
$\Phi_{pp}(\omega)$	wall pressure frequency spectrum
ρ	fluid density
ρ_o	mean fluid density
σ_{ij}	viscous stress tensor
$\boldsymbol{\omega}$	vorticity curl $\mathbf{v}$
ω	radian frequency
B	total enthalpy $w+\frac{1}{2}v^2$
c	speed of sound
c_o	mean sound speed
D/Dt	$\partial/\partial t + v_j\partial/\partial x_j$
D_i	drag force
F_i	surface force applied to fluid
$\mathbf{k}$	planar wavenumber $(k_1,0,k_3)$
k	$\lvert\mathbf{k}\rvert$
K_o	vacuum bending wavenumber
M	Mach number
p	pressure
p_o	mean pressure
p_s	wall pressure
p_{ij}	compressive stress tensor
$\mathrm{P}(\mathbf{k},\omega)$	wall pressure spectrum

$\mathrm{R}(\omega)$	elastic wall refection coefficient
$\mathcal{R}(x_1, x_3, t)$	wall pressure correlation function
(r, θ)	polar coordinates in the x_1x_2-plane
s	specific entropy
t	time
T	temperature
T_{ij}	Lighthill stress tensor
$\mathbf{U}$	mean velocity
U_c	convection velocity
$\mathbf{v}$	velocity
v_*	friction velocity
w	specific enthalpy
$\mathbf{x}$	(x_1, x_2, x_3)
$\mathbf{y}$	(y_1, y_2, y_3)
X_i	$x_i - \varphi_i^*(\mathbf{x})$
Y_i	$y_i - \varphi_i^*(\mathbf{y})$

REPORT DOCUMENTATION PAGE

Form Approved
OMB No. 0704-0188

1. AGENCY USE ONLY *(Leave blank)*	2. REPORT DATE	3. REPORT TYPE AND DATES COVERED
	9 January 1998	Final. 1 July 1997 - 31 Dec. 1997

4. TITLE AND SUBTITLE
Reference Manual on the Theory of
Lifting Surface Noise at Low Mach Numbers

5. FUNDING NUMBERS
G N00014-97-1-0963

6. AUTHOR(S)
Michael S. Howe

7. PERFORMING ORGANIZATION NAME(S) AND ADDRESS(ES)
Boston University
College of Engineering
110 Cummington Street
Boston MA 02215

8. PERFORMING ORGANIZATION REPORT NUMBER
AM-98-001

9. SPONSORING/MONITORING AGENCY NAME(S) AND ADDRESS(ES)
Office of Naval Research
Code 333
Dr. L. Patrick Purtell

10. SPONSORING/MONITORING AGENCY REPORT NUMBER

11. SUPPLEMENTARY NOTES

12a. DISTRIBUTION/AVAILABILITY STATEMENT
Approved for Public Release

12b. DISTRIBUTION CODE

13. ABSTRACT *(Maximum 200 words)*

A summary review is made of the theory of aerodynamic sound in low Mach number flows, with particular emphasis on procedures for estimating the influence of solid boundaries on sound production. Special consideration is given to the production of sound by nominally steady flow over a lifting or control surface. Four categories of interactions are discussed involving (i) a large, nominally flat surface, (ii) a large surface with a trailing edge, (iii) a lifting surface of compact chord and finite span, and (iv) a trailing edge with a streamwise slot or part-span flap. The results can be combined with steady state numerical predictions to express the radiation in terms of calculated mean flow properties.

14. SUBJECT TERMS	15. NUMBER OF PAGES
Aerodynamic sound, lifting surface noise, vortex sound, trailing edge noise, blade noise, slots and side-edge flap noise	93 + ii
	16. PRICE CODE

17. SECURITY CLASSIFICATION OF REPORT	18. SECURITY CLASSIFICATION OF THIS PAGE	19. SECURITY CLASSIFICATION OF ABSTRACT	20. LIMITATION OF ABSTRACT
Unclassified	Unclassified	Unclassified	